

Antenna Modeller for Synthetic Aperture Radar Applications

Electromagnetic and Radiometric Considerations

Master Thesis Dissertation

by Irena Calafell Rueda

Advisor: José María González Arbesú

Barcelona, January 2011

Universitat Politècnica de Catalunya

Teoria del Senyal i Comunicacions

Master of Science in Research on Information and Communication Technologies



Index

1	INTRODUCTION.....	5
1.1	FRAMEWORK OF THE MASTER THESIS WORK	5
1.2	MOTIVATION	6
1.3	STATE OF THE ART.....	6
1.4	SCOPE.....	6
1.5	ORGANIZATION OF THE DISSERTATION	7
2	ARCHITECTURAL MODELLING OF AN ANTENNA MODELLER.....	9
2.1	THE ANTENNA MODELLER	9
2.1.1	<i>Brief Description of the Antenna Modeller Functionalities.....</i>	<i>9</i>
2.1.2	<i>The Antenna Modeller GUI.....</i>	<i>10</i>
2.2	COMPUTING RADIATION PATTERNS WITH AMOR.....	15
2.2.1	<i>Patterns Computation from SA patterns.....</i>	<i>15</i>
2.2.2	<i>Computing Directivities with AMOR.....</i>	<i>17</i>
2.2.3	<i>Elevation (EL) and Azimuth (AZ) Planes.....</i>	<i>18</i>
2.2.4	<i>Computing the AZ Beam Table for a Spotlight Beam.....</i>	<i>22</i>
2.3	COMPUTING ERRORS WITH AMOR.....	22
2.3.1	<i>Mechanical and Thermoelastic Errors</i>	<i>22</i>
2.3.2	<i>Transmit-Receive Module Errors.....</i>	<i>23</i>
3	OPTIMISATION TOOL FOR AMOR: DESIGN AND RESULTS.....	25
3.1	BRIEF DESCRIPTION OF THE OPTIMISER FUNCTIONALITIES.....	25
3.2	AMOR OPTIMISATION TOOL FOR PAZ.....	25
3.2.1	<i>Genetic Algorithm Overview.....</i>	<i>25</i>
3.2.2	<i>Variables of the GA</i>	<i>27</i>
3.2.3	<i>Optimization Tool Variables</i>	<i>29</i>
3.2.4	<i>Fitness Function.....</i>	<i>30</i>
3.2.5	<i>Algorithm Stopping Criteria.....</i>	<i>36</i>
3.2.6	<i>Initial Population</i>	<i>37</i>
3.2.7	<i>Optimiser Development Procedure</i>	<i>38</i>
3.2.8	<i>AMOR Optimiser GUI.....</i>	<i>40</i>
3.3	OPTIMISATION TOOL RESULTS AND GUIDELINES	47
3.3.1	<i>Characterisation of the Optimiser Behaviour</i>	<i>48</i>
3.3.2	<i>Optimiser Guidelines.....</i>	<i>56</i>
3.3.3	<i>Guidelines Application</i>	<i>58</i>

4	BUILDING BLOCKS OF AMOR	65
4.1	DIRECTORY TREE	65
4.2	MAIN SUBROUTINES	66
5	CONCLUSIONS AND FUTURE WORK.....	69
APPENDIX A	STATE OF THE ART.....	71
A.1	MISSIONS OVERVIEW.....	71
A.2	ANTENNA DESCRIPTION	76
A.3	ANTENNA MODEL	79
A.3.1	<i>TerraSAR-X</i>	79
A.3.2	<i>RADARSAT-2</i>	80
A.3.3	<i>COSMO-SkyMed</i>	80
A.3.4	<i>SEOSAR/PAZ</i>	81
APPENDIX B	SIMULATION RESULTS	83
APPENDIX C	AZIMUTH AND ELEVATION PLANES INCONSISTENCE	87
APPENDIX D	PUBLICATIONS.....	89
REFERENCES AND BIBLIOGRAPHY	95
R.1	CHAPTER 2	95
R.1.1	<i>References</i>	95
R.2	CHAPTER 3	95
R.2.1	<i>References</i>	95
R.2.2	<i>Bibliography</i>	96
R.3	ANNEX A.....	96
R.3.1	<i>References</i>	96
R.3.2	<i>Bibliography</i>	97
ACRONYMS		99

1 INTRODUCTION

In measurements of any nature, the objective is to determine as accurately as possible some characteristics of an object, material or living being. To be precise, the instrument used to measure needs to be as perfect as possible. i.e., the readings that provides need to be determined or adjusted. That is exactly the meaning of calibration.

Calibration is a crucial step in a SAR (Synthetic Aperture Radar) mission, where the main objective is Earth Observation (EO). The measured data is translated into SAR images, and from these images information on the ocean's salinity, wind speed, terrain deformation, or urban sprawl, among others, is extracted. Depending on the calibration quality, these SAR images would be more or less reliable.

One of the most critical tasks in the calibration of a SAR is the definition of an antenna model taking into account in a dynamical way all the possible variations in the active antenna array based on the information coming from the instrument internal calibration. To do so, many radiometric parameters need to be considered and need to be properly related to antenna parameters.

The model has to be capable of optimizing the excitations (complex) in order to predict the antenna patterns on-earth and used to compute the desired instrument behaviour before being launched and without needing in-flight measurements. This will help to compute on-ground the compensations to apply to the excitations of the antenna system caused by some of the active elements fail or degradation.

This extreme importance and necessity of an antenna model comes from the fact that the huge antenna arrays physical dimensions used in SAR and the high number of beams which can be generated make highly difficult their complete characterization on-earth.

Although the aim of this Master Thesis is developing the beam optimizer of an antenna model for a generic SAR mission, during that development we have the exclusive opportunity of applying the tool to a practical test case such as the Spanish mission SEOSAR/PAZ. This mission is in the framework of the Spanish Earth observation program (SEOSAR) and includes the design of an X-band synthetic aperture radar.

1.1 Framework of the Master Thesis work

The origin of the work presented in the present Master Thesis comes from collaboration between *Universitat Politècnica de Catalunya* (UPC) and the Spanish contractor *EADS Casa España* (ECE), responsible for the satellite development and construction. Two different investigation groups within the Signal Theory and Communications Department (TSC Department) at UPC take part in the project: the antenna laboratory (AntennaLab) and the remote sensing laboratory (RSLab). Since the UPC is providing a multidisciplinary technical support to ECE, not all the members involved in the project have a theoretical domain of all the covered areas.

The Antenna Modeller is developed by the AntennaLab investigation group; the group in which the author of this thesis is involved. As its name indicates, the main group activity is centred in the design and characterization of antennas and antenna materials and/or radiating systems. The RSLab main activity is the Earth observation by means of radar sensors and the image processing for different applications (cartography, environment protection...).

1.2 Motivation

One of the main missions of the antenna model is to generate all the possible antenna beams required to calibrate. Starting from a set of radiometric parameters previously defined, the antenna model has to generate the complex excitations from which the different satellite operating swaths are obtained. It is indispensable to verify the coincidence between the numerically generated patterns and the measurements which will be carried out once the satellite is in-flight. Another of its main functions is to optimise the beam excitation coefficients of the antenna array. These excitation parameters can be optimised to create an antenna pattern with high gain, or a desired pattern with suppressed side-lobes, for instance. The optimisation is also important to re-compute the excitations in case of failures or drifts in the transmission and reception modules (TRMs) with which the antennas forming the array are fed. It is also important to determine the errors in the patterns caused by phenomena such as thermal drifts or offsets in the subarrays positioning.

It is necessary to duly formalize the procedures involved in the design of an antenna model for the present and also future SAR missions. This should be done with the sufficient efficiency and reliability, really necessary in this kind of missions. To do so, practical and complete software is developed to be used from earth. It will be used to apply corrections once the satellite is in-orbit.

1.3 State of The Art

During the last decade, many SAR missions have been planed, designed and carried out by different countries. Their main objective is the Earth Observation (EO), for different purposes. Some recent SAR missions, sorted by order of satellite launch date are: ENVISAT (Environmental Satellite), ALOS (Advanced Land Observing Satellite), TerraSAR-X, RADARSAT-2 (RADAR Satellite), COSMO-SkyMed (Constellation of Small Satellites for Mediterranean Basin Observation) and, of course, the one to which the present work is applied, SEOSAR/PAZ (Spanish Earth Observation Synthetic Aperture Radar).

Regarding the antenna model, in the case of Envisat/ASAR instrument the SAR system uses in-orbit antenna pattern measurements for correction in calibration process. This is possible because ASAR acquires SAR images with only eight different antenna beams (a low number of beams). At ASAR an antenna model was implemented and the method used to optimise has been the Genetic Algorithm approach. Further the approach in which is based the Envisat antenna model was applied to TerraSAR-X. In the ALOS/PALSAR case, the number of beams is 23, still being a low number of beams. However, there is no public information found on the antenna modeller used. There is some information on a developed antenna model in the RADARSAT-2 and COSMO-SkyMed missions. These antenna models are also based in Genetic Algorithm in order to perform the antenna pattern optimisation.

Further information on the different mentioned missions and the antenna models developed for them can be found in Appendix A, devoted to describe in a more extensive way than in this introduction the state of the art in SAR missions.

1.4 Scope

The antenna model definition and the associated software development is one of the thousands of tasks to be carried out during the different steps on which consists a SAR mission. A SAR mission implies a huge amount of professionals in different disciplines from different institutions and companies or contractors working in parallel and even replicating work in order to ensure the validity of the data provided by the satellite, for the sake of reliability. However - and precisely because the wide range of issues that this kind of missions implies - , the present Master Thesis cannot describe deeply the whole process. The reader is encouraged to consult the references and bibliography in order to have a general perception of the hazards that implies a mission of such a magnitude.

This Master Thesis document includes the definition and implementation description of an antenna model. In particular, this antenna model is being used in the SEOSAR/PAZ mission, which is a Spanish Earth Observation mission (more information is provided in Appendix A). The antenna model, however, comprises many functions; i.e.: antenna pattern analysis, error computation, or antenna pattern optimisation, for instance. The present document focuses in the part specially developed in the Master Thesis work; i.e.: the antenna pattern optimisation.

1.5 Organization of the Dissertation

The present Master Thesis dissertation is divided in 5 chapters. In this chapter the thesis goal is introduced; i.e. the development of an optimizer software for the antenna model developed for SAR missions. In the second chapter, the specific antenna model designed for the Spanish mission is briefly introduced. This includes a description of its functions as well as an introduction to the formulation used to generate the theoretical antenna patterns needed.

The main work developed during the thesis is presented in Chapter 3. The optimiser is described in detail, both from the functional and the algorithmic point of view. In addition, this chapter shows some results obtained with the optimiser once integrated in the antenna model software and relative to the SEOSAR/PAZ mission in the pre-calibration stage. In Chapter 4 the folder tree and main routines of the code of the antenna modeller optimisation software are briefly described.

The concluding remarks and the work to be done in the future are issued in Chapter 5. Appendices with detailed information on some topics treated or mentioned during the thesis are found at the end of the document, right before the references and bibliography, which close it. Appendix A is devoted to introduce the state of the art in SAR missions worldwide, with special interest on the antenna models developed in each of them. Additional results complementary to the ones presented in Chapter 3 are located in Appendix B. In Appendix C one can find useful information needed in Chapter 3 when analysing the obtained results. Finally, Appendix D contains information on published work related with this Master Thesis. At the end of the document, a list of the acronyms used throughout the chapters is presented for reference.

2 ARCHITECTURAL MODELLING OF AN ANTENNA MODELLER

Before dealing with the antenna patterns optimisation, it is important to describe the overall antenna model where the optimizer is embedded and understand the mathematical basis which uses to analyse antenna patterns, since this mathematical basis for the antenna pattern generation is used in the optimizer as well. Therefore, the purpose of this chapter is to describe and explain the functionalities and the software mathematical basis implementing the antenna model developed in this Master Thesis. Its name is AMOR (Antenna MOdelleR) and is used to:

- *theoretically characterize a generic SAR antenna instrument from a set of ideal or measured subarray patterns*
- *synthesize the different beams supported by the satellite operational modes in order to fulfil the SAR mission expected performance*
- *evaluate the influence of mechanical and/or thermoelastic errors in the fabrication or set-up procedure of the antenna instrument, and on the instrument performance characteristics*

Another aspect that is duly explained is the algorithmic for computing the elevation and azimuth pattern planes for the satellite operational modes. Firstly, the array coordinate system and the mathematics required for computing the fields radiated by the satellite antenna are presented. Secondly, the directivity computation is also indicated.

Finally, there is also a section devoted to explain the mechanical and thermoelastic errors considered in the Antenna Modeller. The failures in the transmit/receive modules to be accounted for are also explained.

The procedure to optimize the excitation coefficients feeding the TRMs will be described in detail in the next chapter.

2.1 The Antenna Modeller

The antenna model is the antenna mathematical description. It should allow the antenna radiation patterns reconstruction from a set of on-ground characterized parameters and excitation coefficients. Then, the antenna model will help to reduce the number of beams to be measured and, once in-flight, to update them as a function of measured information.

The on-ground parameters used to design and improve the model are the measured data of a single subarray in free space. The present version of the software (AMOR 4.0) is able to work with the measured patterns of 32 embedded subarrays of a panel. However, measured data was not available at the moment the present MT document was finished to be written.

In this section the functionalities of AMOR will be enumerated, and the antenna modeller Graphical User Interface (GUI) of the optimiser is presented. For the instrument description, please refer to Annex A.

2.1.1 Brief Description of the Antenna Modeller Functionalities

In order to fulfil the radar instrument best performance and to correct the SAR radiometric images, different functionalities are provided by the Antenna MOdelleR (AMOR). These functionalities are listed in Table 2.1.

The Antenna MOdeller
<ul style="list-style-type: none"> Allows the antenna radiation patterns reconstruction by means of superposing the measured (or simulated) embedded subarray patterns weighted by beam excitation coefficients. To this end, it is necessary to consider the antenna geometry and the elements location. The current version of the Antenna Modeller, AMOR 4.0, works at panel level. Hence, it uses the measured patterns of 32 embedded SAs. In this way, the antenna modeller will provide an accurate estimate of the actual antenna pattern for each of the multiple beams that can be generated by the different instrument operating modes. Computes the beam excitation coefficients in order to optimize the instrument SAR performance. This optimization can currently be made in terms of range ambiguities, antenna gain, antenna beamwidth, and null deep at Nadir. Nonetheless, other antenna and radiometric parameters could further be defined to get the excitation coefficients. Allows excitation coefficients re-computation in case of TRM failure or degradation. Makes possible the analysis of the effects caused by subarray misalignment and planarity errors, favouring in this way to better fit the patterns generated to the actual ones. Other effects like the influence of thermo-elastic deformations are assessed.

Table 2.1: AMOR functionalities.

AMOR is a flexible antenna model since all of the previous analysis and computations can be done:

- at any frequency
- taking into account any number of subarrays and any disposition of these subarrays within the antenna array (whit the only restriction that the antenna is bidimensional and planar)
- considering any measured or simulated subarray patterns (the electric field radiated by each SA conforming the antenna is read by the software)

The functionalities of AMOR are distributed through several GUI windows (that will be further introduced in the next section). Figure 2.1 summarizes these previous functionalities in the corresponding window where they can be found.

2.1.2 The Antenna Modeller GUI

The AMOR GUI is intended to design the antenna patterns for all the foreseen SAR antenna operational modes. This is done with the objective of achieving maximum performance sensing data in an operational basis. For this reason, the GUI makes a distinction between the Synthesis and Analysis procedures, subsequent to an Array Description definition procedure. In addition, the influence of errors (mechanical, electronic, and/or thermoelastic) in the antenna performance can also be considered (some of them mot in AMOR 4.0 but in future versions) through inputs in the Errors window. An Error Analysis tool will be included in the code in the Errors window.

The toolbar in the Antenna Modeller main window shown in Figure 2.2 is the link to the windows performing the previously mentioned functionalities (Figure 2.1). The antenna modeller is being implemented using Matlab® and is designed to run on personal computers.

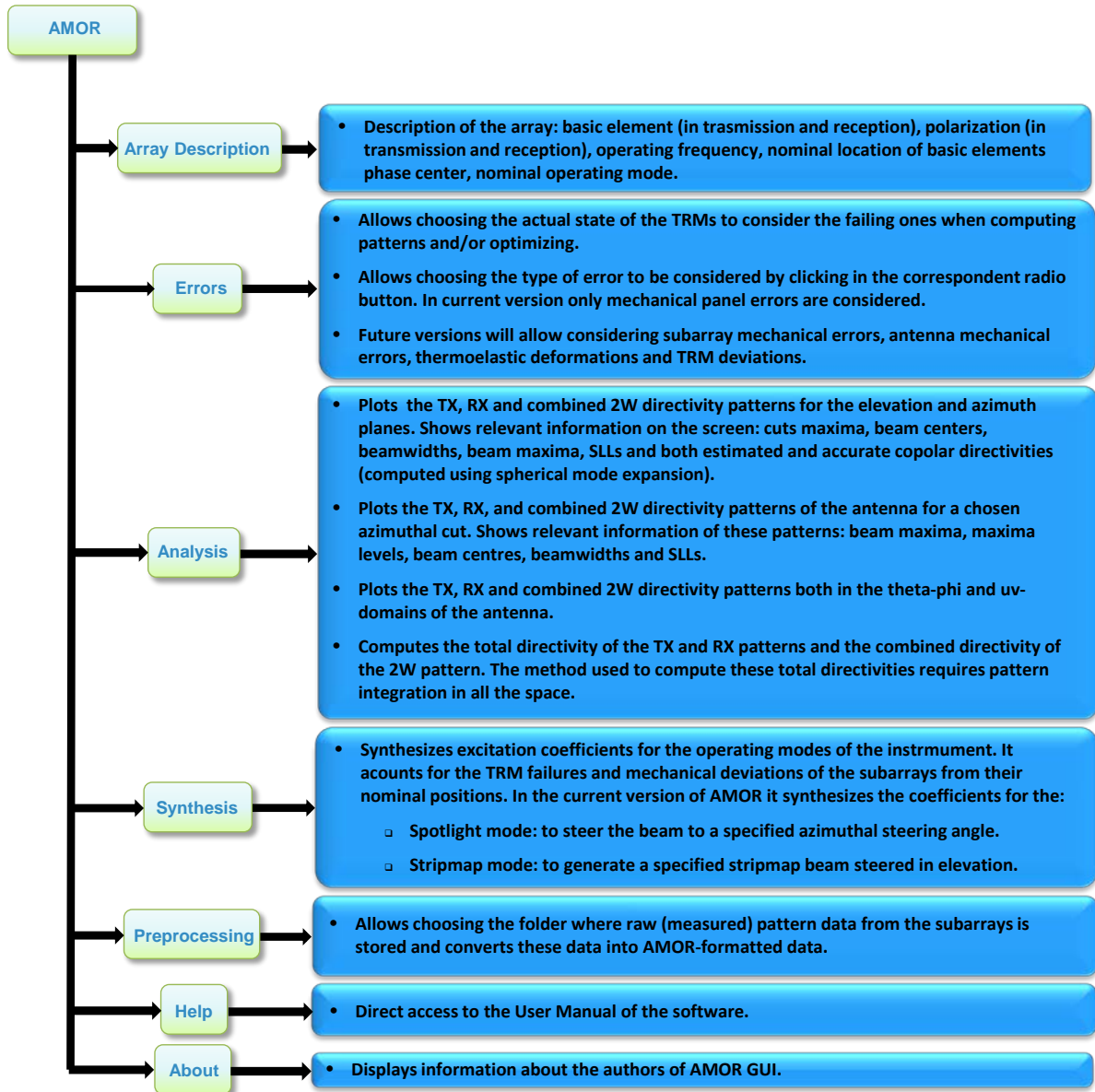


Figure 2.1: Functionalities of AMOR.

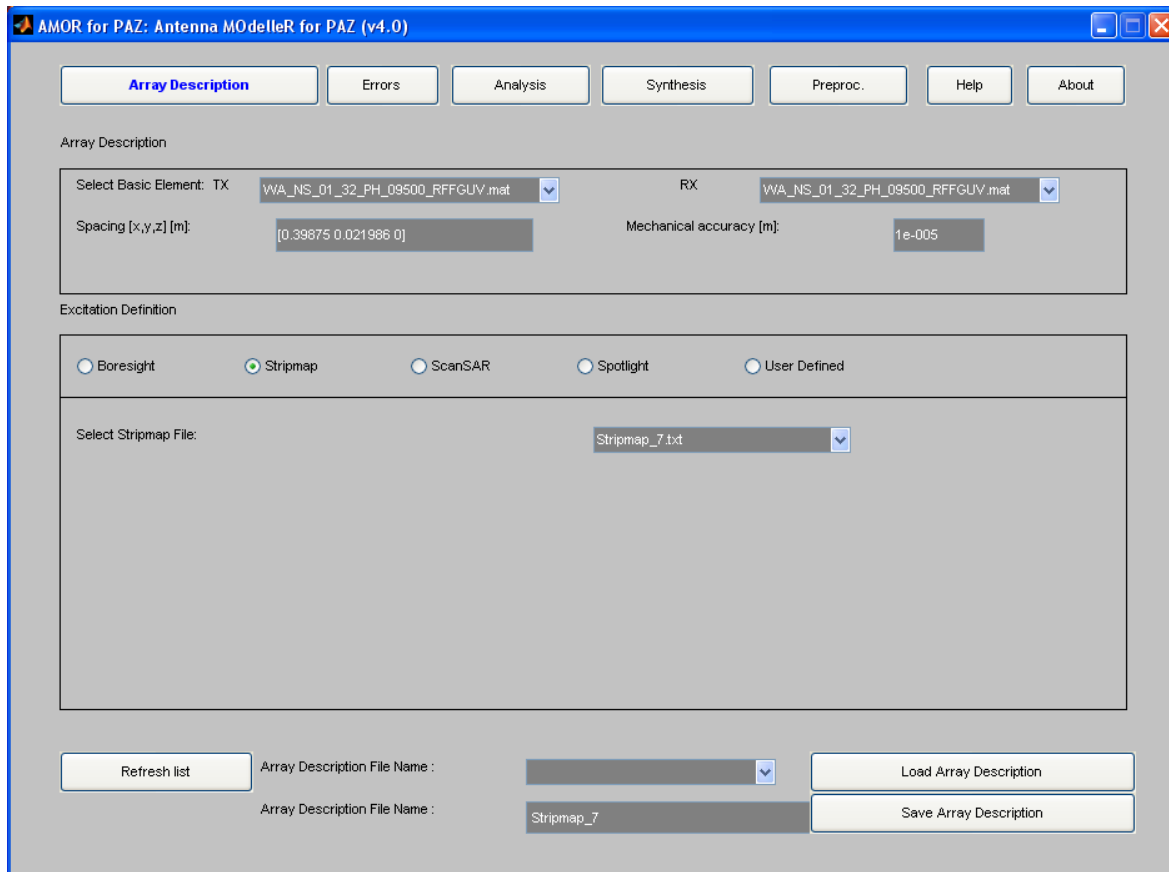


Figure 2.2: Antenna Modeller main window (Array Description Window). In the upper side of the window there are the buttons that make visible the windows performing the different functionalities of the tool. Some of them are the Error analysis tool, the array Analysis tool and the Synthesis of excitation coefficients tool.

AMOR allows the computation of the copolar and crosspolar transmitting (TX) and receiving (RX) antenna patterns of the SAR instrument together with the copolar and crosspolar two-way (2W) antenna patterns. The subarrays patterns can be different in transmitting or receiving modes due to the chosen polarization, being either vertical or horizontal depending on the instrument operating mode. The resulting patterns can be visualized in a standard Cartesian presentation for the elevation and azimuth planes and the pattern main parameters automatically determined for a quick analysis of the results. Also, three dimensional power patterns plots can be generated to assess the absence of notorious secondary lobes out of the main elevation (EL) and azimuth (AZ) plane cuts. The accurate antenna directivity computation for the TX and RX pattern is an additional functionality included in AMOR.

To compute these patterns the software current version (AMOR 4.0) uses several measured (or simulated, if desired) SA patterns simultaneously in order to account for the slight differences in the SAs radiation patterns when embedded in different positions in the whole array. More precisely, the software uses the measured radiation pattern of 32 embedded SAs (that is, a whole panel). In the current version of AMOR the SAs patterns are stored as far-field samples in the uv-domain.

As previously mentioned, and by means of its Analysis Window (Figure 2.3), the software is able to analyze the different instrument operational modes (Stripmap, ScanSAR, Spotlight), and also a User Defined set of coefficients for designing and/or testing purposes. The coefficients that generate a given antenna configuration are the combination of TRM TX/RX phase and RX gain values stored in look up tables like in the satellite. In Figure 2.5 a snapshot of the Analysis tool and some of its results are shown when characterizing a Stripmap beam, while Figure 2.6 highlights the resulting 3D pattern. The 3D power patterns are useful to assess that no grating lobes are present in the EL and AZ cuts.

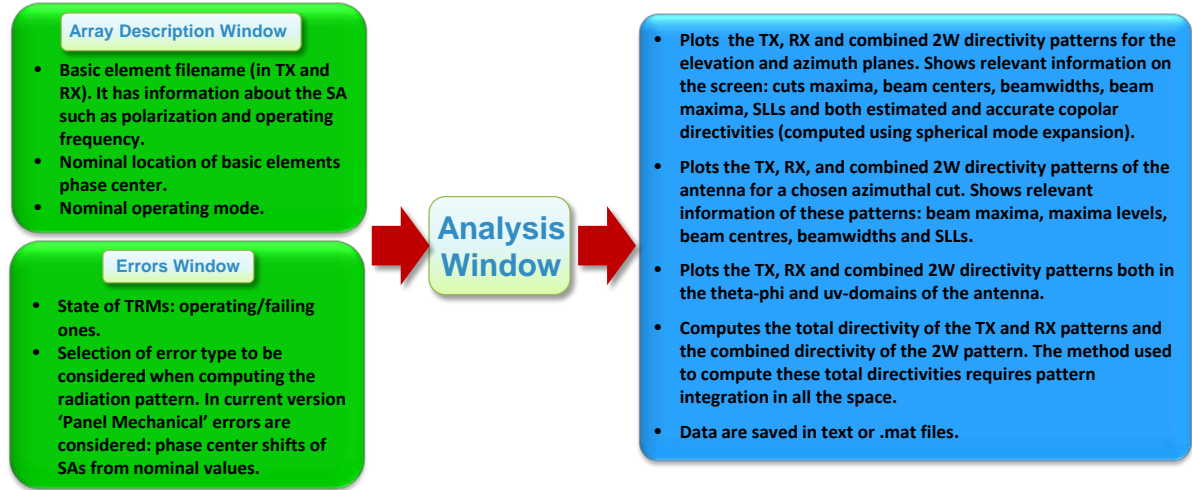


Figure 2.3: Summary of inputs and functionalities of the Analysis Window.

Mechanical errors due to imperfections in the antenna manufacturing and its deformation in-flight due to the variation of thermal conditions at panel and antenna level (modelled as shifts along x, y , and/or z -axis with respect to their nominal positions and a rotation along each of their axis –yaw, roll, pitch) are going to be considered in future versions of AMOR when computing the SAR instrument radiation pattern. The influence of failing TRMs or mechanical deviations of SA phase centres from their nominal values is already implemented in the current version of AMOR.

An important objective of the code is the capability of synthesizing (or re-synthesizing) the excitation coefficients to be applied to the TRMs through its Synthesis tool (Figure 2.4). This synthesis procedure has to derive an optimized 2W antenna pattern matching a given template. The template is related with several instrument gain and main lobe beamwidth, side lobe levels, elevation and azimuth beam pointing directions, gain variations within the swath, range ambiguity level, null positions in certain directions and higher gain towards higher elevation angles within the main lobe (R^3 compensations). The possibility to include deviations in the TRM settings or failing modules either in TX and RX or both is also considered when computing the coefficients. The optimisation is applied to radar parameters, each one weighted with an assigned coefficient. The weighting is used in order to translate to the template the relevance of each parameter. These radar parameters are directly related with antenna parameters.

In addition the Synthesis tool is able to compute the excitation coefficients to steer (spotlight) beams toward a given spatial direction in the AZ plane.

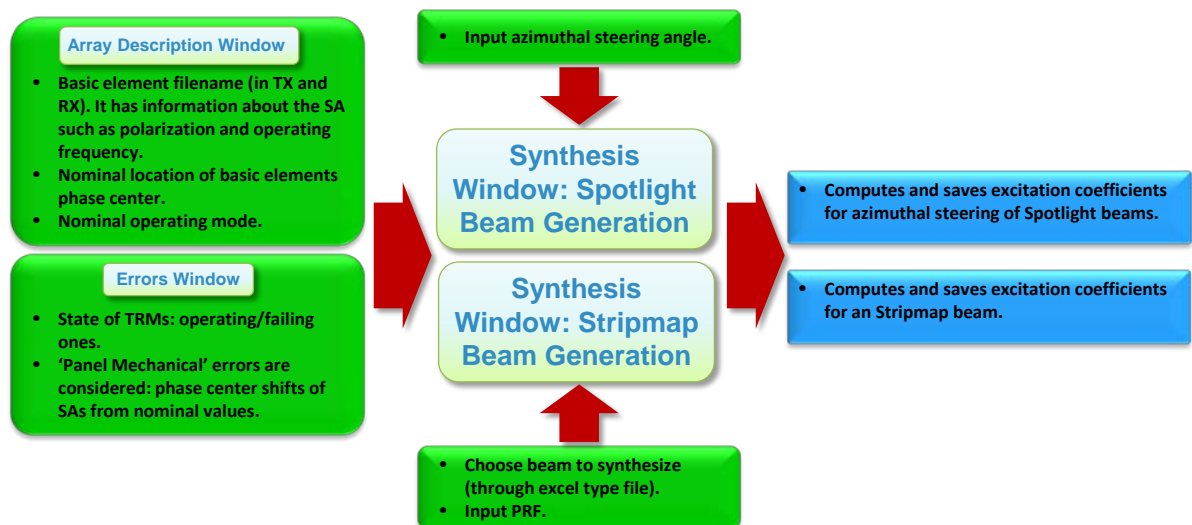


Figure 2.4: Summary of inputs and functionalities of the Synthesis Window.

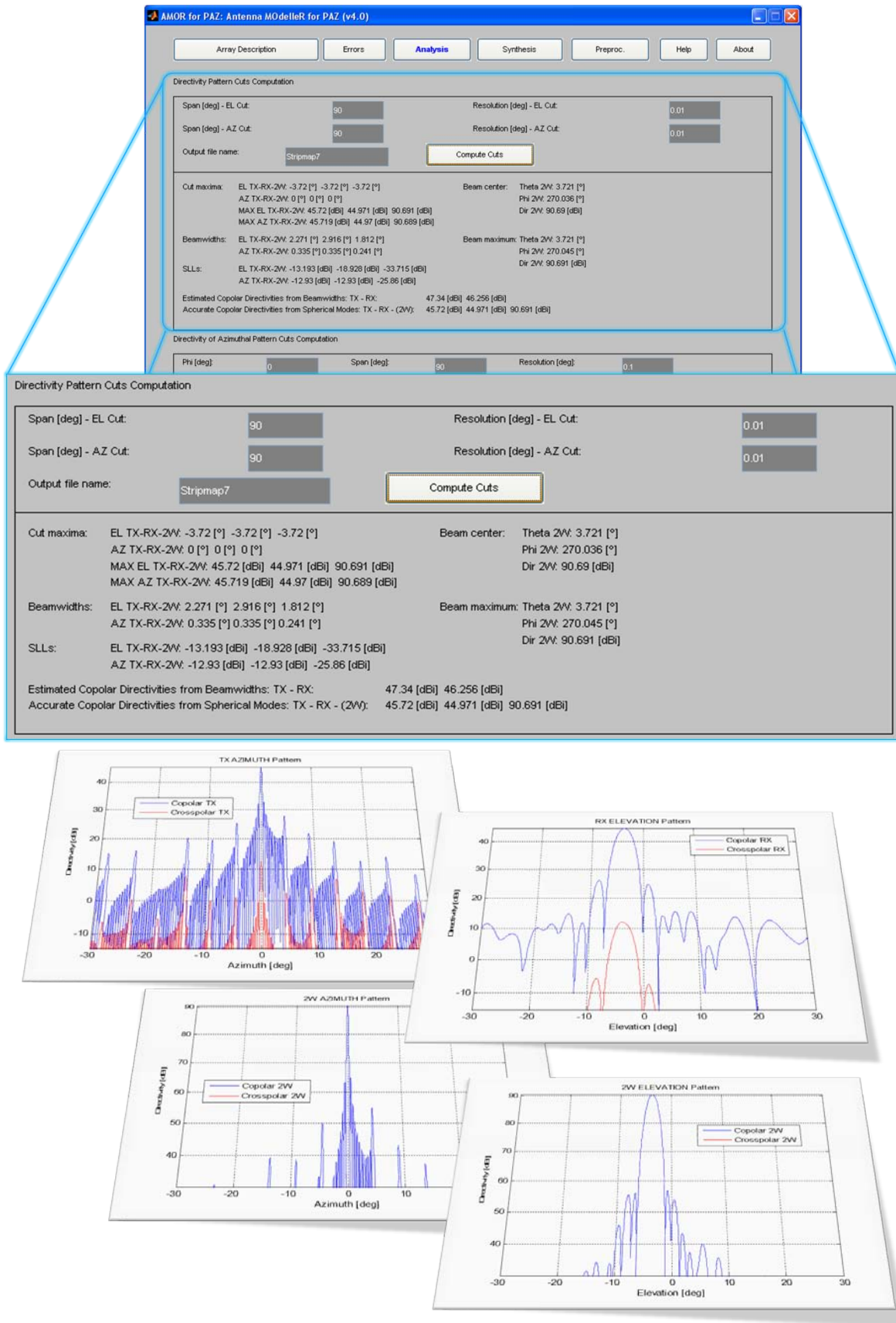


Figure 2.5: Analysis window of AMOR. The main parameters of interest for the resulting patterns are shown in the Analysis window. Some of the resulting pattern cuts (for the TX azimuth plane, RX elevation plane and 2W elevation and azimuth plane) are shown on the bottom.

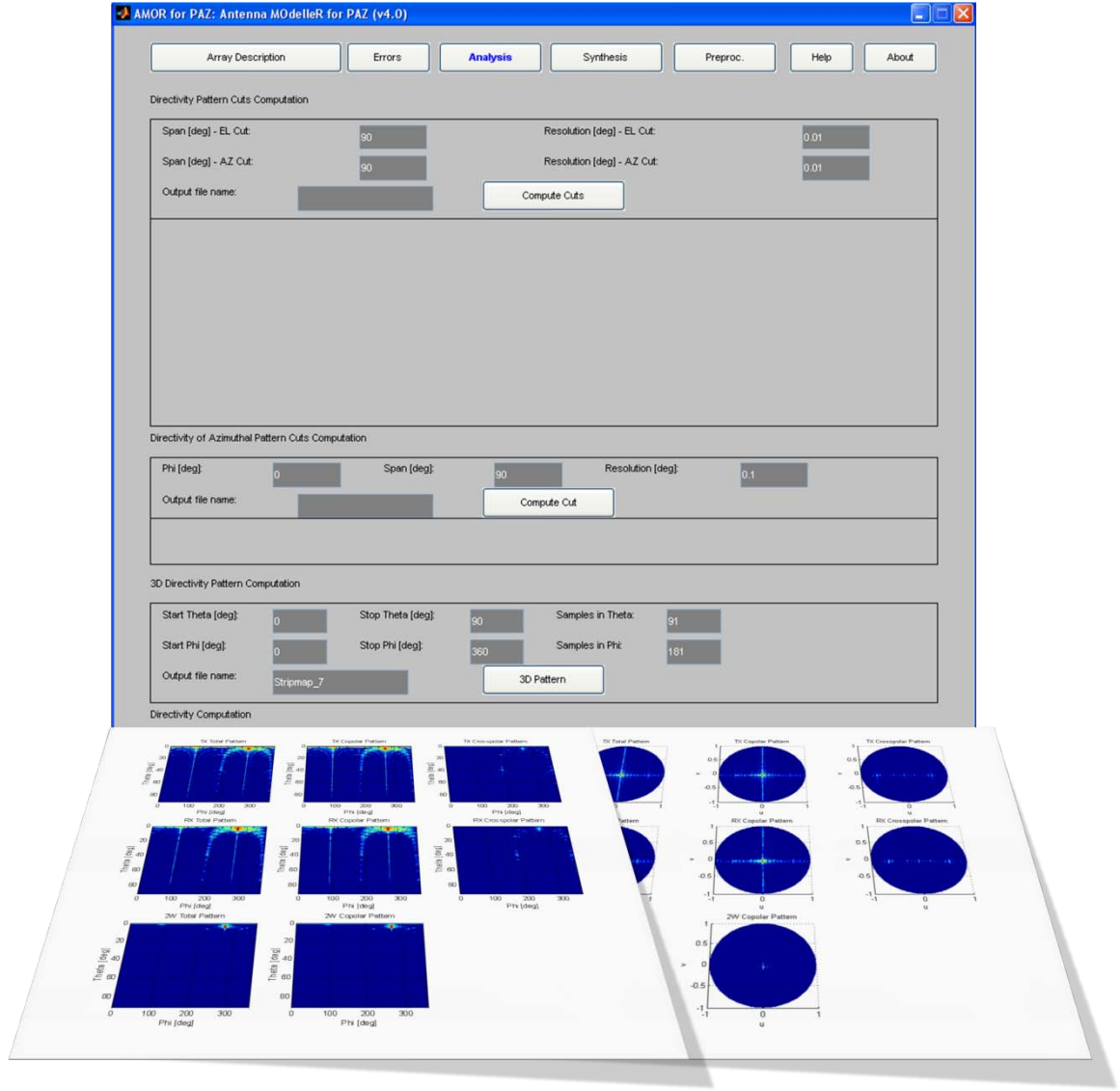


Figure 2.6: Analysis window of AMOR. Two ways of showing the three dimensional TX, RX and 2W copolar and crosspolar power patterns.

2.2 Computing Radiation Patterns with AMOR

The mathematics of pattern and directivity computations is described in this section. How the elevation and azimuth planes are chosen will also be described.

2.2.1 Patterns Computation from SA patterns

The antenna modeller calculates radiation patterns by superposition of the on-ground measured patterns of subarrays (embedded) weighted by beam excitation coefficients and taking into consideration the antenna geometrical dimensions (in fact the subarrays accurate positions with respect to the antenna coordinate system). For the mathematical modelling of the problem a coordinate system local to the satellite antenna array (antenna reference system) has to be defined. The antenna reference system is also used to define the SAR subassemblies locations and orientations. The antenna coordinate axes side view is depicted in Figure 2.7.

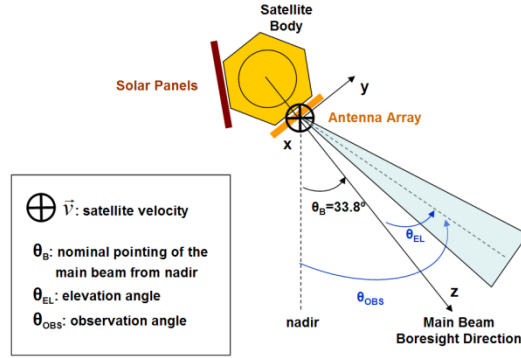


Figure 2.7: Antenna Reference System. In SAR terminology, θ_B is named the antenna tilt angle, and the observation angle θ_{OBS} name is look angle.

The antenna reference system origin is at the geometric centre of the antenna radiating plane. The x-axis direction is parallel to the antenna largest dimension and is pointing towards the satellite flight direction. The y-axis direction is in the antenna plane and is parallel to the shortest antenna side in the opposite direction to the nadir. Finally, the z-axis direction is pointing along the antenna mechanical boresight, which is normal to the antenna plane. The main beam nominal pointing is at boresight when the antenna beam points towards the z-axis. This direction is at $\theta_B = 33.8^\circ$ from nadir. The yz-plane defines the elevation plane, and the xz-plane defines the azimuth plane. The antenna beam rotation about the x-axis is defined as elevation, whilst the antenna beam rotation about the y-axis is defined as azimuth rotation. The PAZ antenna should have the possibility to point its main beam towards a given direction in the elevation plane. This direction is called observation angle θ_{OBS} , and is measured with respect to the nadir. This observation angle is named elevation angle θ_{EL} when measured with respect to the antenna coordinate system z-axis.

In Figure 2.8 (upper) another view of the coordinate system of the PAZ satellite antenna is shown. The rectangle in the figure represents the antenna aperture. The x-axis, as above mentioned, is the satellite flight direction. In Figure 2.8 (lower) the standard definitions of a spherical coordinate system are also shown.

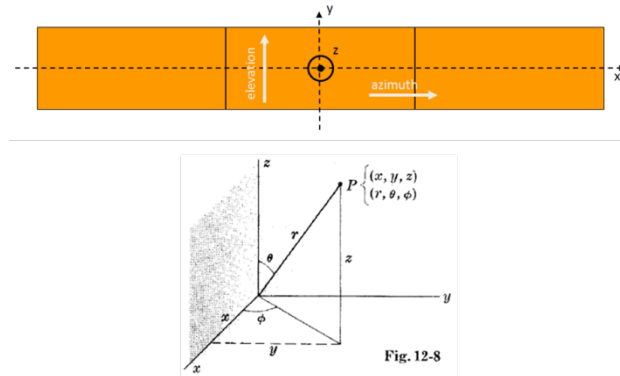


Figure 2.8: PAZ satellite array coordinate system (upper). Spherical coordinate system (lower) [2.1].

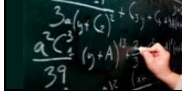
As seen in Figure 2.8 the coordinate system used for the antenna analysis is centred in the array aperture. The antenna angles θ and ϕ are related with these coordinates by Equation 2.1:

	$\begin{pmatrix} x \\ y \\ z \end{pmatrix} = r \cdot \begin{pmatrix} \sin\theta\cos\phi \\ \sin\theta\sin\phi \\ \cos\theta \end{pmatrix} \text{ with } \begin{cases} 0 \leq \theta \leq \pi \\ 0 \leq \phi \leq 2\pi \\ 0 \leq r \leq \infty \end{cases}$	Equation 2.1
--	--	--------------

However is very common to use the sin θ -space coordinates (u, v) defined as Equation 2.2:

	$\begin{pmatrix} u \\ v \end{pmatrix} = \begin{pmatrix} \sin\theta\cos\phi \\ \sin\theta\sin\phi \end{pmatrix} \text{ being } \begin{cases} -1 \leq u \leq 1 \\ -1 \leq v \leq 1 \end{cases} \text{ and } u^2 + v^2 \leq 1$	Equation 2.2
--	---	--------------

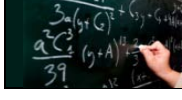
The pattern $\vec{F}_{total}(u, v)$ of the PAZ satellite is computed as a superposition of the fields radiated by the $N \times M$ (elevation x azimuth) subarray patterns $\vec{F}_{mn}^{SA}(u, v)$ weighted by a_{mn} the complex excitation coefficients given by the TRM setting. Subindex m and n specify a subarray by column and row, respectively, in the antenna array. The subarray patterns are considered to be embedded in the total antenna so all relevant effects are considered in the simple formula of Equation 2.3.



$$\vec{F}_{total}(u, v) = \sum_{n=1}^N \sum_{m=1}^M a_{mn} \vec{F}_{mn}^{SA}(u, v)$$

Equation 2.3

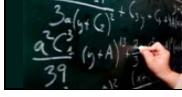
In case that the measured subarray was not embedded in the total antenna, Equation 2.4 takes into account the phase shift of the subarray pattern due to the position.



$$\vec{F}_{total}(u, v) = \sum_{n=1}^N \sum_{m=1}^M a_{mn} e^{j\vec{k}\vec{r}_{mn}} \vec{F}_0^{SA}(u, v)$$

Equation 2.4

In Equation 2.4 vector \vec{k} is the wave vector that can be defined as a function of the spatial angles or in the uv-domain (Equation 2.5). The position of each subarray measured in the antenna coordinate system is given by the vector \vec{r}_{mn} .



$$\vec{k} = \frac{2\pi}{\lambda} (\sin\theta\cos\phi, \sin\theta\sin\phi, \cos\theta) = \frac{2\pi}{\lambda} (u, v, \sqrt{1-u^2-v^2})$$

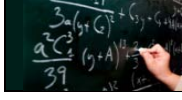
Equation 2.5

2.2.2 Computing Directivities with AMOR

To compute the partial directivity of a pattern (copolar component), four procedures have been implemented in the Antenna Modeller. Two of them are not time consuming but less accurate than the third and fourth methods, both based on the 3D pattern integration of the array under test.

2.2.2.1 Directivity Estimate for a Directional Pattern from Beamwidths

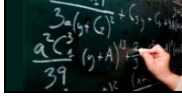
To avoid the time consuming computation of the maximum directivity an estimate of its value can be found using Equation 2.6, valid for directive antennas:



$$D_{cop,max} = \frac{4\pi}{\Delta\theta_{AZ} \Delta\theta_{EL}}$$

Equation 2.6

being $\Delta\theta_{AZ}$ the -3 dB beamwidth in the azimuth plane and $\Delta\theta_{EL}$ the -3 dB beamwidth in the copolar pattern elevation plane. Both angles are given in radians. If beamwidths are known in degrees, Equation 2.7 can be used:



$$D_{cop,max} = \frac{41253}{\Delta\theta_{AZ} \Delta\theta_{EL}}$$

Equation 2.7

For planar arrays [2.2] indicates that Equation 2.8 is a better approximation.



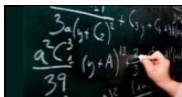
$$D_{cop,max} = \frac{32400}{\Delta\theta_{AZ} \Delta\theta_{EL}}$$

Equation 2.8

The difference between Equation 2.7 and Equation 2.8 is 1.05 dB. In the present version of AMOR the equation implemented is Equation 2.6.

2.2.2.2 Directivity Estimate from Subarray Radiated Power Integration

The TX and RX copolar patterns directivity is computed by calculating the antenna array total radiated power. This radiated power is obtained by summing up the radiated power of each subarray [2.3], as done in Equation 2.9.



$$D_{cop} = 4\pi \frac{|E_{32x12}^{cop}(\theta, \phi)|^2}{\int_0^{2\pi} \int_0^\pi [|E_{SA}^{cop}(\theta, \phi)|^2 + |E_{SA}^{cross}(\theta, \phi)|^2] \sin\theta d\theta d\phi \sum_{n=1}^{32} \sum_{m=1}^{12} |a_{mn}|^2}$$


Equation 2.9

In Equation 2.9, a_{mn} are the excitation coefficients that feed the TRMs; $|E_{32x12}^{cop}(\theta, \phi)|$ is the copolar field magnitude radiated by the whole antenna $|E_{SA}^{cop}(\theta, \phi)|$ and $|E_{SA}^{cross}(\theta, \phi)|$ are, respectively, the copolar and crosspolar field magnitudes of the subarray; n is the subarray number inside a panel ($1 \leq n \leq 32$); and m is the panel number ($1 \leq m \leq 12$).

The partial directivity accuracy computed with Equation 2.9 depends on the accuracy on the subarray radiated power computation, and this depends on the sampling interval given in the subarray measurement. Unfortunately, this formula is not accurate when SAs are coupled, being the case in the modeller.

2.2.2.3 Directivity Computation by Integrating the Total Array Pattern

The directivity for the TX and RX copolar patterns can be accurately computed by integrating the total field radiated by the subarray using Equation 2.10:



$$D_{cop,max} = 4\pi \frac{|E_{32 \times 12}^{cop}(\theta, \phi)|^2}{\int_0^{2\pi} \int_0^\pi [|E_{32 \times 12}^{cop}(\theta, \phi)|^2 + |E_{32 \times 12}^{cross}(\theta, \phi)|^2] \sin\theta d\theta d\phi}$$

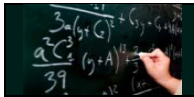
Equation 2.10

In Equation 2.10, $|E_{32 \times 12}^{cop}(\theta, \phi)|$ and $|E_{32 \times 12}^{cross}(\theta, \phi)|$ are the copolar and crosspolar field magnitudes radiated by the whole antenna.

As aforementioned, this computation is time consuming because it requires a fine grid step in the spatial directions domain to integrate the array total pattern.

2.2.2.4 Directivity Computation Using the Spherical Mode Expansion

This computation directivity approach is based in the formulation proposed by Hansen in [2.4]. According to this, the electric field in a source-free region of space can be written as a weighted sum of two spherical wave functions, $\vec{F}_{smn}^{(c)}$, which are closed and known expressions (s indicates which of the two spherical wave functions is used $\vec{F}_{1mn}^{(c)}$ or $\vec{F}_{2mn}^{(c)}$). Hence the electric field can be written as in Equation 2.11:




$$\vec{E}(r, \theta, \phi) = k\sqrt{\eta} \sum_{c=3}^4 \sum_{s=1}^2 \sum_{n=1}^{\infty} \sum_{m=-n}^n Q_{csmn}^{(c)} \vec{F}_{csmn}^{(c)}(r, \theta, \phi)$$

Equation 2.11

The variable c indicates whether the travelling modes are standing waves ($c=1$ and $c=2$), outward travelling waves ($c=3$) or inward travelling waves ($c=4$). The m and n variables indicate the number of modes considered in the electric field computation from the spherical wave functions.

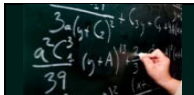
The expression for the power radiated by outward travelling modes is then as simple as:



$$P_{rad} = \frac{1}{2} \sum_{s=1}^2 \sum_{n=1}^{\infty} \sum_{m=-n}^n |Q_{smn}^{(3)}|^2$$

Equation 2.12

In practice the summations will always be truncated to a maximum value of n and m ; N and M respectively. The way to choose these values can be consulted in [2.4], but the basic idea is that for a given N and M , using higher n and m values than N and M , respectively, has no significant effect in the electric field computation because with N and M it is sufficiently well approximated. In AMOR M is considered equal to N , and N is found from the diameter D of the minimum sphere enclosing the whole antenna array plus an integer found empirically:

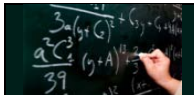


$$N = \left\lceil k \frac{D}{2} \right\rceil + 100$$

Equation 2.13

Where the symbol $\lceil \bullet \rceil$ in Equation 2.13 yields the ceil integer of the mathematical operation between brackets.

The Q coefficients are obtained from Equation 2.11, following the procedure described in [2.4] and implemented in *Sub_SN2FFT_ModesComputation.m* (described in Chapter 4), since the known information is the electric field and the spherical wave functions. From the former expression the directivity can then be computed through the known expression in Equation 2.14.



$$D = \frac{4\pi}{r^2} \frac{|\vec{E}|^2}{2\eta P_{rad}}$$

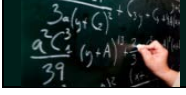
Equation 2.14

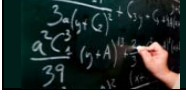
This method is slower but more accurate than the one explained in Section 2.2.2.2.

2.2.3 Elevation (EL) and Azimuth (AZ) Planes

Elevation (EL) and azimuth (AZ) radiation pattern planes of the antenna beams are required to fully characterize the SAR instrument radiometric performance.

The definitions of the azimuth and elevation planes are done according to document [2.5]. For a given beam scanning direction, defined by the pair (u_0, v_0) in the $\sin\theta$ -space, the azimuth and elevation pattern cuts are:

	$\vec{F}_{total, AZ}(u, v_0) = \sum_{n=1}^N \sum_{m=1}^M a_{mn} e^{j\vec{k} _{v=v_0} \cdot \vec{r}_{mn}} \vec{F}_0^{SA}(u, v_0)$	Equation 2.15
---	--	----------------------

	$\vec{F}_{total, EL}(u_0, v) = \sum_{n=1}^N \sum_{m=1}^M a_{mn} e^{j\vec{k} _{u=u_0} \cdot \vec{r}_{mn}} \vec{F}_0^{SA}(u_0, v)$	Equation 2.16
---	--	----------------------

An example of these cuts for a hypothetical beam pointing towards the direction $(\theta_0, \phi_0) = (21^\circ, 1^\circ)$, that is, $(u_0, v_0) = (0.358, 0.006)$ is shown in Figure 2.9.

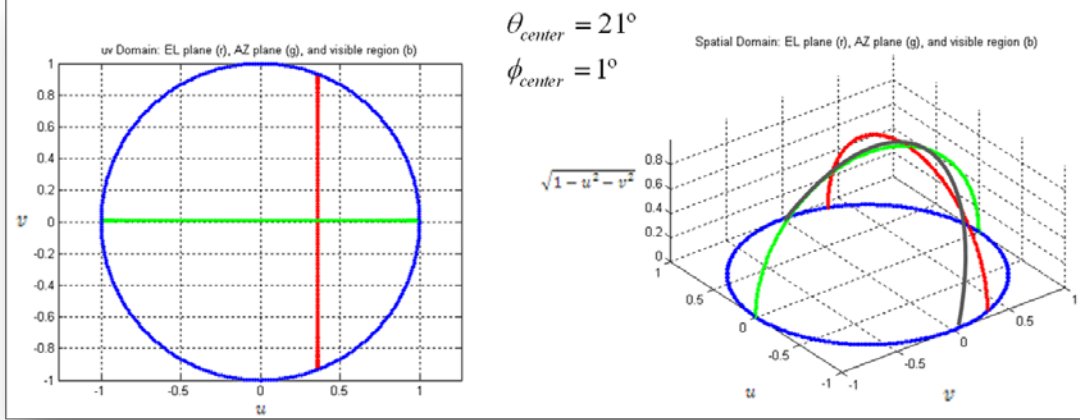


Figure 2.9: Example of azimuth (green) and elevation (red) pattern cuts for beam scanning at $(\theta_0, \phi_0) = (21^\circ, 1^\circ)$: (left) pattern cuts in the uv -domain (or $\sin \theta$ -space domain) and (right) projection of the direction samples in a unity radius sphere.

The algorithm implemented in AMOR for computing and plotting the EL and AZ radiation patterns is in Figure 2.10. The algorithm required for finding the beam centre of a two way (2W) power pattern is in Figure 2.11.

In these figures, θ_{max}^{EL} and $\Delta\theta^{EL}$ define the angular range in which the pattern has to be computed in the elevation plane being, respectively, the angular span with respect to the boresight direction and the spacing between the angular samples. Meanwhile θ_{max}^{AZ} and $\Delta\theta^{AZ}$ are used to define the angular range in the azimuth plane. Accordingly to the algorithm described in Figure 2.10 the beam centre of the 2W pattern in the uv -domain is found first, that is, it is found the direction where the beam centre is pointing. Once this direction is found, the spatial directions corresponding to the EL and AZ planes are found in the $\theta\phi$ -domain and the power patterns for the TX, RX and 2W computed. The range centre where the beam is 3 dB below the beam maximum is considered to be the direction where the beam is pointing, as shown in Figure 2.11.

A detailed description on how the beam centre of a 2W pattern is computed is shown in Figure 12. Basically it is an iterative procedure that makes a zoom of the 2W pattern in the uv -domain starting from a range of values corresponding to the region where maxima are expected. In each iteration, the uv -region is meshed and the 2W pattern computed for this region. The -3dB contour below the beam maximum is found and the beam centre calculated. The angular shift (for θ and ϕ) between the current spatial direction of the beam centre and the spatial direction computed for the previous iteration is used to stop the iterative procedure of the zoom. Specifically, the zooming is stopped when the beam centre variation between iterations is below the angular resolution of the pattern to be plotted.

In Figure 2.12, the angles $\theta_{beam_center}^k$ and $\theta_{beam_maximum}^k$ refer to beam centre and beam maximum pointing directions at iteration k in the plane under consideration, when computed in the whole space. Angles $\theta_{beam_center}^k$ and $\phi_{beam_center}^k$ refer to the beam centre direction when computed in the whole space, at iteration k . The associated values in the uv -domain are $u_{beam_center}^k$ and $v_{beam_center}^k$.



Figure 2.10: Algorithm for azimuth and elevation pattern cuts computation; Tx: transmission, Rx: reception, 2W: two-way, EL: elevation, AZ: azimuth, 3D: all the spatial directions.

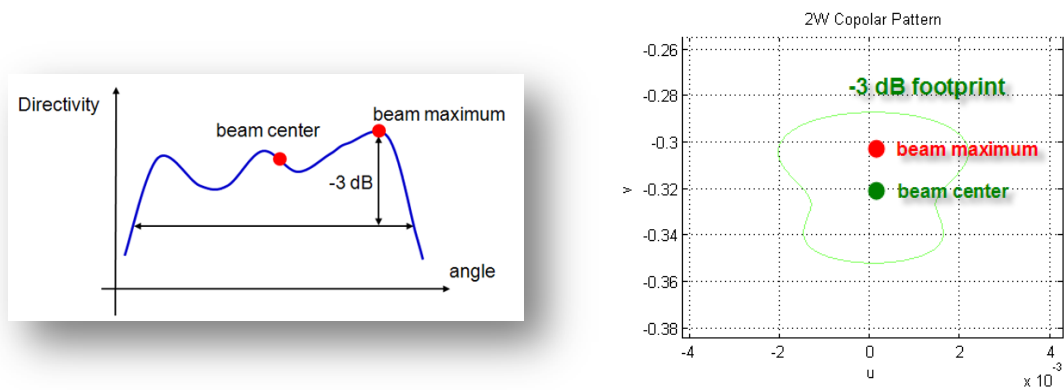


Figure 2.11: Beam maximum and beam centre in an angular domain, θ or ϕ (left) and in the uv-domain (right).

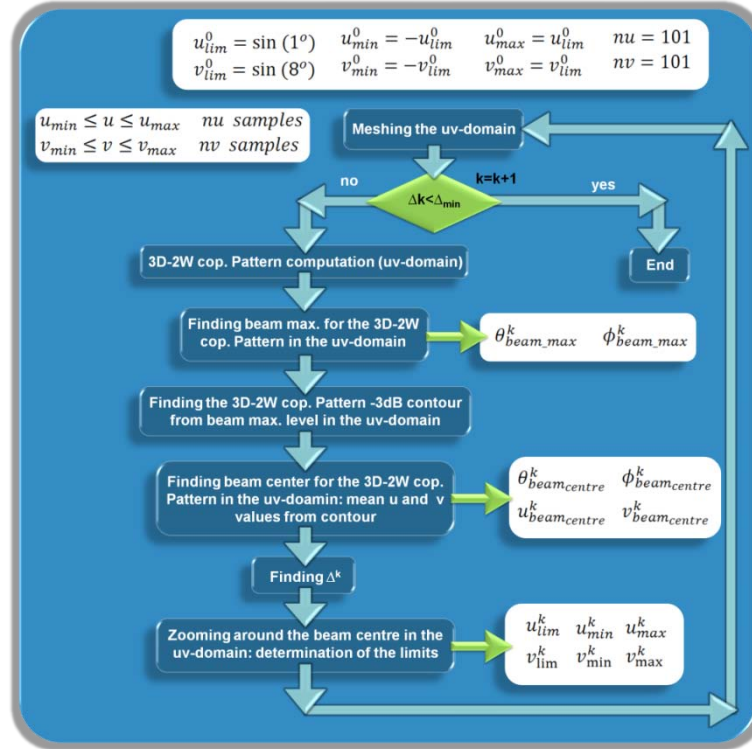


Figure 2.12: Algorithm for finding the beam centre (and also beam maximum) of a two way pattern; k : iteration, Δ : movement of beam centre between iterations. The angular values used in the first iteration ($u_{lim}^0 = \sin(1^\circ)$ and $v_{lim}^0 = \sin(8^\circ)$) are used because there is an a priori knowledge of the beam widths which can be obtained in a practical situation.

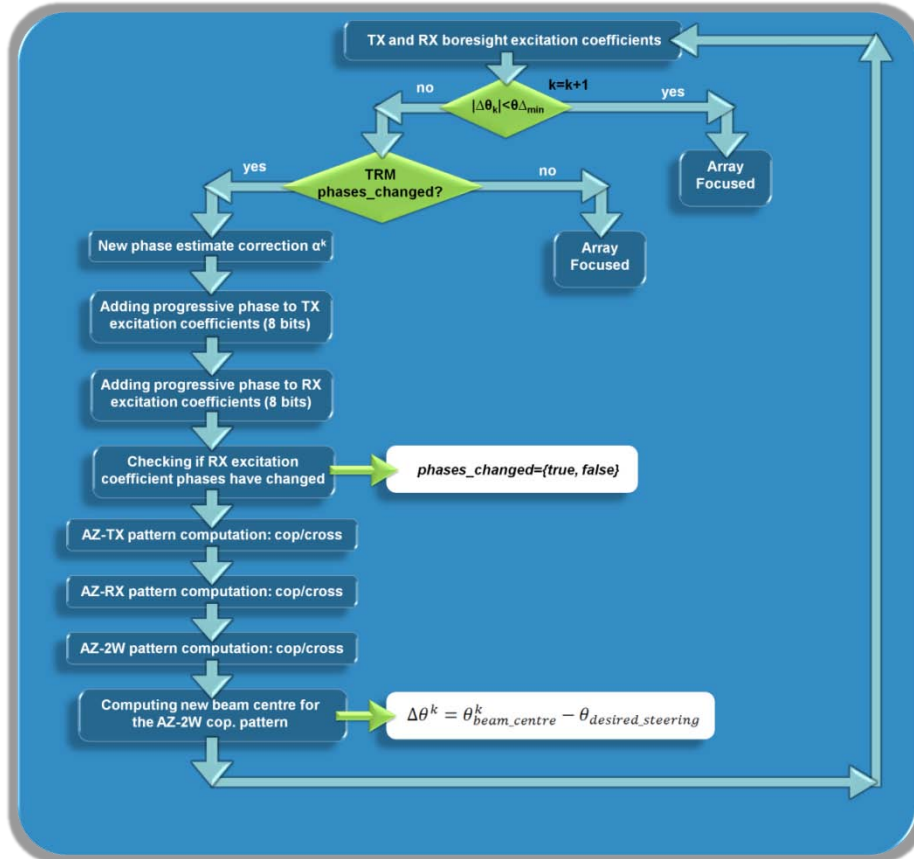



Figure 2.13: Algorithm for beam steering spotlight modes.

2.2.4 Computing the AZ Beam Table for a Spotlight Beam

The beam tables used for steering spotlight beams in the AZ plane can also be computed using AMOR. These tables are obtained by steering a boresight beam. The algorithmic for getting the beam table is shown in Figure 2.13.

The algorithm is iterative and corrects inaccuracies in the solution of the equation that models the steering of a uniform isotropic array of isotropic radiators. The equation for the initial estimate progressive phase α^0 for the theoretical array of isotropic elements is given by:




$$\alpha^0 = -\frac{360}{\lambda} d_x \sin(\theta_{\text{desired steering}})$$

Equation 2.17

where λ is the operating frequency wavelength, d_x is the separation between subarrays in the azimuth direction, and $\theta_{\text{desired steering}}$ is the angle in the AZ-plane where the beam centre should be pointing after the steering.


The inaccuracies between the desired steering angle and the resulting steered angle are compensated using Equation 2.18:



$$\alpha^k = \frac{\alpha^{k-1} - \alpha^{k-2}}{\theta_{\text{beam centre}}^{k-1} - \theta_{\text{beam centre}}^{k-2}} (\theta_{\text{beam centre}}^{k-1} - \theta_{\text{desired steering}})$$

Equation 2.18

The specific phase to be applied to each TRM follows the Equation 2.19, taking into consideration the progressive phase solution of the iterative procedure and the panel number m :



$$\alpha_{mn} = \frac{(2m-1) - M}{2} \alpha_{\text{solution}}$$

Equation 2.19

Phases are discretized to 8 bits prior to their storage in the AZ beam table. However when computing the patterns after applying the AZ beam table to a given beam the phase shifters resolution is reduced by taking the first 6 bits of the solution (starting from the MSB).

2.3 Computing Errors with AMOR

The influence of two error types has to be considered when simulating the SAR instrument performance with the antenna modeller: mechanical errors due to imperfections in the antenna manufacturing and its deformation in-flight due to the thermoelastic conditions variation; and errors due to TRM failures or deviations from their nominal values.

2.3.1 Mechanical and Thermoelastic Errors

Mechanical deformations can be simulated at different levels. These levels are presented and explained in Table 2.4:

Subarray level
This deformation is introduced by thermal variations and affects only the subarray largest dimension. It can only be simulated theoretically as a displacement of each of the annular slots along the z-axis following a parabolic shape within the subarray edges affected by a maximum deviation chosen by the user.
Panel level
It consists in a deviation of the subarrays positions with respect to their theoretical positions in x, y, and z due to different subarray width or mounting in the structure and a rotation of each subarray along each of their axis (roll, pitch and yaw). It can be simulated as a variation of the individual position when computing the array factor and a rotation of each of the measured subarray patterns along the three axes. The user should be able to define individually, for each subarray, the displacements and rotations through a format to be determined. Initial separation in the z-axis is around $\pm 0.5\text{mm}$.

Antenna level

Consisting of a displacement of each of the panels, especially in the z-axis direction and a rotation in each of the three axes (i.e. a rotation of all subarray patterns). These values need to be specified independently from the previous errors and added up when computing the final antenna patterns. Initial values can be taken as 0.2° rotation in elevation and azimuth (yaw, pitch) and ± 1 mm deviations along the z-axis.

Table 2.4: Different levels to simulate mechanical deformations.

The thermoelastic deformations are panel parabolic torsions or the complete antenna. Along the x-axis (flight direction) the panel torsion is equivalent to the subarray deformation. The antenna torsion is equivalent to a parabolic deformation of a maximum value at the edges with respect to the SA center. Along the y-axis, this deformation can be simulated as a displacement of the subarray positions also following a parabolic shape.

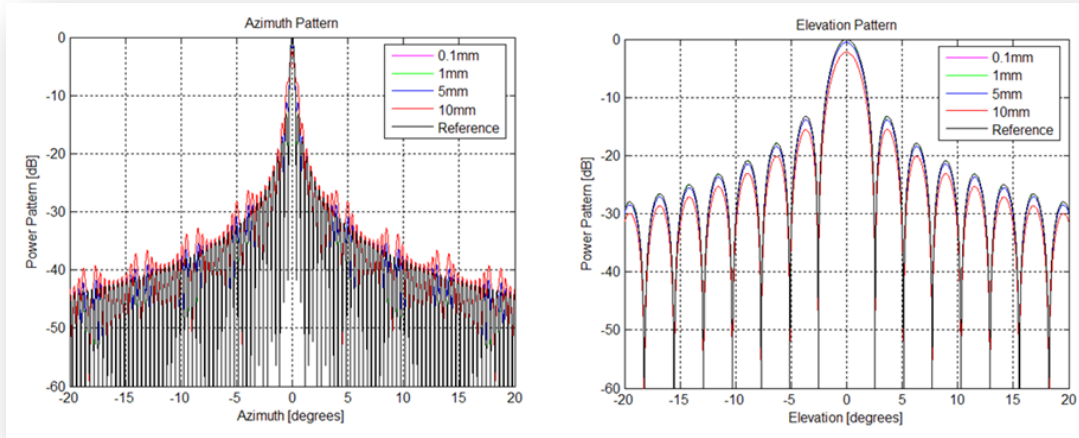


Figure 2.14: Normalized azimuth and elevation pattern cuts for a one-way boresight array having a theoretical subarray of rectangular patches as basic element [2.3]. Thermoelastic distortion following a parabolic shape along the z-axis has been considered with different maximum deviations in the borders of the PAZ array.

2.3.2 Transmit-Receive Module Errors

Errors in the TR modules can be considered at two levels: by a failure of the module in transmit, receive or both, or by a statistical module amplitude and phase deviation.

TRM failures

Specified through the GUI by the selection of any of the 384 modules either in transmit receive or both. There shall be the possibility to perform an iteration of M simulations of N random TRM failures to get a worst case mask.

TRM deviations

This shall be simulated as a Gaussian distribution centered in zero with an expected 3σ value to be determined by the user (in principle 0.5 dB, 5°) which will be added to the commanded values. Other errors such as deviations due to voltage or temperature variations will also be modelled through the 3σ value. TRM settings variations due to variations with temperature when the temperature compensation is not activated will directly be considered as variations of the TRM coefficients.

3 OPTIMISATION TOOL FOR AMOR: DESIGN AND RESULTS

The aim of the present chapter is to present and explain the optimisation tool embedded in AMOR, both from the functional and the algorithmic point of view.

In the next sections the Genetic Algorithm (GA) optimization technique is briefly described. The use of the GA applied to a SAR mission is addressed, and the connection between the instrument specification and GA variables explained. In a SAR mission the fitness function combines both antenna and radiometric parameters, like in the case of the SEOSAR/PAZ mission where the optimizer presented in this thesis could be used.

Next, the pattern requirements to be optimized for getting the instrument best performance are introduced and the fitness function definition is presented. Actually, the abovementioned requirements combination is what defines the fitness function to be minimised by the optimiser. This combination and the procedure followed to get the best solution for the excitation coefficients are explained in detail in the last sections of this chapter.

Finally, the specifications for three test cases are presented to define the examples that will be used in order for the reader to completely understand the optimization tool.

3.1 Brief Description of the Optimiser Functionalities

In Table 3.1 there are listed the functionalities offered by the optimiser developed in this Master Thesis.

The Optimiser for AMOR	
<ul style="list-style-type: none"> ▪ ▪ ▪ 	Allows the optimisation of all the possible antenna patterns in order to reach a maximum gain in the swath, reduce the gain variation within the swath, enforce gain nulls on certain directions (for instance in the nadir direction), and reduce the range ambiguities in the swath.
	Makes possible to optimise the antenna beams generated by the antenna in case of any deviation or error in the operation of the antenna elements.
	Permits to adjust the generated beams to the real ones after measurements.

Table 3.1: AMOR optimizer functionalities.

These functionalities are reflected in the *Synthesis* window of the Antenna MOdelleR GUI, as shown in section 3.2.8.

3.2 AMOR Optimisation Tool for PAZ

The optimization tool designed for AMOR is implemented using genetic algorithms. In the next sections the relationship between the electromagnetic and SAR parameters and the genetic algorithm variables are described. Additionally, the input and output parameters of the tool are overviewed, together with the way it operates to reach a solution. The objective is such that the instrument performances are optimised.

3.2.1 Genetic Algorithm Overview

In SAR applications the instrument array pattern has to reach certain goals, not only according to typical antenna parameters (gain, steering, crosspolar levels, null positions...) but also some SAR parameters (range ambiguity level, flatness in the swath). One example of these parameters is the gain variation within the swath, which determines the acquired image degradation caused by the gain variation in the main lobe borders.

In a scenario where the pattern shape is conditioned by many practical constraints, optimization techniques should be used. The optimization objective is to reach a trade-off (which is mathematically represented by a global maximum or minimum, depending on the algorithm) having into account absolutely the whole set of constraints. There exist a copious number of optimisation techniques devoted to find a function maximum or minimum: trial and error techniques, combinatorial methods, gradient descent or ascend, Newton's method, etc. Genetic algorithms (GA) are a particular case of evolutionary optimization technique, such as *Particle Swarm Optimization*, *Ant Colony Optimization* or *Bacteria Foraging Optimization* algorithms. All of them mimic natural selection and evolution concepts.

The reasons to use GAs as the optimization technique have been: the proven reported success in many electromagnetic applications, such as antenna design or pattern synthesis [3.1]; and the rapid implementation of the optimization tool by using an existent MatLab® GA Toolbox.

Genetic algorithms operate on a group of trial solutions in parallel. This group of solutions is called **population**. Each solution in the group is named **individual**. An individual is any point where the optimisation function is evaluated, and is sometimes referred to as a **genome**. The vector entries of an individual are referred as **genes**. The vector can be composed of double type numbers or bits. The initial population can be chosen in a more or less effective and determined way; i.e., the initial population can be left to be totally random or partially determined in case the effect of introducing a specific characteristic in an individual is known to be positive.

A member of a current generation is named **parent**, while a member of the next one is called **child**. The generations are populations created iteratively (hence also referred as the algorithm iterations). A **chromosome** is a coded form of a trial solution or individual. Finally, the **fitness** is the positive number assigned to an individual in order to compare it with the other individuals in a population and represents a measure of goodness of each solution.

A generic GA is explained through Figure 3.1. In the reproduction cycle individuals with best fitness (parents) are selected to combine their genes creating a new solution (child) for the next generation. The parameter to control the crossover, or combination, is the crossover probability. The higher the **crossover** probability, the higher the number of individuals coming from crossover in the next generation is. Another mechanism to create the next generation is **mutation**. Mutation randomly introduces new "genetic material" in the new population individuals. The parameter controlling this mechanism is the mutation probability. Finally, another mechanism is the **elitism**, by which the bests (or best, depending on the elitism parameter) individuals in a given generation directly go through the next one without changing its chromosomes.

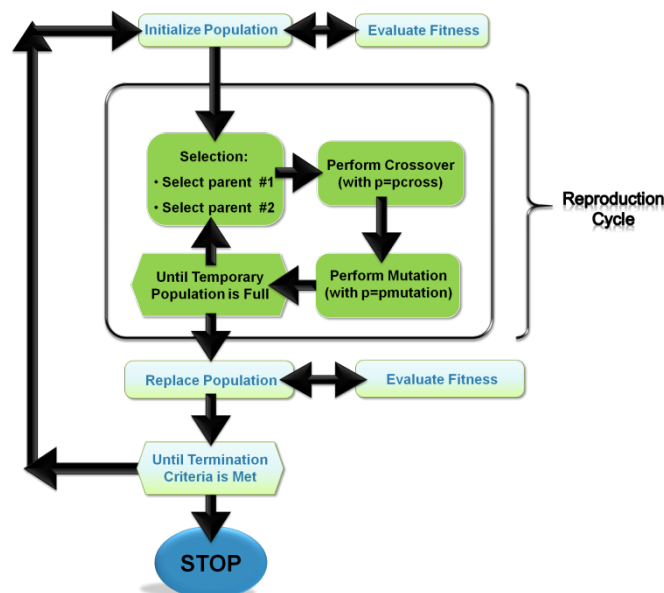


Figure 3.1: Genetic algorithm optimizer block diagram [3.1].

More detailed information on genetic algorithms and their applications can be found in [3.1].

3.2.2 Variables of the GA

In this section the electromagnetic and SAR parameters used by the genetic algorithm and their translation into genetic algorithm variables are explained.

3.2.2.1 General parameters

For the GA proper operation some general parameters need to be specified; for instance the GA stopping criterion, and the number of individuals per generation.

In many cases these parameters cannot be intuitively deduced but can be matched from a series of trial and error tests, such as the variables involved with the crossover, mutation and elitism probabilities. For this reason, these parameters will not be open for the user to be modified.

3.2.2.2 Individuals

The goal of the optimization tool is that the EL plane of the 2-way (2W) radiation pattern of a given satellite mode of operation (Boresight, Stripmap, Scansar or Spotlight) meets user-defined specifications in order to acquire high quality Earth images. Hence, during the GA optimization procedure, the GA should test several 2W gain patterns until specifications are met. Because each 2W gain pattern is defined by a set of *complex excitation coefficients*, this will be the *individual* of the Genetic algorithm.

In the present implementation of the optimizer, the set of excitation coefficients will be coded in binary format to be in concordance with the problem we are dealing, as it will be explained in the following lines.

Previously, let us consider again the SAR array physical structure. As shown in Figure A.13, the antenna has 12 panels along the azimuthal (AZ) flight direction. In each panel there are 32 subarrays (SA) in rows (in the elevation direction, EL). There is one Transmit-Receive Module (TRM) feeding each subarray. The TRMs set-up is represented by a complex excitation coefficient. The excitation coefficients have a magnitude and phase with discrete values in the range from 0dB to -31.5dB and 0° to 360°, respectively. However, the temperature correction applied during the in-flight calibrations reduces the amplitude ranges from 0dB to -20dB. Anyway, the optimisation is performed using 6 out of 8 bits (starting from the MSB) to discretize both magnitude and phase in steps of 0.5dB and 5.625°, respectively.

The previously mentioned set-up is stored in two look-up tables, one for the TX pattern and another one for the RX pattern. In the optimization tool each table is represented by a matrix of 32 rows per 24 columns (odd columns represent magnitudes and even columns represent phases). The format of these matrices is seen in Figure 3.2.

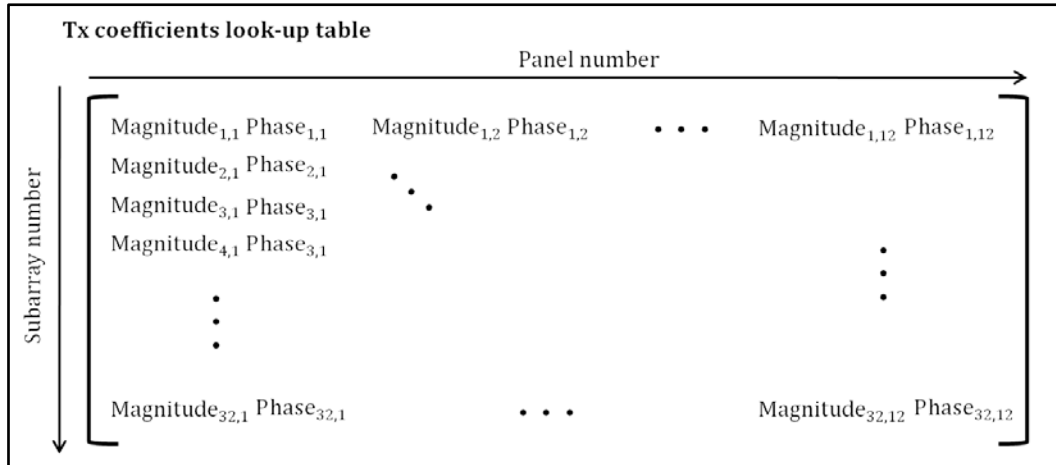


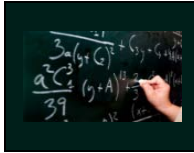
Figure 3.2: Look-up tables format containing the TRMs coefficients. Magnitudes are stored in dB and phases in degrees. Given that no steering is considered in the AZ direction, all the columns are equal by pairs.

Therefore, a given antenna configuration is obtained by superposition of measured embedded subarray patterns weighted by beam excitation coefficients. These coefficients are the combination of 384 amplitude and phase excitation coefficients to be applied to the TRMs in transmission and reception, with the constraint that TRMs in transmission always work around the saturation point (maximum transmission gain) so that the TX gain cannot be

commanded (TX and RX gain and phase values stored in the look-up tables like the ones on-board PAZ satellite). Tables are decoupled in elevation (left and right looking independent tables) and azimuth directions. This means that, for a given antenna configuration, 32 values must be selected for elevation and 12 for azimuth. For TX and RX separate beam tables are used, and consequently the beam shaping can be different for TX and RX for the same beam pointing direction [3.2].

Since (magnitude) tapering and steering is only possible in the EL plane (for the operating beams considered), all the column vectors (taken by pairs) are equal. TX magnitudes are always set to 0dB for the instrument to work with maximum radiated power. The TRM phases can be different in TX and RX.

Therefore, to generate each of the look-up tables described above (TX and RX) only a column vector of 32 complex coefficients is needed. Let us call the coefficients in this vector A_i . The total generated 32x12 coefficient matrix can be expressed as shown in Equation 3.1.



$$\begin{pmatrix} A_1 \\ A_2 \\ \vdots \\ A_{32} \end{pmatrix} (B_1 \ B_2 \ \dots \ B_{12}) = \begin{pmatrix} C_{1,1} & C_{1,2} & \dots & C_{1,12} \\ C_{2,1} & C_{2,2} & \dots & C_{2,12} \\ \vdots & \vdots & \ddots & \vdots \\ C_{32,1} & C_{32,2} & \dots & C_{32,12} \end{pmatrix}$$

Equation 3.1

Being A a 32x1 column vector and B a 1x12 row vector where all B_i coefficient phases are set to 0° and modules to 0 dB (1 in lenear). The resultant is the matrix $[C]$, with the same format than the look-up tables containing the TRMs modules and phases in TX or RX.

The A_i coefficients are generated by the GA and for each element of the population the matrices $[C]_{TX}$ and $[C]_{RX}$ are therefore extracted. The pattern cuts are computed from these matrices (using the same procedure than in the analysis case, with the difference that in the analysis the $[C]$ matrices are read from a file), and hence the fitness function is evaluated. With this fitness value, the algorithm evolves and generates another individual if it's the case.

Magnitudes are coded with 6 bits (the more significant bit is the latest) in steps of 0.5 dB, and the dynamic range is limited from 0dB to -20dB. Phases are defined in a range from 0° to 360° , and also coded with 6 bits in steps of 5.625° .

Considering that the magnitude and the phase of an excitation coefficient is codified with 6 bits, each pattern can be generated using a chromosome of 576 bits (see a clarifying sketch in Figure 3.2) where:

- the TX pattern magnitudes are always 0 dB (A_{TX} modules)
- 32x6 bits correspond to the RX pattern magnitudes (A_{RX} modules)
- 32x6 bits correspond to the excitation coefficient phases for the TX pattern (A_{TX} phases)
- 32x6 bits correspond to the excitation coefficient phases for the RX pattern (A_{RX} phases)

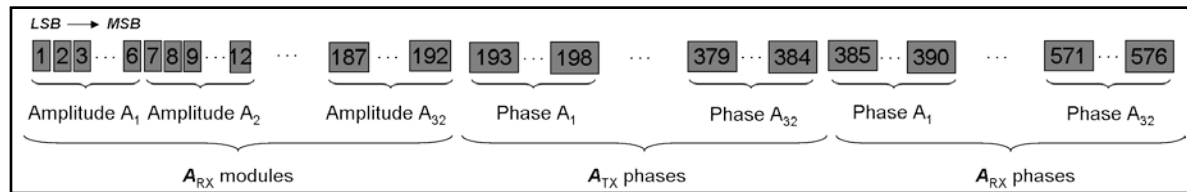


Figure 3.2: Sketch of the chromosome of the individuals considered in the GA implementation used in AMOR.

Aside from the excitation look-up tables (Figure 3.2), error tables containing information of possible TRMs failure or phase drifts are available. There are four tables: phase drifts in the TRMs in Tx, phase drifts in the TRMs in Rx, TRMs amplitude in Tx, and TRMs amplitude in Rx. The amplitude matrices are masks formed by zeros and ones (zeros for the failing TRMs and ones for the operative TRMs).

These error tables are used in the optimisation process in order to recompute the excitation coefficients when TRM failures occur. These matrices are combined with the nominal excitation matrices to obtain the actual pattern for a failing TRMs scenario. This pattern is degraded with respect to the nominal one. Both patterns are compared, and the degraded pattern is enforced to evolve to the nominal one.

3.2.3 Optimization Tool Variables

This section describes the parameters taken into account when the AMOR Synthesis tool was designed. The input parameters of the optimization tool designed for AMOR are mainly related to SAR parameters. As specified in [3.3], the instrument parameters that drive the antenna pattern synthesis are:

	Gain of the main lobe	The main lobe gain requirement implicitly affects the instrument sensitivity across the swath (i.e. $NE\sigma^0$ specification). The gain shall be achieved within the main lobe width. The main lobe gain is intended to reach the theoretical maximum, that depends on the operating frequency and the antenna effective aperture (considered to be the array whole surface).
	Width of the main lobe in elevation	The -3dB beamwidth is basically defined by the on-ground swath projection in terms the angular coordinates. The swath width will be provided by the user as an elevation angle $\Delta\theta$ in order to keep the same incidence angle on-ground along the orbit, taking into account the satellite altitude variation.
	Gain variation within the swath	The peak-to-peak gain variation represents the gain difference between the maximum and the minimum within the swath specified in [dB]. In order to optimize the final images quality, the 2-way elevation antenna pattern needs to be as flat as possible, since in the calibration process the elevation antenna pattern inverse is applied and the noise distribution in the images directly follows that modulation.
	Higher gain towards higher elevation angles	The signal power received by the instrument depends on the R^4 (transformed to R^3 after azimuth compression), so the image intensity falls towards far range; this effect can be compensated by applying an antenna pattern with a positive slope in gain towards far range within the main lobe. The compensation law (proportional to R^3 shape) shall be applied in AMOR Synthesis tool in the angular range covering the main lobe and be transparent with respect to the user, which is given only the choice to trigger or not this option. This additional gain shall be added to the one specified under point 1 taking as reference the near range angle.
	Range ambiguity	The antenna sidelobes level directly impacts on the range ambiguities, so the Synthesis tool shall have the capability to compute the Range Ambiguity-to-Signal Ratio (RASR) during the optimization process. The user is given the possibility to specify a RASR level in [dB] and the number of the ambiguities to be calculated.
	Elevation and azimuth pointing direction	The elevation pointing direction is defined by the swath geometrical parameters, thus the look angle respect to the antenna boresight direction. In the azimuth direction the antenna pattern shall always be pointed towards zero degrees (i.e. zero-Doppler geometry) except for Spotlight mode where the azimuth squint angle determines a Doppler frequency different from zero. The elevation angle with respect to boresight will be input by the user. This will correspond to the swath centre.
	Null position on certain directions	In order to avoid ambiguous nadir echoes the instrument commanding is designed such that the reception window is not open when the Nadir return reaches the satellite. However, this cannot be ensured for all combination of satellite altitudes and terrain heights, so the option to include a null in the nadir direction shall be provided. The user shall be able to select the direction (in elevation) of the desired antenna pattern null and the level of this null.

Table 3.2: Parameters used in the antenna pattern optimisation process.

In order to have a clearer idea of each of the above described parameters meaning, a detail of the mask in the main lobe region is depicted in Figure 3.3:

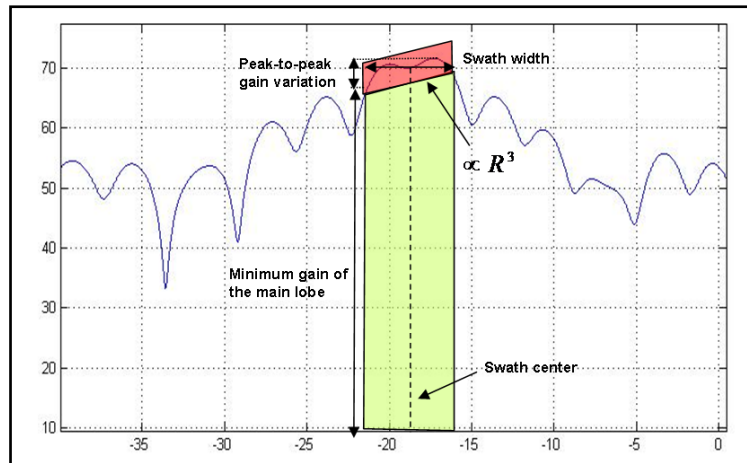


Figure 3.3: Mask detail in the main lobe [3.3].

All the above identified parameters are used as constraints in the synthesis process and the user is able to stress some of them by means of weights through the implemented fitness function. The use of these parameters is explained in the next section.

Since the optimization could be performed for different polarization combinations (i.e. HH, VV, HV, VH) only one of them (chosen by the user) will be considered in the process. However results for all possible combinations should be computed and displayed in order to evaluate the different trade-offs against the masks requirements.

Additionally, the possibility to include deviations in the TRM settings or failing modules either in transmission, reception or both shall be considered when computing the coefficients. The module shall consider the nominal elevation pointing based on nominal antenna pointing plus the pointing accuracies or shifts.

Different coefficients shall be obtained for right and left looking, by modifying the antenna nominal pointing parameter.

3.2.4 Fitness Function

The fitness function is the function helping to decide which the best solution to the optimization is. This function has to be minimized and should combine anyhow the parameters mentioned in the previous section into a single number. This process can be done by means of:

- A combination of the aforementioned parameters into a mask or **template** that the solution has to fit closely;
- or by means of the definition of a fitness function based in the proper **weighting** of these parameters.

The current version of AMOR considers a weighted combination of parameters to define the fitness function. However, finding the adequate combination of parameters to define the fitness function is not trivial, and is the most difficult task in the GA application to any problem. The fitness function has to be tailored to the specific problem, and this is really hazardous since there is not a unique manner to define it.

In the following sections some solutions applied to our particular scenario are presented.

3.2.4.1 Template

Obtaining the fitness function value from a template is quite simple. The defined template consists on the definition of the desired gain value for each angle in the elevation angle range considered $[-90^\circ, 90^\circ]$. The possibility to define a high and a low template is offered. These kinds of templates impose restrictions in the gain. Different scenarios are possible for each elevation angle in the range:

1. High template: a high template (HT) is defined to limit the antenna gain pattern (GP) to a maximum value in a region of the antenna pattern; $GP < HT$.
2. Low template (LT): to enforce the gain to reach a minimum value for some elevation angles; $GP > LT$.

3. High and low template: the gain must be between the values specified by the templates; $LT < GP < HT$.
4. Specific template (ST): the gain must equal the most as possible a template with the desired antenna pattern; $GP = ST$.

From these four cases, number 3 is used in the *Delimiting Template* approach, and number 4 corresponds to the *Fitting Template* approach (both described next).

The criterion to evaluate the fitness function depends on the kind of template used, as shown in Table 3.3:

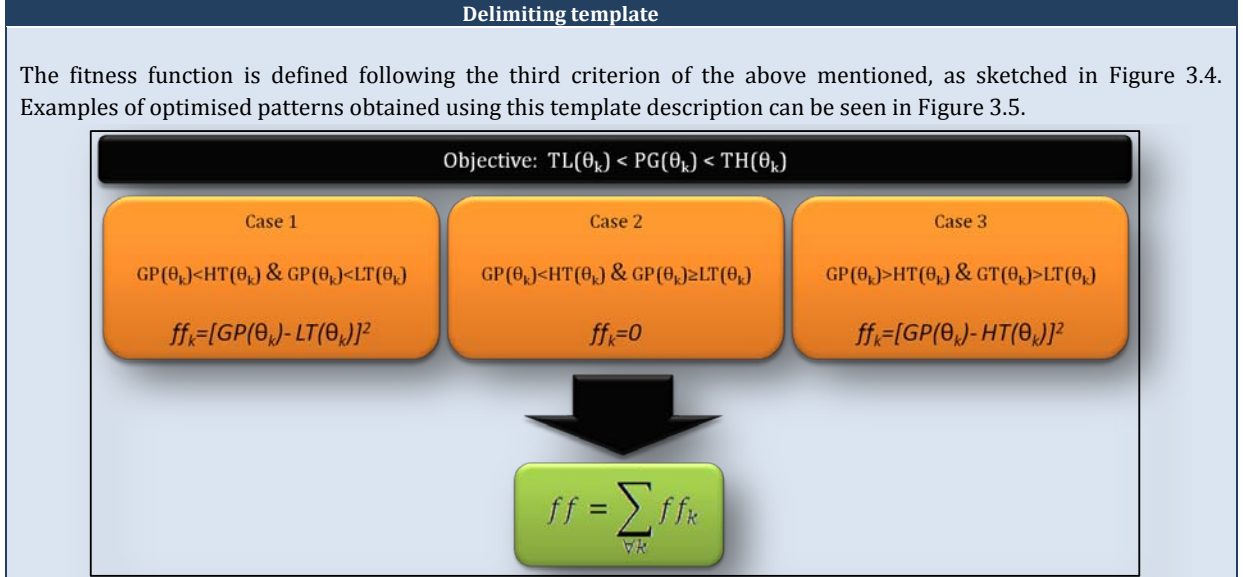


Figure 3.4: Partial fitness function assignation. The fitness function is denoted by ff , and the partial fitness functions (partial because it is computed for each elevation angle sample) are denoted by ff_k . k is the number of angular samples in the angular range considered.

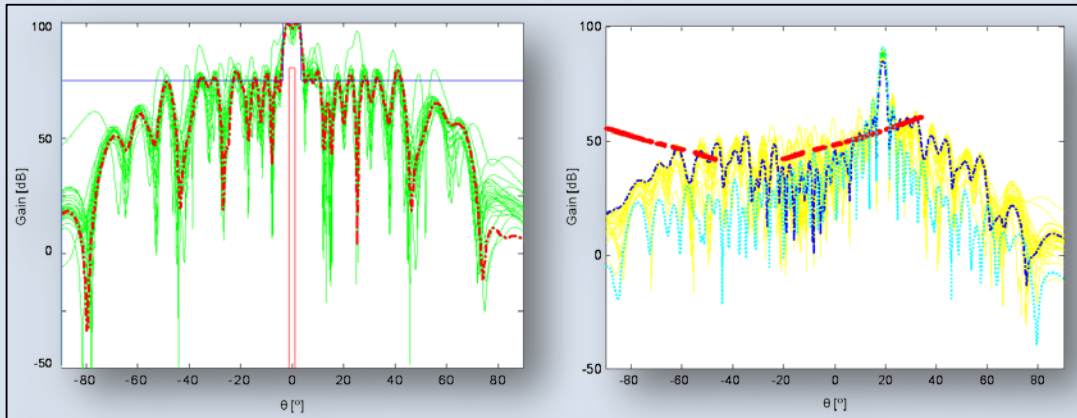


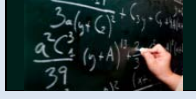
Figure 3.5: Examples of optimised EL patterns using the delimiting template technique.

Figure 3.5 (left) shows the algorithm convergence, from a random initial population, to a pattern similar to the desired one. The template used is very simple and does not correspond to the application of any specific criterion based in radiometric quality parameters. In this figure the high template is marked in blue, while the low template is red. The final algorithm solution is the red dash-dotted line, while the green lines correspond to the intermediate solutions or the solutions of each generation.

In Figure 3.5 (right) the cyan pattern is the best within the initial population, yellow patterns are the best results of the consecutive generations, and the blue pattern is the best individual in the last generation. The red template (high template) defines the antenna pattern side lobe region, where the antenna gain must be below to reduce the ambiguities level. The green template (low template) in the main lobe region indicates the minimum gain providing sufficient energy to illuminate the swath.

Fitting template

The objective is to obtain an antenna pattern as similar as possible to a given pattern (the fourth of the type of objectives described before). The fitness function is then obtained as simply as computing the sum of all the squared difference between the template and the candidate patterns at each generation for all the angles in the elevation range (Equation 3.2).



$$ff = \sum_{k=1}^N [template(\theta_k) - pattern(\theta_k)]^2$$

Equation 3.2

Being p the number of elevation angle samples considered.

This technique is suitable to optimise patterns after TRM failures to obtain a new pattern as equal as possible to the original one (before the TRM failure).

Table 3.3: Fitness function definition using templates.

3.2.4.2 Weighting

The input parameters mentioned in the last section are used in the optimization tool to define a fitness function, that is, to assign a fitness figure to each individual analyzed during the GA evolution. This figure summarizes the 7 parameters described in section 3.2.3 and is computed in four steps, each throwing a partial fitness ff_1 , ff_2 , ff_3 and ff_4 , respectively, as exposed in Equation 3.3:



$$ff = \sum_{p=1}^4 w_p \cdot ff_p$$

Equation 3.3

From all the optimization variables presented in 3.2.3, the different partial fitness functions are extracted, as explained in Table 3.4:

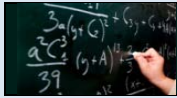
Computes the distance between simulated gain and the maximum gain achievable in the main beam.

This partial fitness function has the following input parameters:

- the main lobe minimum achievable gain (depends on the whole antenna aperture size and the operating frequency)
- the elevation beamwidth
- the swath centre or pointing direction
- the R^3 gain compensation values (for a given number of points inside the main beam)

With these parameters a $Pattern_{desired}$ is defined in the main beam area. A ff_1 value from the patterns generated in each algorithm generation is computed as shown in Equation 3.4:

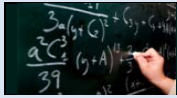
ff_1



$$ff_1 = \Psi_{limit} \left(DR, slope, a, Param_{desired} ; \sqrt{\frac{\sum_k ff_1(\theta_k)}{numpoints^2}} \right)$$

Equation 3.4

Where $ff_1(\theta_k)$ is computed as indicated in Equation 3.5:



$$ff_1(\theta_k) = |Pattern_{desired}(\theta_k) - GP(\theta_k)|^2$$

Equation 3.5

Somehow, we are also using a template and the criterion is the fourth of the explained in section 3.2.4.1. GP is the pattern generated by the GA that is being evaluated, and Ψ_{limit} the function (Equation 3.9) used to limit the dynamic range of the ff_k 's that is explained (together with the DR , $slope$, a and $Param_{desired}$) further in this section. The variable $numpoints$ is the number of angular samples considered in the main beam that depend on the angular resolution chosen for the optimisation tool (by default 0.1°).

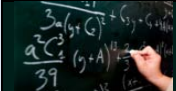
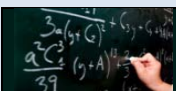
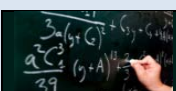
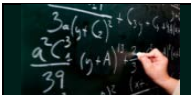
ff_2	<p>Computes the gain ripple in the swath. To compute this value the considered parameters are:</p> <ul style="list-style-type: none"> the gain variation within the swath and the slope in the main lobe (defined by the compensation law proportional to R^3 shape) <p>The gain GP variation within the swath, ΔG, is computed from the corrected swath (with the R^3 compensation law) and used to derive ff_2:</p>
	<div>  <div> $ff_2 = \Psi_{limit}(DR, slope, a, Param_{desired}; \Delta G)$ </div> <div>Equation 3.6</div> </div>
ff_3	<p>Computes the worst RASR in the swath. The worst RASR value is computed for the pattern generated by the GA. Then the third partial fitness function value is computed using Equation 3.7:</p>
	<div>  <div> $ff_3 = \Psi_{limit}(DR, slope, a, Param_{desired}; RASR_{worst})$ </div> <div>Equation 3.7</div> </div>
ff_4	<p>Computes the null to maximum gain ratio. The null value with respect to the GP maximum gain value is computed and used directly to obtain the ff_4 value:</p>
	<div>  <div> $ff_4 = \Psi_{limit}(DR, slope, a, Param_{desired}; Null)$ </div> <div>Equation 3.8</div> </div>

Table 3.4: Partial fitness function definition.

The Ψ_{limit} function is used in order to have a limited dynamic range for each partial fitness function ff_k . In fact, the partial fitness ranges are limited from 0 to 1. This is very important to have balanced partial costs for each of the four parameters according to the weighting values w_p .

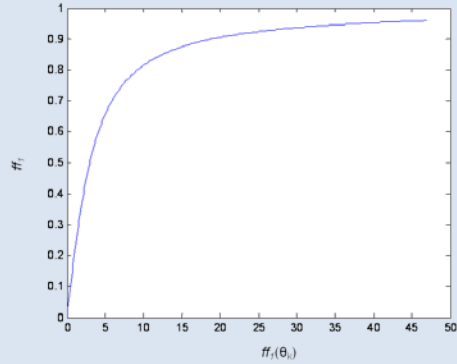
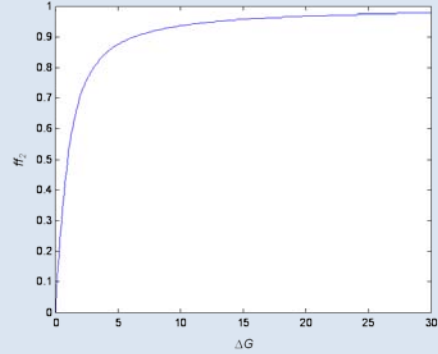
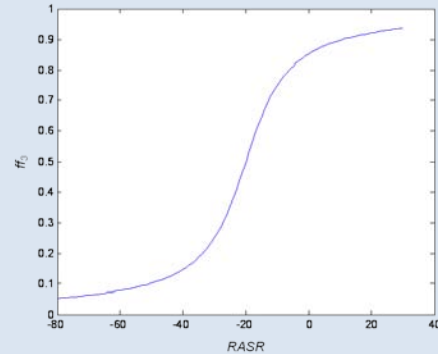
The mentioned Ψ_{limit} function is the following:



$$\Psi_{limit} = \frac{DR}{\pi} \cdot \left[\arctan\left(\frac{Param_{actual} - Param_{desired}}{slope}\right) + a \right]$$

Equation 3.9

The *arctangent* function is used to limit the dynamic range from $-\pi$ to π . Four parameters should be defined to get the output of Ψ_{lim} in the range from 0 to 1 for the expected values of $Param_{actual}$, DR , $Param_{desired}$, $slope$ and a . The resulting parameters after tuning are summarised in Table 3.5:

	Parameter Values	Graphical Representation of the Limiting Function
ff_1	<p>Distance to maximum achievable gain in the swath.</p> <ul style="list-style-type: none"> Maximum gain is computed from the area A_{geom} of the whole array. If an aperture efficiency of 100% is considered the maximum achievable gain in the swath is found as: $G_{max}=10*\log(4\pi A_{geom}/\lambda^2)$. It is considered that when the mean difference between maximum and actual gains is 5dB fitness should be 0.7. Then: $Param_{desired}=G_{mean_diff}=5$ and $\Psi_{limit}(DR, slope, a, Param_{desired}=5)=0.7$. Finally: <ul style="list-style-type: none"> $DR=2$ $slope=3$ $a=0$ $Param_{desired}=0$ 	 <p>The $slope$, DR, and a parameters are fixed in order to obtain a rapid fitness decrease when "better" values of $ff_1(\theta_k)$ are reached. The increase of the ff_1 value when the input parameter increases its value is softer.</p>
ff_2	<p>Ripple ΔG in the swath.</p> <ul style="list-style-type: none"> The user input is ΔG. In this example it is considered that $\Delta G = 2$dB is the maximum value allowed. Consequently: $Param_{desired}=\Delta G = 2$ and $\Psi_{limit}(DR, slope, a, Param_{desired}=2)=0.5$. Then: <ul style="list-style-type: none"> $DR=2$ $slope=1$ $a=0$ $Param_{desired}=0$ 	 <p>The $slope$, DR, and a are tuned to obtain a high descending slope for values approaching $\Delta G = 0$dB (the desired ones). The slope is softer in the undesired region, because in this region it does not matter the worst the value is but the fact that it is a bad value.</p>
ff_3	<p>Maximum RASR in the swath.</p> <ul style="list-style-type: none"> In this example the desired maximum value of RASR in the swath is -20dB. It is always considered that when the worst RASR in the swath is -80dB fitness is 0.05. Then, $Param_{desired}=RASR_{worst}=-20$ and $\Psi_{limit}(DR, slope, a, Param_{desired}=-20)=0.5$. Finally: <ul style="list-style-type: none"> $DR=1$ $slope=10$ $a=\pi/2$ $Param_{desired}=-20$ 	 <p>Higher values than -20 are considered worst, and lower values better. However, obtaining a very low value implies negative effects on other parameters such the maximum obtainable gain, and is not as important as obtaining a value lower than -20dB. For this reason the $slope$, DR, and a parameters are adjusted to have:</p> <ul style="list-style-type: none"> a steep slope around the desired value and a saturation of the ff_3 value when the RASR input value is further from the desired one.

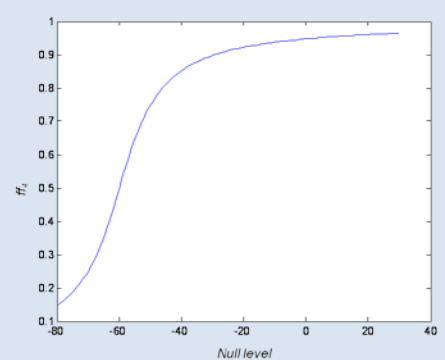
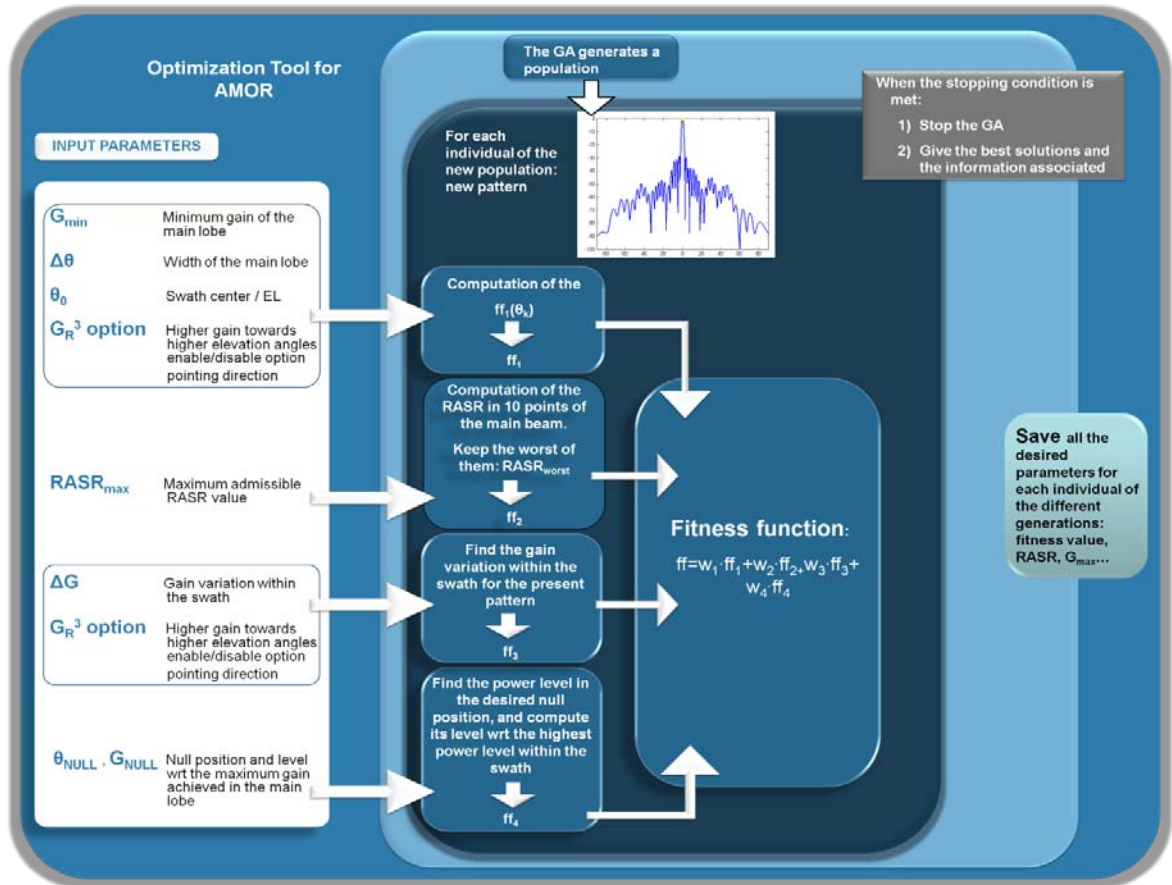
<p>Null to maximum gain ratio.</p> <ul style="list-style-type: none"> In this example the desired null gain wrt maximum gain is -60dB. Then: $Param_{desired}=Null_{level}=-60$ and $\Psi_{limit}(DR, slope, a; Param_{desired}=-60)=0.5$. It is always considered that when the null gain wrt maximum gain is 0dB fitness is 0.99. Then: <ul style="list-style-type: none"> $DR=1$ $slope=10$ $a=\pi/2$ $Param_{desired}=-60$ 	 <p>In this case, the curve is adjusted to reach a 0.5 value when Null=-60dB.</p> <p>The curve has been tuned to have:</p> <ul style="list-style-type: none"> As the value obtained in the studied pattern is better, the slope quickly descends. And, on the contrary, as this value is worse the slope ascends slowly.
--	--

Table 3.5: Partial fitness function adjustments.

An optimization procedure block diagram when the weighting approach is applied is shown in Figure 3.6:


Figure 3.6: Optimiser block diagram. Fitness function weighting method approach. The weights w_k are user defined.

In the figure the input parameters and their connection with the optimization process are sketched. The soft blue boxes indicate actions that are made in the routine that performs the fitness function computation, ff . Therefore these actions are executed $(\#individuals_per_population) \times (\#generations + initial_generation)$ times.

Once the fitness function is obtained, the algorithm internally waits to the end of each generation to compare the fitness of the individuals and therefore perform elitism, mutation and crossover and hence create the next population. The best individual of the next generation will have a better, or at least equal, fitness than the one in the previous generation.

Whereas the stopping condition is not met, the algorithm goes on with the iterations. The stopping criteria are diverse: a maximum number of generations, a given fitness value, a lasting time for the optimization process, a stopping order given by the user, or any combination of the previous conditions (see next section).

Although the former Figure refers to the weighting method, it is quite general. If the template approach is used, w_2 , w_3 , and w_4 are set to 0 and w_1 to 100. The ff_1 term input is the defined template and is computed depending on the definition of fitness function used (Figure 3.4 or Equation 3.2). Irrespective of the chosen weights and template definition, the historic of all the parameters involved in the optimisation is stored for further analysis.

In addition if null to maximum gain ratio does not need to be fulfilled, just assigning a value of 0 to w_4 cancels its influence in the algorithm evolution.

3.2.5 Algorithm Stopping Criteria

The best way to stop the algorithm would imply results active monitoring for each generation by a skilled user. This is not a convenient solution, because it makes the optimising process non automatic. There are plenty of conditions through which the algorithm can be commanded to stop, some of the most intuitive and used are:

Algorithm Stopping Approaches	
▪	Maximum number of generations. The algorithm can be stopped if the number of generations exceeds a fixed limit. A drawback of this stopping method is that there is not an intuitive rule to determine the convenient number of generations before stopping the algorithm. The number must be established after studying the particular optimisation case in order to avoid stopping the algorithm before having reached a sufficiently good solution or to avoid spending too much time optimising when the optimal solution is reached many generations before. However, it can be considered as a stopping method in our particular case.
▪	Fitness value limit. In this case the algorithm stops when the fitness value obtained for a given solution is less than or equal to a specified fitness limit. Similarly to the former method, in some situations it is difficult to establish that limit in the fitness function value. In our particular case, the obtained fitness value meaning is highly difficult to relate with the algorithm inputs and outputs (as explained in the former section), hence making unsuitable this stopping criterion.
▪	Time limit. The algorithm stops after running for an amount of time equal to a specified time limit. This is a dangerous stopping method. Beforehand, it is practically impossible to know the time the algorithm will need to reach a solution susceptible of being qualified as truly optimal for a given problem. Therefore, this method is not used in AMOR.
▪	Manually. This option can be used to stop the algorithm when checking its progression and a sufficiently optimal solution is found.

Table 3.6: Different possible algorithm stopping criteria.

The method used in the AMOR software is the limit number of generations. This value is accessible to the user although, as abovementioned, this number is not intuitive and it must be carefully determined in the design of the optimiser. Additionally, there is an option to stop the algorithm manually.

3.2.6 Initial Population

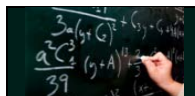
One of the initial steps while running a Genetic Algorithm is providing the code with an initial population of individual for the algorithm to evolve towards an individual with the lowest fitness as possible. Typically the initial population generation is random. However, it is possible to feed the initial population with a set of individuals known to or expected to have low fitness values, or even with individuals having certain properties expected to be in the algorithm best solution.

In AMOR, the individuals of the initial population are generated using different criteria:

- Some of them are generated fully randomly.
- Others are generated considering a boresight solution steered towards the direction of the desired steering one (specified by the user).
- Another group of individuals is generated using a squinted beam in RX steered towards the direction of the desired steered direction. The squinted beam is generated adding two beams: one is the resulting beam from shifting a boresight beam $+\alpha$ degrees from the desired steering angle, and the other is the resulting beam from shifting a boresight beam $-\alpha$ degrees from the desired steering angle. These individuals have a flat response in the main beam of their RX pattern whereas have a pencil beam in their TX pattern.
- Finally the individual that is the solution for a planar array of equally spaced subarrays of ideal resonators has also been considered. This array is assumed to have all its subarrays working properly. Albeit not exact in terms of SAR parameters, this optimised solution is very similar to the one obtained considering embedded subarrays.

The solution for the actual array having subarrays at nominal positions and maybe some failing TRMs is expected to be close to the ideal one (meaning that excitation coefficients would not be much different). A light version of the GA code has been implemented to find this solution. This light version of the code is especially implemented to solve an array of equally spaced set of subarrays of ideal resonators being its execution times faster than the code solving the actual array. That is the reason why the optimization tool is configured to run the lite version of the GA code during more generations than the actual array GA code and with a higher number of individuals in the initial population.

Figure 3.7 summarizes the tasks carried out by the optimization algorithm. The inputs to the algorithm are the SAR parameters to be considered and the working/failing TRMs (both through external files). First the template for having maximum gain at swath and all the range ambiguities are computed. The individuals for the initial population to be used in the lite GA code (for the case of an equally-spaced array of ideal subarrays) are generated. The solution for this lite GA is computed and included in the set of individuals that describe the initial population to be used in the GA that will find the solution for the actual array of embedded subarrays. The resonator radiation power pattern is given by Equation 3.10.

	$t(\theta, \phi) = (0.05 + 0.95\cos\theta)^2$	Equation 3.10
---	---	----------------------

Due to its computation speed to calculate the actual subarrays pattern directivities the GA uses the method of subarray radiation power integration (section 2.2.2.2). Once the GA best solution is found the pattern directivity is accurately computed using the spherical mode expansion (section 2.2.2.4).

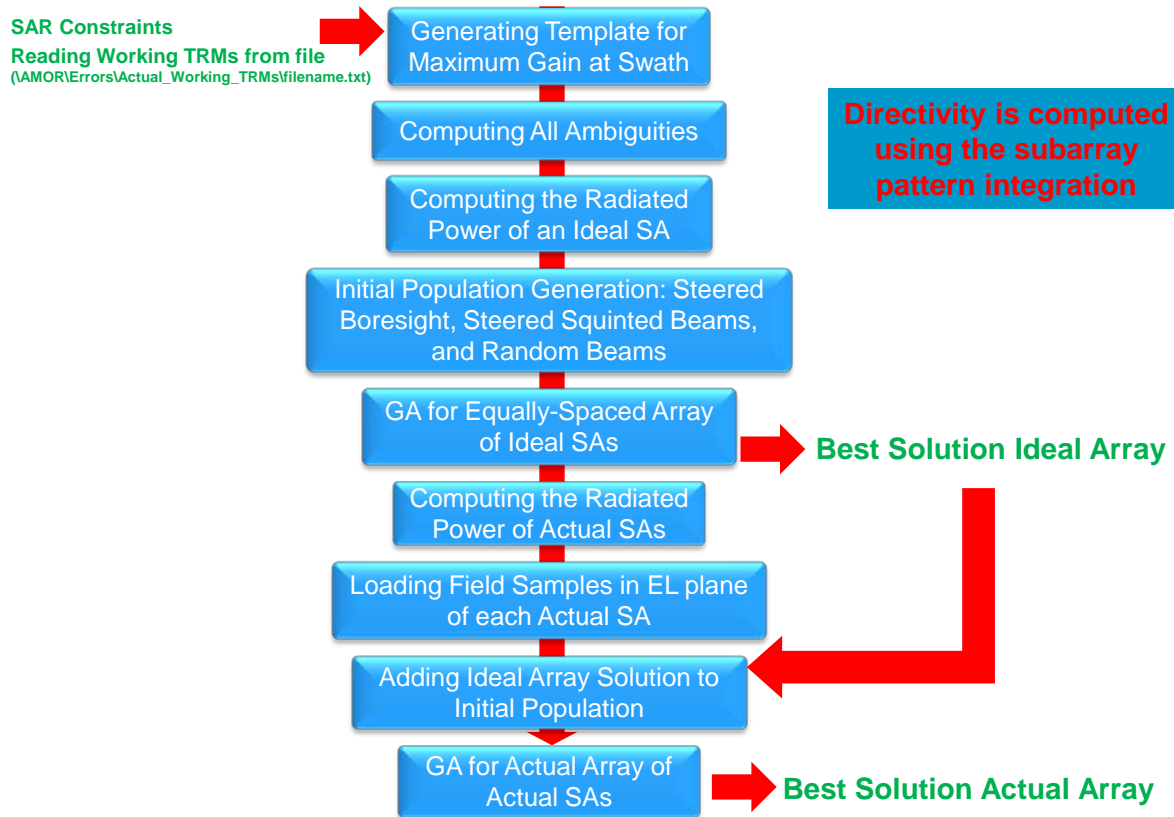


Fig. 3.7: Optimizer algorithm.

3.2.7 Optimiser Development Procedure

The optimisation is based in the Genetic Algorithm approach. This algorithm is iterative, and reaches a solution after an intensive tuning of the consecutively intermediate solutions. In parallel, the development of the optimisation tool is an iterative process itself in which the inputs are fixed by quality parameters that the outputs have to fulfil.

The way these quality parameters are translated to the optimizer core can need to be redefined in successive steps. Many modifications in the definition of the fitness function inputs and the fitness function itself have been needed in order to obtain sufficiently accurate results within a reasonable time slot.

In the former section the optimiser design and implementation process are described in detail, making special emphasis on the most hazardous parts of the design and the solutions proposed. The optimiser development is based on an iterative process in which some definitions and parameters are refined in order to obtain an optimiser sufficiently tuned to our particular needs. The overall optimiser development procedure is sketched in Figure 3.8:

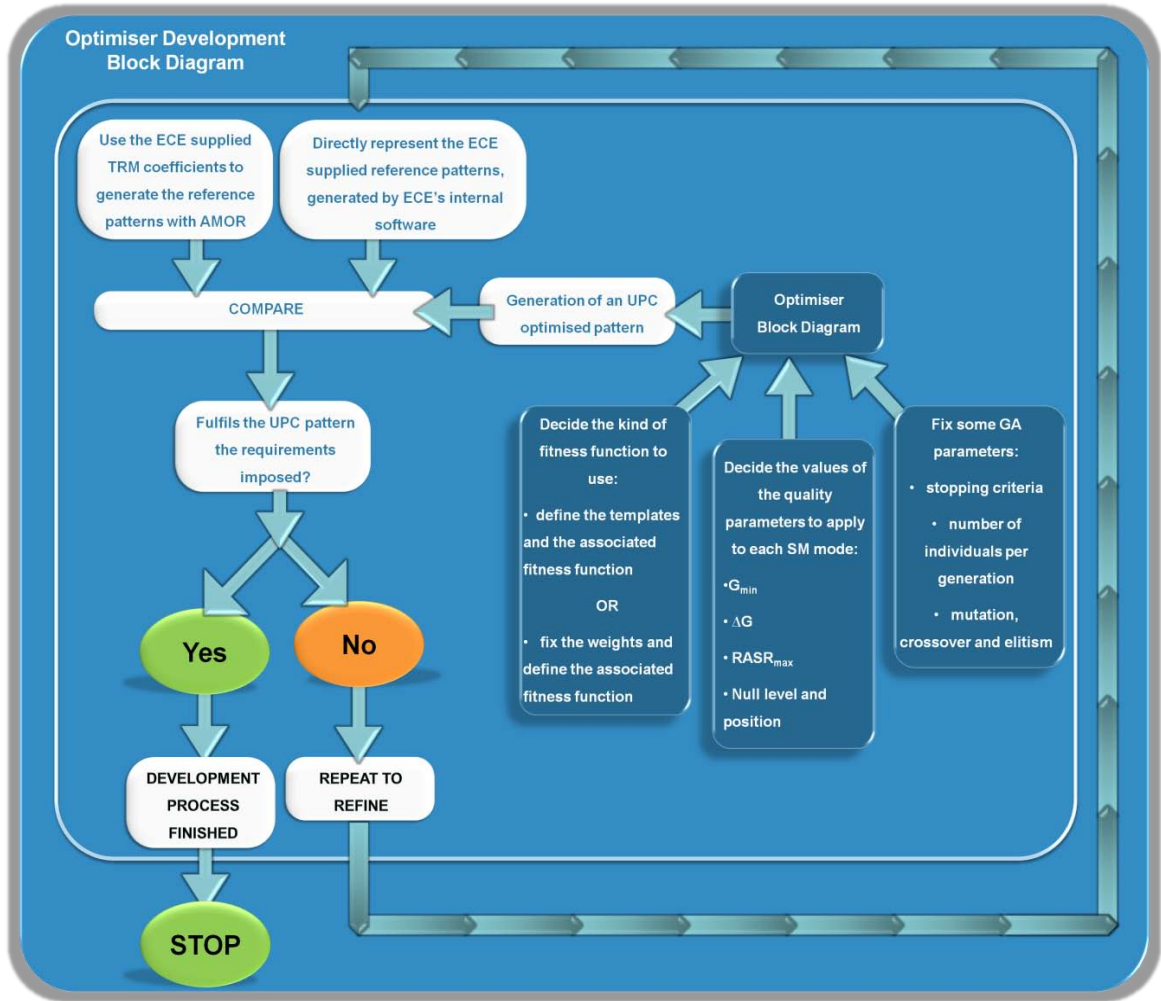


Figure 3.8: Optimisation development block diagram.

The comparison between ECE's supplied patterns and the AMOR optimiser obtained ones is part of the optimisation development procedure. It is necessary and useful as a means to pre-validate the software (although the complete prelaunch validation will not be complete until some of the synthesised beams are compared with the correspondent measured ones). However, it does not tight the AMOR optimiser to obtain any specific result previously obtain with the ECE tool. Moreover, the AMOR optimisation tool has been designed to overcome the ECE tool restrictions and trying to improve its results.

In this process, the results obtained using AMOR are compared to the ones supplied by ECE. Some of the most important difficulties found in the adjustment procedure of the AMOR optimiser are related with the fact that UPC does not know the way the ECE tool derives its results. It is neither known the analytical expression of the basic element used, nor the kind of algorithm used. Moreover, some important details like the planes used to define the AZ and EL plane of the beams are unknown. Therefore, whenever the AMOR optimisation tool performed worse than the ECE tool it has been difficult to determine if the patterns compared were exactly the same and under the same conditions.

Anyway, these difficulties are not completely a drawback, since the objective is to develop a new and better Antenna Model tool. To do so, the tool needs to be designed and developed completely independent to any other existent tool.

Hence, the main goal is that, fixed the desired design parameter values the GA optimum pattern has to fulfil them.

3.2.8 AMOR Optimiser GUI

This section is aimed to demonstrate the operation of the optimiser GUI, and specifically concerning to the Stripmap beams optimization, through the simulated results of the Stripmap SM1 beam. The Spotlight and ScanSAR beam generations are easier and quicker and fall out of the scope of this thesis. The Spotlight beam generation objective is to steer a given pattern to a specified angle in AZ, while the ScanSAR beam generation will be based in the Stripmap one, steering a given Stripmap beam in AZ and without needing to apply GAs.

First of all, the basic element to be taken into account in the optimizer as the actual SA has to be selected in the *Array Description* window, as depicted in Figure 3.9. In this case the *WA_NS_01_32_PH_09650_COSGUV.mat* element, both in TX and RX. This basic element data is based in an ideal model of the SA pattern, based in a cosines-like shape as observed in Equation 3.10. The other possibility is *WA_NS_01_32_PH_09650_ISOGUV.mat*, taking an isotropic element as a basic element of the phased array antenna. AMOR allows considering as basic element any kind of radiating element. In future versions of the software another configuration is planned to be added: the one considering measurements.

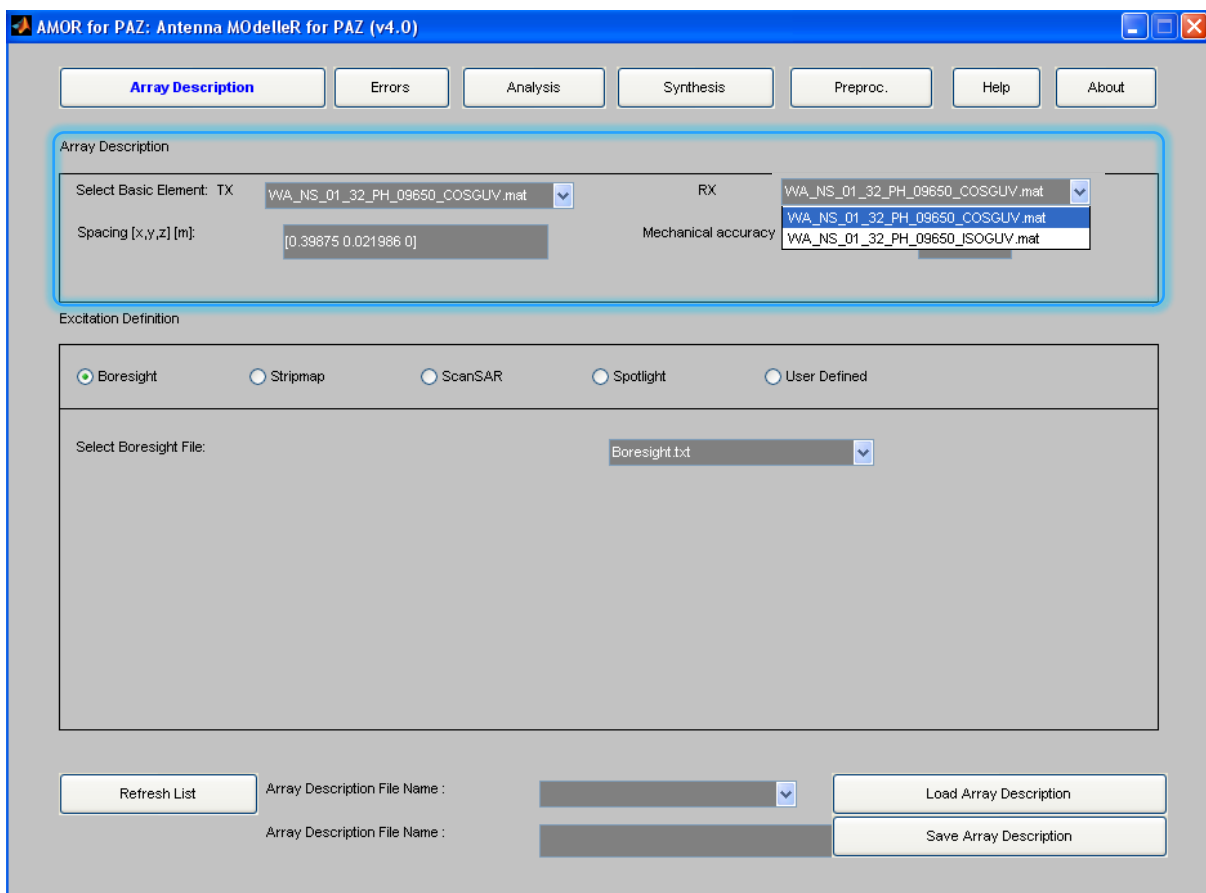


Fig.3.9: AMOR Array Description window. The desired TX and RX antenna configurations have to be chosen.

Then, in the *Errors* window, a file containing the description of the failing TRMs can be selected if needed. In addition, another kind of errors can also be taken into account: mechanical errors made when assembling the antenna, or detected deviations in the nominal values of the phase shifters or amplifiers, among others. An example can be observed in Figure 3.10. In this example and the simulations performed in the rest of the chapter, no errors are considered. Those errors, if selected, are taken into account in the second part of the optimisation process, when considering the actual SA.

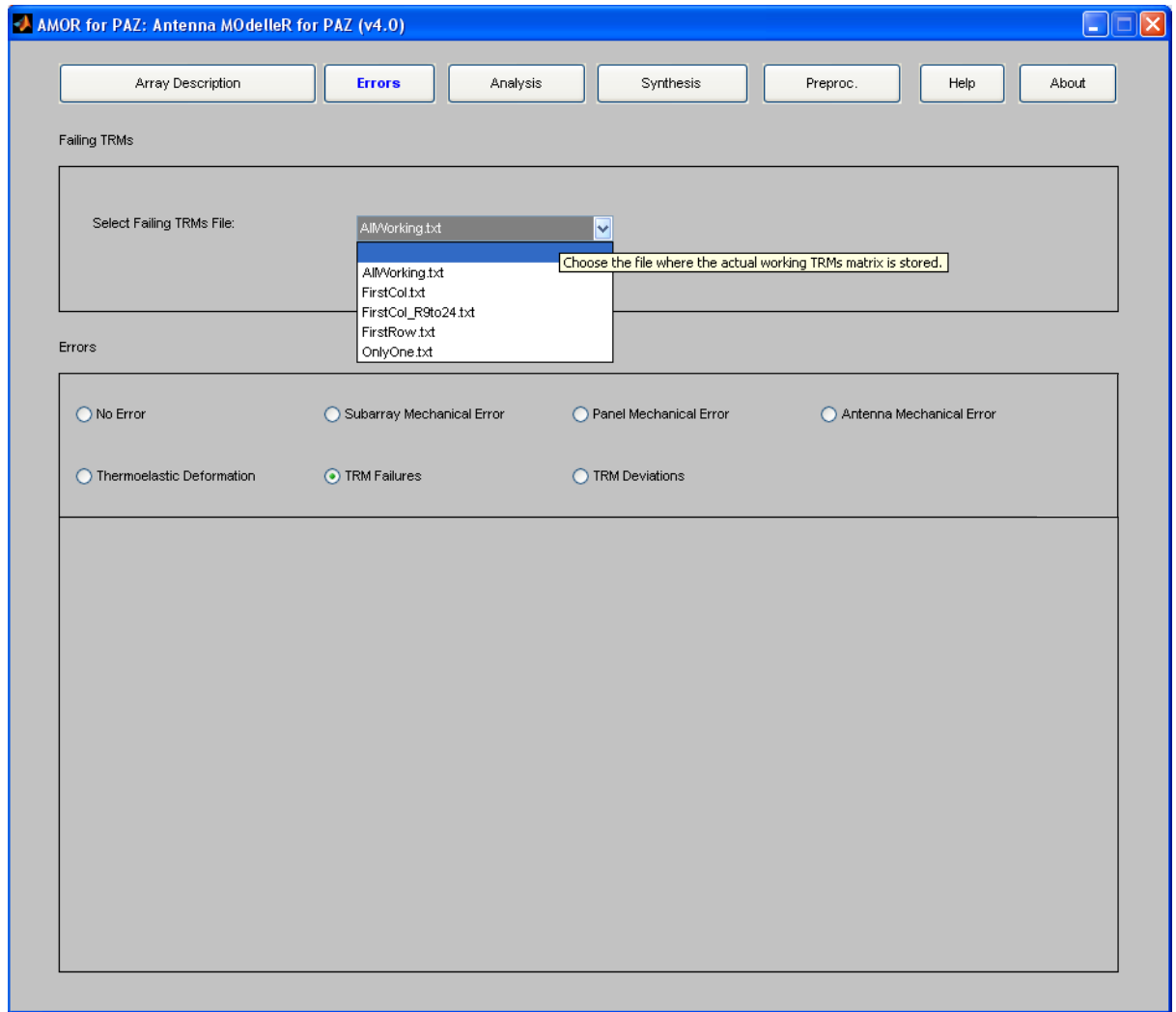


Fig.3.10: AMOR Errors window. The desired errors to be taken into account can be chosen.

After these preliminary adjustments, the *Synthesis* window of the AMOR simulator has to be selected. The Stripmap optimisation tool is placed in the left part of the window. Figure 3.11 depicts the initial state of the Stripmap optimisation window.

There are some hints indicating the required action to be done anytime in order to carry out the optimisation using the AMOR GUI. These hints appear when placing the pointer over a pushbutton, or an edit text box, for instance. In the Figure 3.11, the first step is to decide whether the swath filename to be used is the default one or not. The *Load Swath File* pushbutton has the hint "Press to load the chosen swath file" associated. The swath file, which is an excel file with a predefined format, contains information on the possible swaths of the Stripmap operating mode, such as the default PRF or the desired pointing direction. This information defines the main characteristics of the desired Stripmap beams, and is part of the information required to optimise each of them.

Once the chosen file containing information on the swath is loaded, some beam characteristic parameters are printed on the window, along with the more relevant GA parameters. This is shown in Figure 3.12.

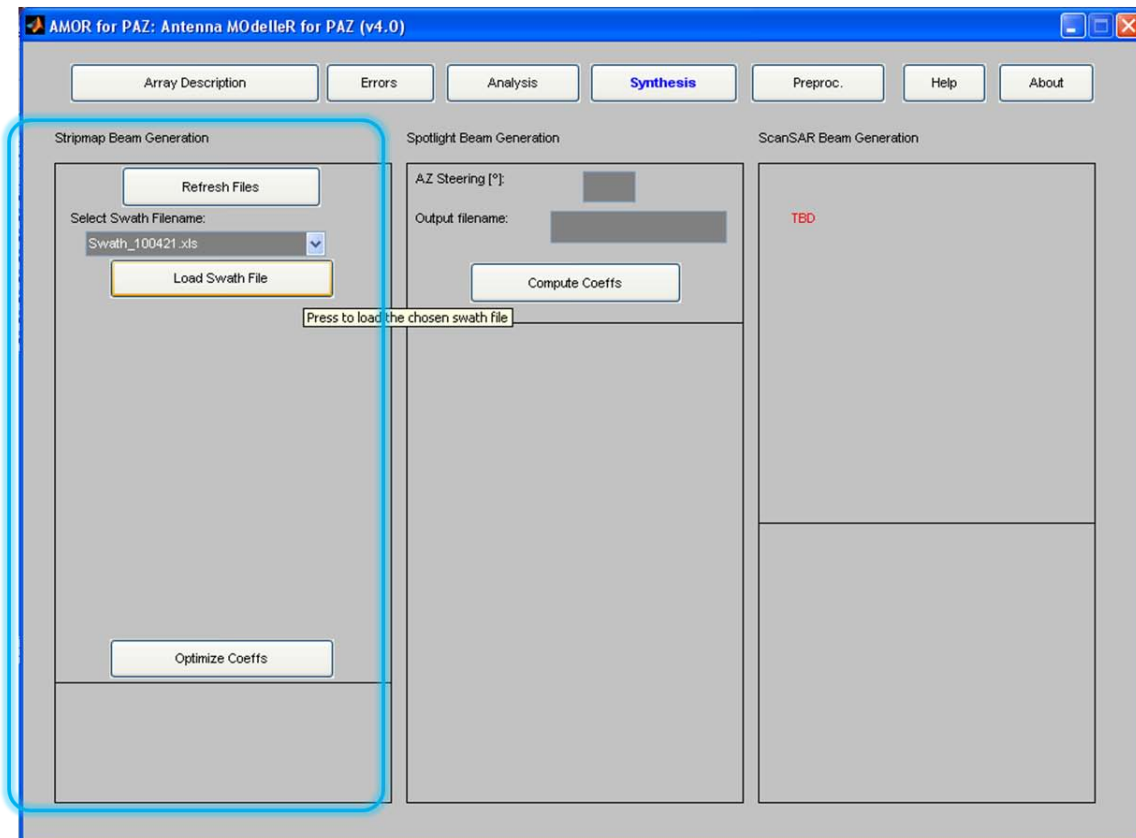


Fig.3.11: AMOR Synthesis window. The Stripmap optimisation is placed in the left part of the window, under the name Stripmap beam generation, and is marked in blue.

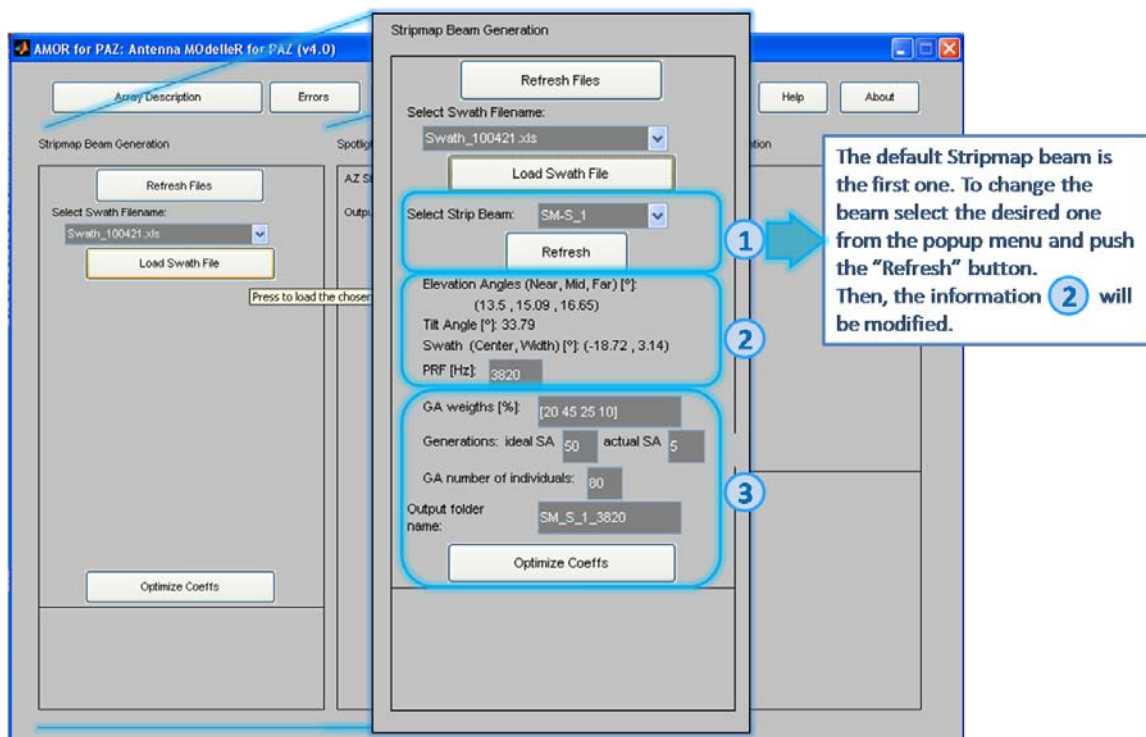


Fig.3.12: AMOR Synthesis window. Beam information of the first Stripmap beam, SM-S_1, (second blue square), and relevant GA parameters (third blue square) appear in the Stripmap Beam Generation window right after pushing the Load Swath File button. Since the SM1 may not be the desired beam to be optimised, a popup menu to select the desired one also appears. By means of selecting the strip beam name and pushing the Refresh button, the information printed on the window relative to the beam characteristics is actualised.

After pushing the *Load Swath File* button, information on the first Stripmap mode, SM-S_1, appears printed in the *Stripmap Beam Generation* window (blue square 2 in Figure 3.12). The SM-S_1 is the default value for the strip beam, but one might want to optimise another beam. For this reason, a popup menu with a list of the possible beams for the swath defined also appears (blue square 2 in Figure 3.12). Choosing the desired Stripmap beam and pushing the *Refresh* button, the beam information printed in the window changes. Finally, some relevant GA parameters are also printed in the window inside edit text boxes. These parameters are editable by the user. These values are made editable in order to allow the user to interact with the algorithm, but they need to be chosen carefully since, as explained in previous sections, its values are not easily deduced by mere intuition.

Note that the design parameters are neither editable nor visible. Remember that these parameters are: the mean gain in the swath, the RASR, the ΔG within the swath (considering the R^3 correction) and, optionally, the gain at nadir with respect to the gain at maximum. The objective is to achieve the maximum mean gain in the swath, the minimum possible value of RASR in the swath, the minimum gain variation within the swath and, if specified, the minimum possible gain in nadir. The GA is a global optimizer, and hence the pattern best fitting all the mentioned requirements at the same time (or reaching a convenient trade-off of its values) will be the optimal.

Once the desired strip beam is selected (in this example SM-S_1) and the GA parameters are checked, by pressing the *Optimize Coeffs* button the algorithm described in Figure 3.7 begins to run. During the optimisation, the following information is printed in the Matlab® command window:

```

1 Stripmap Optimization: Defining templates.
2 Stripmap Optimization: Computing ambiguities.
3 Stripmap Optimization: Computing radiated power of the ideal subarray of resonators.
4 Stripmap Optimization: Generating the GA initial population.
5 Stripmap Optimization: Starting the GA for an antenna having the subarray of ideal resonators.
6 Stripmap Optimization: ideal Subarray, computed generation: 1 of 50
...
54 Stripmap Optimization: ideal Subarray, computed generation: 49 of 50
55 Stripmap Optimization: ideal Subarray, computed generation: 50 of 50
56 Optimization terminated: maximum number of generations exceeded.
57 Elapsed time is 145.316804 seconds.
58 Stripmap Optimization: Computing the patterns of THE BEST RESULT for the antenna having the subarray of ideal resonators.
59 Stripmap Optimization: Computing the radiated power of the actual subarrays.
60 Stripmap Optimization: Loading the elevation patterns of each actual subarray.
61 Stripmap Optimization: Adding the best solution of the ideal antenna to the GA initial population of the actual antenna.
62 Stripmap Optimization: Starting the GA for the actual antenna.
63 Stripmap Optimization: actual Subarray, computed generation: 1 of 5
64 Stripmap Optimization: actual Subarray, computed generation: 2 of 5
65 Stripmap Optimization: actual Subarray, computed generation: 3 of 5
66 Stripmap Optimization: actual Subarray, computed generation: 4 of 5
67 Stripmap Optimization: actual Subarray, computed generation: 5 of 5
68 Optimization terminated: maximum number of generations exceeded.
69 Elapsed time is 96.335307 seconds.
70 Stripmap Optimization: Computing the best result for the actual antenna.
71 Stripmap Optimization: Plotting ALL THE ANALYZED excitations for the antenna having the subarray of actual resonators.
72 Stripmap Optimization: Plotting THE BEST excitation for the antenna having the subarray of actual resonators.
73 Stripmap Optimization: Saving the resulting coefficients from optimization.
74 Stripmap Optimization: Computing accurate patterns for GA solution.
75 Computing the spherical mode expansion for the TX beam...
76 Max. Directivity TX Pattern [dBi] (spherical modes, coarse sampling): 45.479
77 Max. Directivity TX Pattern [dBi] (pattern integration, coarse sampling): 45.479
78 Computing the spherical mode expansion for the RX beam...
79 Max. Directivity RX Pattern [dBi] (spherical modes, coarse sampling): 42.595
80 Max. Directivity RX Pattern [dBi] (pattern integration, coarse sampling): 42.596
81 Stripmap Optimization: Plotting TX, RX and 2W patterns.
82 Stripmap Optimization: Results saved in text file...
83 Stripmap Optimization: Erasing variables.
84 Stripmap Optimization: GA optimization ended.
```

The lines 3-61 are the correspondent to the initial quick optimisation from ideal SAs. In this example, the parallelization is not used; however there is the option of using it. Parallelisation is used to make the optimiser more efficient in time consumption. The Matlab® parallelisation tool¹ evaluates the parallelisation possibilities of the hardware used to perform the optimisation and decides if the parallelisation is possible and which number of labs the hardware allows working with.

The lines 62-72 correspond to the optimisation using actual SAs. Since the computations using measured data are slower and the coarse optimisation using ideal SAs is quite precise, only 5 generations are carried out. Note that 5 generations using actual SAs take around 96s while the 50 generations using ideal SAs take around 145s, in this example. Therefore, the total time to optimise is approximately 4 minutes.

The most time consuming part is the one described in lines 73-80; i.e. the computation of the exact directivities of the beams using the spherical mode expansion. It can take more than 10 minutes, depending on the computer used. +

During the optimisation, many figures are plotted. The first figure appearing is the one containing information on the progress of the optimisation using ideal SAs, as shown in Figure 3.13. While running the optimization code the best solution of the more recent iteration is plotted together with its predecessors:

- In the upper part of the figure:
 - in blue, the present iteration solution;
 - in green, the former solutions.
- Down:
 - in blue, the present iteration solution swath without R^3 correction;
 - in red the present iteration swath with R^3 correction;
 - in green the past iterations solution swaths without R^3 correction;
 - and in magenta, the past iterations solutions with R^3 correction.

In addition, information on the maximum gain within the swath, the worst RASR value, the gain at nadir with respect to maximum gain within the swath, the difference in dB between the maximum possible gain and the average gain in the swath, the gain variation within the swath with R^3 correction and the same variation without R^3 correction is provided for the present iteration.

During the optimization process, this figure is replaced by the one containing exactly the same information but for the GA using the actual SA, as further explained. The only of both figures remaining on the screen when the optimization process terminates is the corresponding to the evolution of the GA using the actual SA.

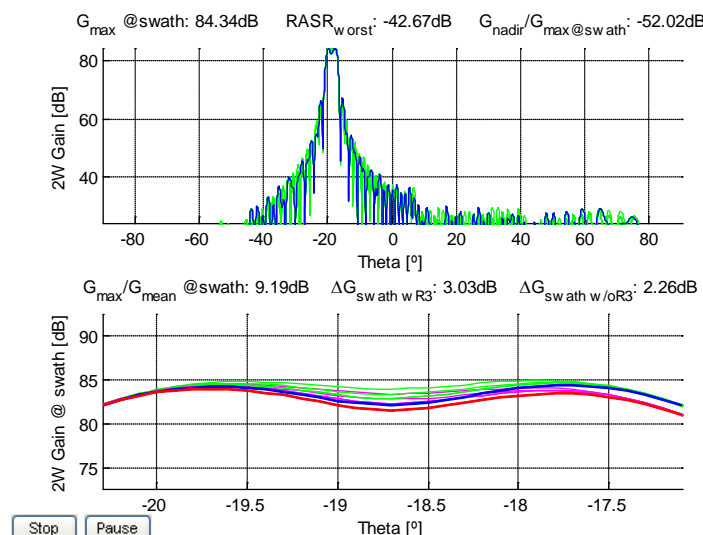


Fig. 3.13: Figure containing information on the evolution of the first optimisation, using ideal SAs. The figure shown is a screenshot of the evolution of the beam for the GA using the ideal SA, although at the end of the optimization the figure remaining on the screen is the one corresponding to the algorithm using the actual SA.

¹ To use the Matlab® parallelization tool it is necessary to have acquired the correspondent toolbox, which is optional and has to be bought apart.

At the end of the first optimisation, the one with the GA using the ideal SA, the optimization using the actual SA begins. The figure above shown is replaced by the one showing the evolution of the second phase of optimization (Figure 3.14), which remains present in the screen at the end of the whole optimization process together with 5 more figures.

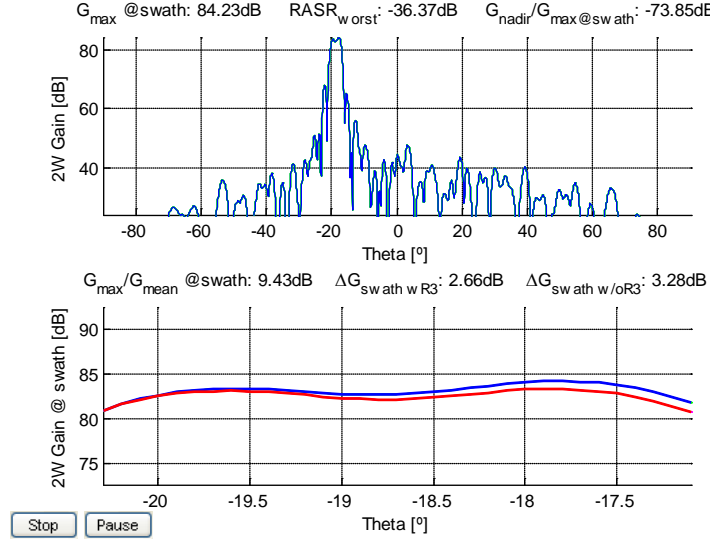


Fig. 3.14: Figure containing information on the evolution of the second optimisation, using actual SAs.

In this case, the evolution can not be appreciated (there are no different beams in green or magenta) just because there is no evolution. Since no errors and no measured data are introduced in the considered actual SA, this SA is exactly the same as the one considered in the ideal GA optimisation. Therefore, little evolution with respect to the GA using the ideal SA is expected.

Another of the resulting figures contains information on the mean ΔG_{wrtmax} , $RASR_{worst}$, and $\Delta Gain_{wR3}$ of all the individuals in all generations (Figure 3.15), and the one shown in Figure 3.16 contains information on the same parameters commented on the former figure, but only for the best individual of each iteration. Only one result is observable in Figure 3.16, for the reason explained in the last paragraph.

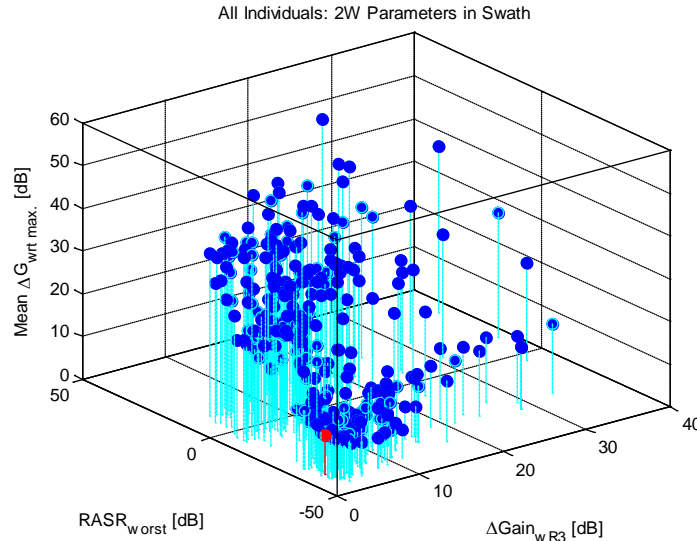


Fig. 3.15: Figure containing information on the evolution of the first optimisation, using ideal SAs. It shows the values of the mean ΔG_{wrtmax} , the $RASR_{worst}$ and the $\Delta Gain_{wR3}$ for all the individuals in the population and for all the iterations carried out.

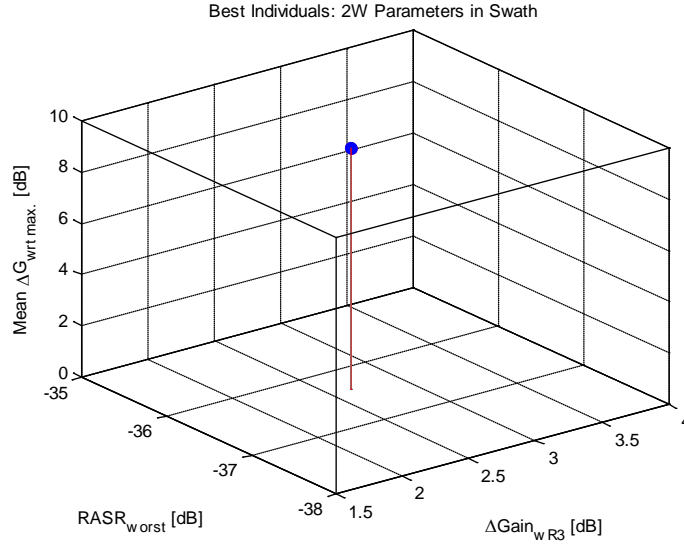


Fig. 3.16: Figure containing information on the evolution of the first optimisation, using ideal SAs. It shows the values of the mean $\Delta G_{wrt max}$, the $RASR_{worst}$ and the $\Delta Gain_{w R3}$ only for the best individuals in the population and for all the iterations carried out.

Finally, three figures with information on the optimum beam for the optimisation using both the ideal SA and actual SA are plotted: one figure with the TX beams, another figure with the RX beam, and a figure with the 2W beams - with R3 compensation (Figure 3.17).

In all them, directivities for the ideal SA are quickly computed using the method described in 2.2.2.2, while for the actual SA are computed using the methods described in 2.2.2.3 (pattern integration) and 2.2.2.4 (spherical modes expansion).

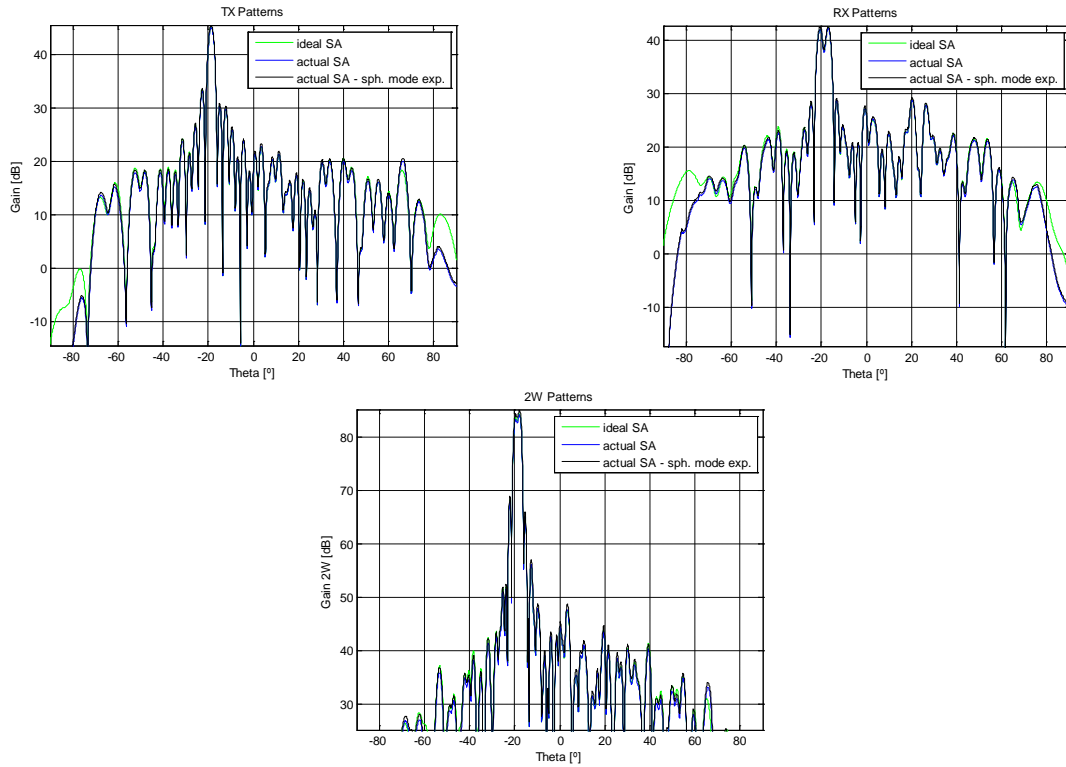


Fig. 3.17: Optimised beam: TX (left up) RX (right up) and 2W (down) gain EL pattern cuts. Both the result for the GA considering the ideal and the one considering the actual SA are presented. For the one considering the actual SA, the result is presented using two different methods for the directivity computation.

In addition, important information on the solution is printed in the *Stripmap Beam Generation* window. This information is highlighted in a blue rectangle in Figure 3.18.

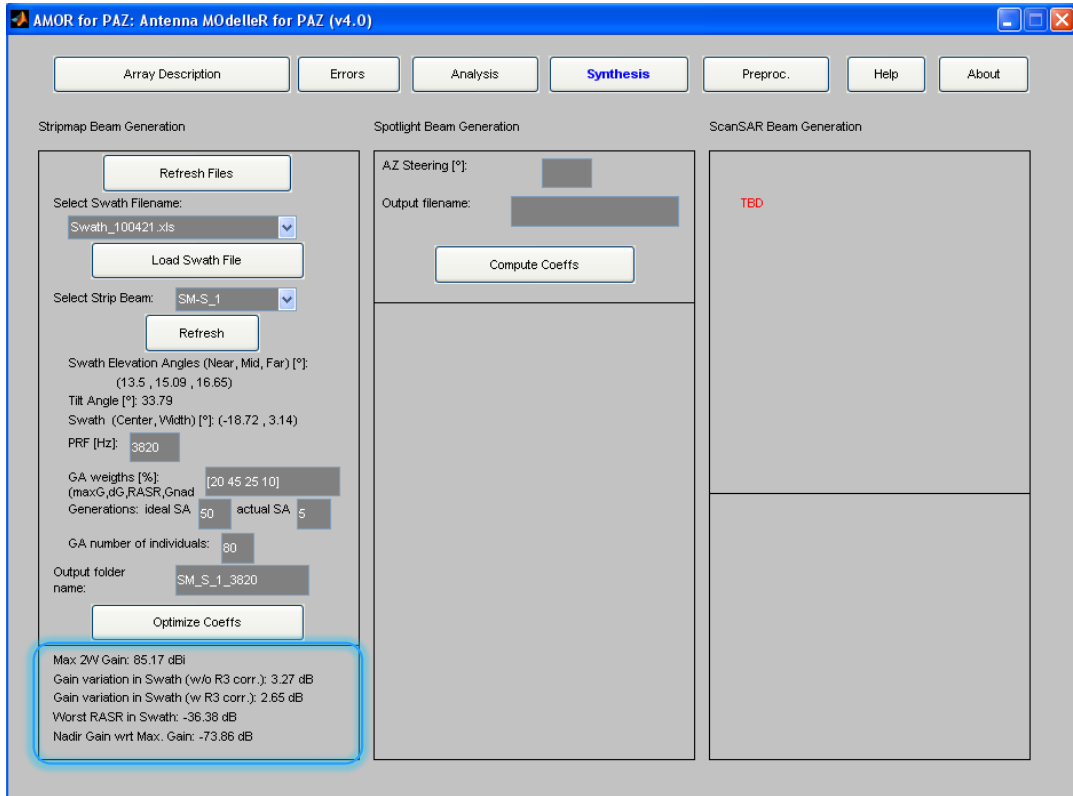


Fig. 3.18: Information on the optimised beam is printed in the *Stripmap Beam Generation* window: the mean 2W gain, the gain variation within the swath (with and without R3 correction), the worst RASR value and the nadir gain with respect to the maximum gain in the swath.

In the example, the requirement of obtaining a variation of the gain within the swath less than 2dB is not fulfilled. In the next section, solutions to the eventual problems encountered when optimising a beam are presented after a detailed study on the effect of some GA options modifications.

3.3 Optimisation Tool Results and Guidelines

The use of the optimiser is not trivial. Although the main decisions are taken by the optimiser, the final decision on whether the result is optimal or not (it matches the specifications) has to be taken by the user. This does not mean that the optimizer is not doing its job, but that the user could have introduced wrong values in the input editable text boxes of the Synthesis window of AMOR. Therefore, at the end, the user has to do the effort of tuning the input parameters according to the beam synthesized. To tune correctly the algorithm helps in reducing the execution time needed to reach the optimal solution.

A sufficiently fulfilled set of specifications for a far range swath, for instance, would be to reach a reduced gain level at Nadir with respect to the maximum gain (under -60dB), an acceptable maximum gain (not too low knowing that the boresight maximum for the PAZ specific antenna is 92.8dB approximately – see Equation 3.10), a good variation of the gain within the swath (maximum 2dB) but a bad RASR level. In far range swaths the RASR is expected to be bad (well above the restriction of -20dB taken as design parameter in the examples – see Figures 3.24 and 3.25). As mentioned in previous sections, all this terms contribute to extract an overall fitness value, the lower the better (since the objective is to minimize the cost). None of the solutions is dismissed if some of the parameters determining the fitness value do not fulfil the specifications; all of them contribute to the optimizer convergence to an optimal result.

The aim of this section is to establish the guidelines to make the most of the optimiser. The SM-S_1 strip beam optimisation is studied by means of observing its repeatability, and changing different GA parameters. At the light of

the results, the AMOR optimiser is characterised and some hints to efficiently use it are listed. At the same time, by reading this section, the AMOR potential user can discover the eventual hazards that he or she might face during the optimisation procedure.

After establishing a methodical procedure, it is applied to three test cases based on real specifications for three different strip beams. The proposed examples are described in terms of radiometric parameter constraints. They will help the reader to completely understand the meaning of the different steps of the optimization tool design described in recent sections. They also help extracting conclusions which could be applied in further revisions of the optimizer in order to continue improving its performance.

3.3.1 Characterisation of the Optimiser Behaviour

As mentioned before, this section intends to characterise the Optimiser behaviour by means of varying the mean parameters modifiable by the user. This study is aimed to save time to a potential user of the software, performing first attempt simulations. The objective is to demonstrate which the adequate changes to be applied to the initial settings are in order to quickly converge to a fairly adequate solution.

The initial simulation, carried out with the default configuration of the different input parameters, referred as Simulation 1 hereinafter, is the starting point of all the variations examined in the following sections. Its GA configuration parameters are gathered in Table 3.7:

GA weights (Maximum gain in swath, gain variation in swath, RASR, nadir gain wrt maximum gain in swath)	20% 45% 25% 10%
Number of individuals per generation	80
Number of generations for ideal SA GA	50
Number of generations for actual SA GA	5

Table 3.7: Default GA configuration parameters.

The results when executing the optimizer code can be found in Table 3.8:

Maximum 2W gain (computed using spherical modes)	85.38 dBi
Gain variation in swath (without R^3 correction)	3.23 dB
Gain variation in swath (with R^3 correction)	2.36 dB
Worst RASR in swath	-37.54 dB
Nadir gain with respect to maximum gain	-67.51 dB

Table 3.8: Results of Simulation 1.

The figures obtained from this execution of the optimizer are gathered in Table 3.9. The first two figures show all the results obtained corresponding to the main design parameters for all the individuals assessed (first figure) and for only the best individuals (second figure), only for the GA using the actual SA. The third figure shows the evolution of the optimized beam while the GA using actual SA evolves: in the upper part of the figure, the blue beam is the solution one while the green beams are the best of previous generation; in the lower part of the figure, the blue line corresponds to the solution pattern swath without R^3 correction, the red line to the solution pattern swath with R^3 correction, the green lines to the previous best individuals swaths in their correspondent generations without R^3 correction, and the magenta lines to the previous best individuals swaths in their correspondent generations with R^3 correction. The fourth, fifth and sixth figures show the resulting 2W, TX and RX beams: in green the resulting beam of the GA using ideal SA, in blue the resulting beam of the GA using the actual SA, and in black the resulting beam of the GA using the actual SA with the directivity computed using the spherical mode expansion method.

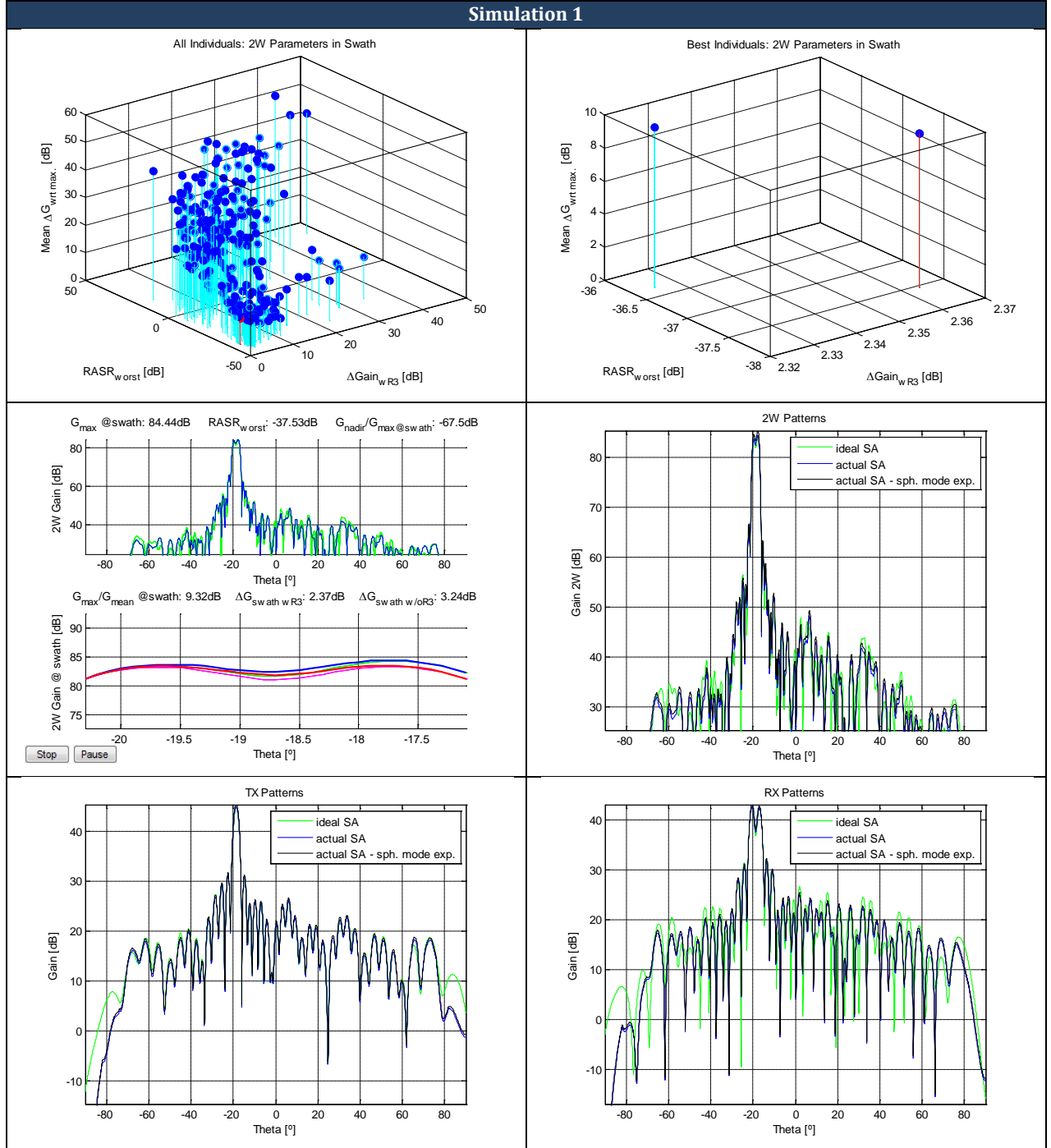


Table 3.9: Resulting figures after executing Simulation 1. They show all the results obtained corresponding to the main design parameters, for the GA using the actual SA; the evolution of the optimized beam while the GA using actual SA evolves; and the resulting 2W, TX and RX beams both for the algorithm considering the ideal and the actual SA.

As previously mentioned, one of the outputs of the GUI is a text file containing the feeding coefficients to obtain the optimised beam pattern. They are plotted and presented in Table 3.10 for Simulation 1:

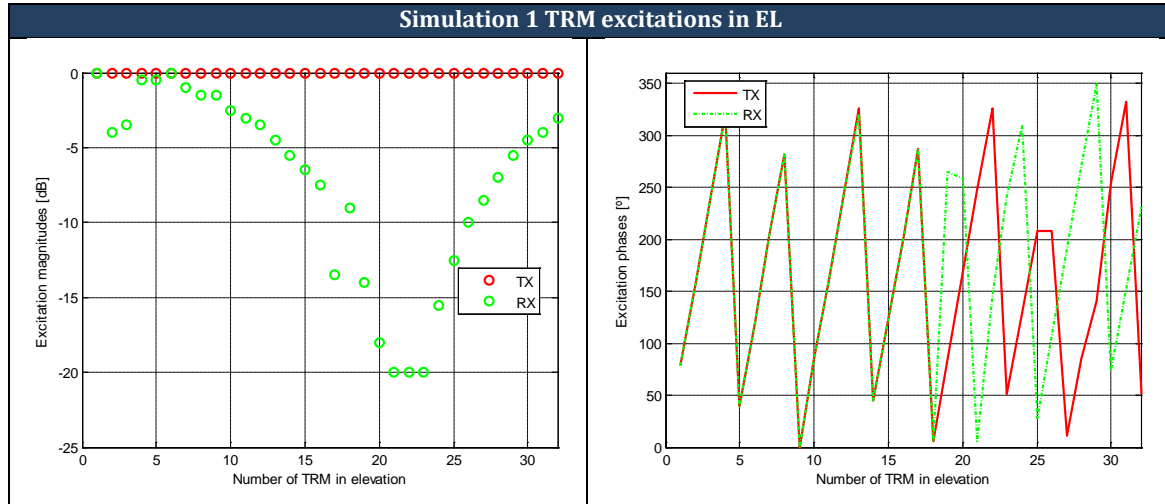



Table 3.10: Representation of the optimal feeding coefficients magnitudes and phases (TX and RX) in Simulation 1. The first figure shows the TX magnitudes for the TRMs in EL plane. The second figure shows the RX excitation magnitudes in the EL plane. Finally, the third and fourth figures show the TX and RX excitation phases in the EL direction.

Remember that the TRM excitation magnitudes and phases are constant in the AZ direction, and for this reason they are not represented in the former figures. In the phase plots it is evident the linear component of the phase, which indicates the beam steering applied.

As explained in previous sections, the specifications fix that the maximum tolerable gain variation in swath (since the specifications are from the radiometric point of view, this gain variation is specified taking into account the R^3 correction) is 2dB. In Simulation 1 the value obtained is 2.36 dB, and does not fulfil the mission needs. The RASR has to be below or equal to -20dB, and the worst RASR value in this case is -37.54 dB. Therefore, the RASR specification is widely fulfilled. The nadir gain with respect to the maximum gain is considered sufficiently low reaching a -60dB value. In this case it is considered that there is a null in the nadir direction. In Simulation 1, the null condition is fulfilled even having assigned a 10% to the correspondent weight of the fitness function. *A priori*, it is difficult to say which the adequate gain is. It can only be assured that the maximum gain possible is desired, and that the maximum achievable gain for the considered array antenna is the one in Equation 3.10 (as mentioned in section 3.2.4.2):



$$G_{max_{1Way}} = 10 \cdot \log_{10} \left(\frac{4\pi \cdot A_{geom}}{\lambda^2} \right) \sim 10 \cdot \log_{10} \left(\frac{4\pi \cdot (4.8m \times 0.7m)}{\lambda_{9.65GHz}^2} \right) = 46.40 \text{ dB}$$

Equation 3.10

This implies that the maximum achievable 2-Way gain is approximately 92.80 dB. However, this value is the maximum achievable at boresight, and the steering of the beam implies degradation in the gain value. In addition, this value is the maximum achievable having a uniform feeding distribution, and with this kind of distribution a pencil-beam like pattern is obtained. Since a maximum gain variation in the swath is imposed, and this implies a certain flatness of the swath, the maximum gain will be also affected for this condition and will be even lower. The gain obtained in Simulation 1 is 85.38 dBi, and hence 7.42 dB under the maximum achievable value. However with only one optimisation it can not be affirmed if this is a good or a bad value.

Starting from Simulation 1 different simulations are performed in order to determine whether the results obtained can be improved, and, if so, how can they be improved. In the following sections the variations performed are the following:

- *Repeatability of the experiment:* 9 new simulations under exactly the same conditions than in Simulation 1 are performed. This is made in order to evaluate the repeatability of the same experiment, knowing that the GAs are intrinsically random, and to establish if a huge or a little variation in results is obtained between different realizations of the same experiment. In principle, a huge variation is not desired. This can imply that the fitness function is not well designed and that the optimizer user would be exposed to uncertainty or that little iterations have been performed.
- *GA weights variation:* 7 new simulations varying the GA weights controlling the importance of fulfilling each of the four principle radiometric specification parameters (maximum 2W gain, maximum gain variation in the

swath, worst RASR in swath, and gain of the null in Nadir with respect to the maximum gain in swath) are performed.

- *GA number of generations' variation:* increasing progressively the number of ideal generations in the 9 first simulations (the ones considering the ideal SA pattern), and also of actual generations in the last 9 simulations (the ones considering the actual SA pattern), the objective is to determine if the results can be improved by doing so².
- *GA number of individuals in the population variation:* according to Rahmat-Samii [3.4], approximately four or five times the binary individual length is the adequate number of individuals in the population in order to quickly converge to an optimal solution in a GA binary problem. This means that in our case, having individuals of 384 bits, the ideal number of individuals would be between 1536 and 1920. By default, this parameter is set to 80 in our tool, which is very far from the indicated one. This number is varied progressively along 9 new simulations, up to 1600. The objective is to determine whether this parameter has a high or a low influence in the improvement of results obtained in Simulation 1.

With this 35 simulations a preliminary optimizers' behaviour statistical study is carried out. From them, conclusions on the optimizer performance can be extracted and some utilization guidelines can be indicated.

3.3.1.1 Repeatability of the experiment

First of all we compare the results of Simulation 1 with 9 more different sets of results under the same conditions (no changes in the editable parameters in the *Stripmap Beam Generation* window). All the results are gathered in Table 3.11 in order to facilitate the comparison of the different simulations.

Simulation number	Maximum 2W gain (computed using spherical modes) [dBi]	Gain variation in swath without R ³ correction [dB]	Gain variation in swath with R ³ correction [dB]	Worst RASR in swath [dB]	Nadir gain wrt maximum gain [dBi]	Total fitness
1	85.38	3.23	2.36	-37.54	-67.51	34.49
2	85.55	3.14	3.67	-40.44	-82.07	37.98
3	84.88	2.43	1.99	-34.76	-80.22	33.87
4	84.34	1.67	1.16	-34.64	-42.98	36.85
5	85.38	3.23	2.36	-37.54	-67.51	34.49
6	85.55	3.14	3.67	-40.44	-82.07	37.98
7	84.88	2.43	1.99	-34.76	-80.22	33.87
8	84.34	1.67	1.16	-34.64	-42.98	36.85
9	84.51	2.25	1.72	-33.99	-67.49	33.45
10	85.38	3.23	2.36	-37.54	-67.51	34.49

Table 3.11: Main resultant parameters when repeating the same simulation (different realisations of the same experiment). Results which are equal between them are marked with the same colour. In blue, results 1, 5 and 10 are equal between the, result 6 is equal to result 2, results 4 and 8 are equal between them, and result 9 is not equal to any other result.

All the results have been generated in different hours and some of them in different days. However, the results are not totally different between them. In fact there are only 5 different results out of 10 simulations. This may seem surprising because the GA behaviour is random. But in fact, ideally (if the algorithm would have been run a sufficient amount of time) the result must be always the same, because the GA is a global optimisation technique. Indeed, the obtained result is not negative at all. It means that although the algorithm to find the optimal solution is random, given the same algorithm settings (number of generations, number of individuals in the population, GA weights, etc) there is a closed set of possible solutions in the short-term. This is positive in the sense that the user has not a high uncertainty in knowing whether if repeating the same experiment highly better results may be obtained.

² Remember that using the ideal SA configuration means that the GA uses a cut of the ideal SA pattern described by Equation 3.10, and equally spaced SAs without any failure in the TRMS or positioning error. Using the actual SA configuration means that the whole pattern generated by the array is considered (3D pattern), and all kind of possible errors are included (positioning of the SAs in the antenna, failures in the TRMs, etc.).

Another different thing is if the SA pattern considered in the analysis when using the actual SA comes from measures or from an analytical formulation. In the present study the SA considered patterns are created analytically, since measures were still not available in the moment that the Master Thesis document was prepared.

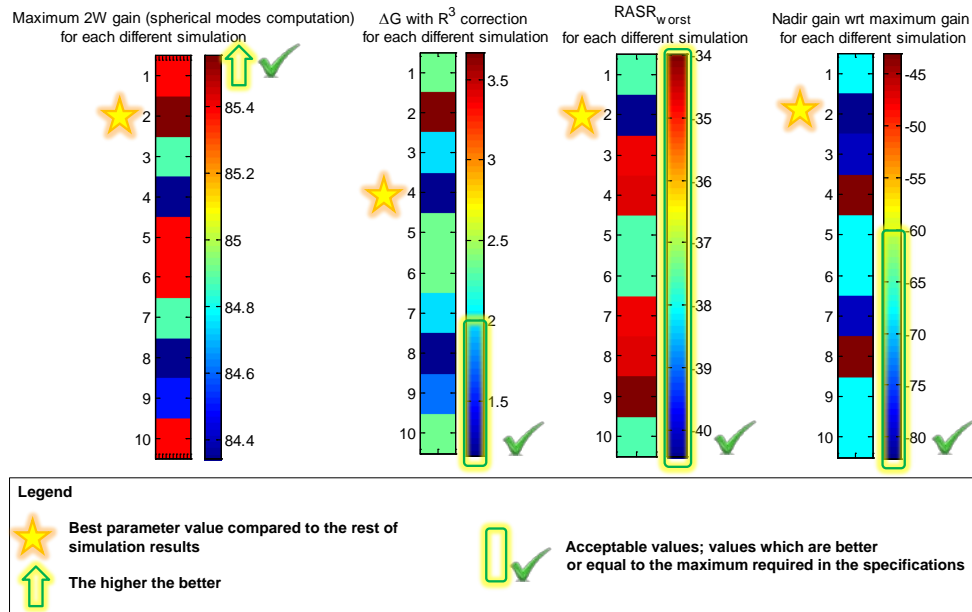


Figure 3.19: Colour plots representing the magnitudes of the different evaluated parameters for the different number of simulation.

But let's take a look to the results obtained in detail. In Figure 3.19, four different colour plots representing the magnitudes of the evaluated parameters for the different number of simulation can be observed. The first colour plot represents the maximum 2-Way gain, from Simulation 1 –the reference one- to Simulation 10. In this case the RASR is always better than the specified. Simulation 2 has the major number of best results (3 stars), except for the gain variation in the swath (3.67 dB) which is notably worse than the 2dB specified. If we concentrate in finding a good gain variation value, simulation 4 would be the best.

However, the null gain and the maximum gain values are poor in this case. Nonetheless, the simulation having a lower overall fitness function value is Simulation 9. Therefore it has to be considered as the best one. In fact, when paying attention to the values reached in this simulation, it turns out that it is the solution reaching the best trade-off between the different design parameters. This means that the fitness function is well designed, and represents mathematically through a single value (the total fitness value) the quality of a solution from a multiple-objective optimisation problem.

From this study it can be concluded that, as expected, when a good gain variation value is obtained (flat-top beam like pattern) the secondary lobes increase its value (therefore poorer null gain with respect to maximum gain values and also poorer RASR values are obtained) and the main lobe value is decreased. Another important conclusion is that the repeatability is fair good, which seems to confirm (even considering a low number of individuals in the population) that the algorithm does searches a fitness function global minimum, as desired.

3.3.1.2 GA weights variation

In this case the GA weights are varied in the 7 new simulations performed. Each variation of the weights performed in the different simulations has a reason (see Table 3.12), and the procedure is below explained:

- Since in Simulation 1, and as mentioned in the former section, the gain variation in swath is too high, the first weight that can be varied is the one related to the gain variation, w_2 . In Simulation 2 w_2 is increased a 10%, and hence the rest of the weights need to be readjusted. We choose to decrease in a 10% the weight w_3 , related to the RASR, since in Simulation 1 the RASR condition is widely fulfilled. With that change, the gain variation in the swath is slightly improved (from 2.36 to 2.16 dB) but the maximum 2W gain is also decreased (from 85.38 to 85.04 dB).
- Simulation 3 is intended to even outperform the results in Simulation 2. In this case, w_2 is increased in a 10% while w_3 and w_4 are decreased a 5%. This is an example of having surpassed the limit of weighting the gain variation in swath parameter in front of the rest. In this case the gain variation in swath obtained is very good, at the expense of having an extremely low maximum gain and a very bad RASR (although concordant with the weight assigned to this parameter in the optimization, of only a 10%). The fact that the nadir gain wrt max gain

is too high is not important, because it is also concordant with the weight assigned to this parameter in the optimization (5%).

- Simulation 4: at the light of the previous results, w_1 is increased a 5% and w_2 decreased a 10%, and w_3 is increased a 5% to compensate the total weighting that needs to be 100%. In this case it can be stated that all the results are satisfactory with respect to the weights assigned. The maximum gain is better (but not better than the initial 85.38 dB), the gain variation has not a good value, 3.34 dB, and the RASR is well below the maximum allowed (-20dB). In the case of the null gain, it has a good value with respect to the maximum considering that its correspondent weight has been set to only a 5%.
- Simulation 5: making less important the maximum gain and more the gain variation. Still too high gain variation value is obtained.
- Simulation 6 makes even more important the gain variation value, but compensates the high weight assigned to this parameter increasing the weight of the RASR. This is done knowing that the weights in simulation 3 have led to very bad results. Still too high gain variation.
- In simulation 7 the gain variation weight is even more increased. The gain variation is finally good enough, but the maximum gain is unacceptable, because it is more than 10dB below the maximum one reached in former simulations.
- Simulation 8 tries to improve the former results increasing a 5% the maximum gain weight, ending with even worse results.

Simulation number	w_1, w_2, w_3, w_4 [%]	Maximum 2W gain (computed using spherical modes) [dBi]	Gain variation in swath without R^3 correction [dB]	Gain variation in swath with R^3 correction [dB]	Worst RASR in swath [dB]	Nadir gain wrt max gain [dBi]
1	20, 45, 25, 10	85.38	3.23	2.36	-37.54	-67.51
2	20, 55, 15, 10	85.04	2.49	2.16	-37.57	-65.64
3	20, 65, 10, 5	68.82	1.30	0.58	-2.22	-18.75
4	25, 55, 15, 5	84.91	2.46	3.34	-39.64	-75.64
5	20, 60, 15, 5	85.39	3.13	2.38	-39.28	-64.82
6	20, 65, 15, 0	85.01	2.59	2.44	-37.65	-44.59
7	15, 70, 15, 0	80.72	1.38	1.01	-27.14	-37.39
8	20, 70, 10, 0	74.66	0.78	0.54	-12.72	-41.70

Table 3.12: Main resultant parameters when varying the GA weights controlling the importance of each design parameter in the optimization process.

From Figure 3.20 it can be affirmed that in this case the simulation having the maximum best results is simulation 4, with 2 stars corresponding to the RASR and null gain. However, the ΔG value is unacceptable. In general, Simulation 2 and Simulation 1 are the ones with the best overall results; although from Table 3.12 we know that the gain variation in swath is 2.16 dB and 2.36 dB, respectively, above the maximum tolerated.

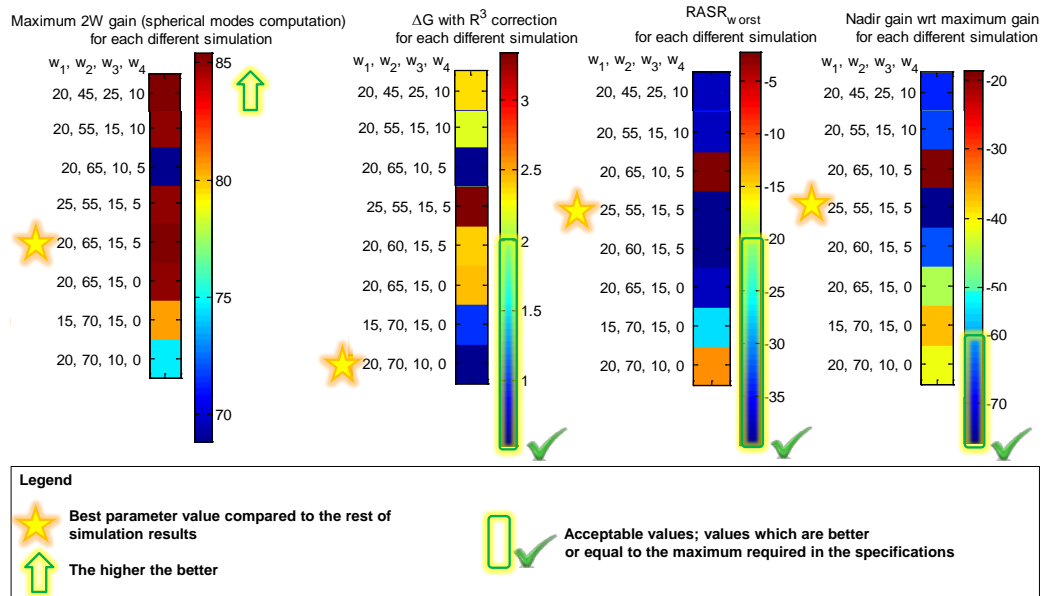


Figure 3.20: Colour plots representing the magnitudes of the different evaluated parameters for the different simulations.

In conclusion it can be stated that it is frankly difficult to adjust the GA weights. In this case, however, the starting weights (the default ones) have been previously adjusted when designing the optimizer. So the results confirm that the default values are the correct ones.

3.3.1.3 GA number of generations variation

First of all, the number of generations considered in the optimization which is varied is the correspondent to the ideal SA GA optimization, maintaining the rest of the default values (reference case, Simulation 1: Table 3.7). The starting number of generations is 50. Since the ideal optimization is, as previously mentioned, the quicker one, this number can be increased with less time consumption increment than in the GA using the actual SA. For this reason the simulations increase progressively the number of generations from 50 to 300, as briefed in Table 3.13:

Simulation number	Number of generations for ideal SA GA	Maximum 2W gain (computed using spherical modes) [dBi]	Gain variation in swath without R ³ correction [dB]	Gain variation in swath with R ³ correction [dB]	Worst RASR in swath [dB]	Nadir gain wrt max gain [dBi]
1	50	85.38	3.23	2.36	-37.54	-67.51
2	60	84.64	2.24	2.19	-34.08	-85.46
3	70	84.69	2.77	2.24	-34.28	-96.41
4	80	84.01	1.54	1.09	-32.67	-64.26
5	90	85.24	3.20	2.52	-36.56	-73.22
6	100	84.58	2.51	1.70	-37.24	-39.72
7	150	83.81	2.08	1.43	-29.19	-74.18
8	200	84.31	1.58	1.10	-36.80	-39.33
9	250	84.40	2.15	2.31	-34.19	-77.47
10	300	84.57	2.55	1.77	-34.10	-77.43

Table 3.13: Main resultant parameters when varying the number of generations in the GA using ideal SA.

In this case the analysis of the results is simpler: the increment of the number of generations in the ideal SA GA process has a fair effect in the improvement of the final results. As easily observed from Figure 3.21, as the number of generations increases, a trade-off between the different parameter values is reached: the maximum gain is not as high as initially, but the gain variation value is acceptable and the other parameters also fulfil the specifications.

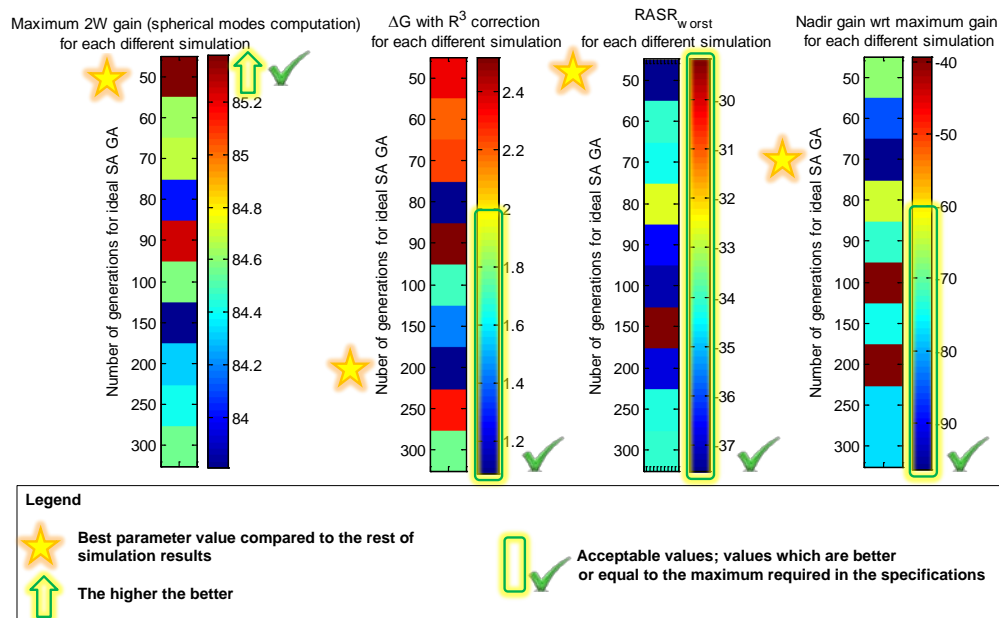


Figure 3.21: Colour plots representing the magnitudes of the different evaluated parameters for the different simulations.

If the number of generations increased is the corresponding to the GA using the actual SA, maintaining the number of generations of the GA using the ideal SA equal to the default one (Table 3.7), the results obtained are the ones gathered in Table 3.14 and Figure 3.22:

Simulation number	Number of generations for actual SA GA	Maximum 2W gain (computed using spherical modes) [dBi]	Gain variation in swath without R ³ correction [dB]	Gain variation in swath with R ³ correction [dB]	Worst RASR in swath [dB]	Nadir gain wrt max gain [dBi]
1	5	85.38	3.23	2.36	-37.54	-67.51
2	6	85.55	3.14	3.67	-40.44	-82.07
3	7	85.73	3.66	2.94	-36.89	-74.64
4	8	84.80	2.97	3.08	-38.66	-76.47
5	9	84.82	3.07	2.78	-31.54	-71.73
6	10	84.37	1.99	1.19	-31.99	-67.66
7	15	85.47	2.91	2.37	-39.91	-44.12
8	20	84.83	2.79	3.12	-37.79	-66.04
9	25	85.57	3.48	2.85	-35.30	-74.56
10	30	84.93	2.24	1.67	-33.03	-41.54

Table 3.14: Main resultant parameters when varying the number of generations in the GA using actual SA.

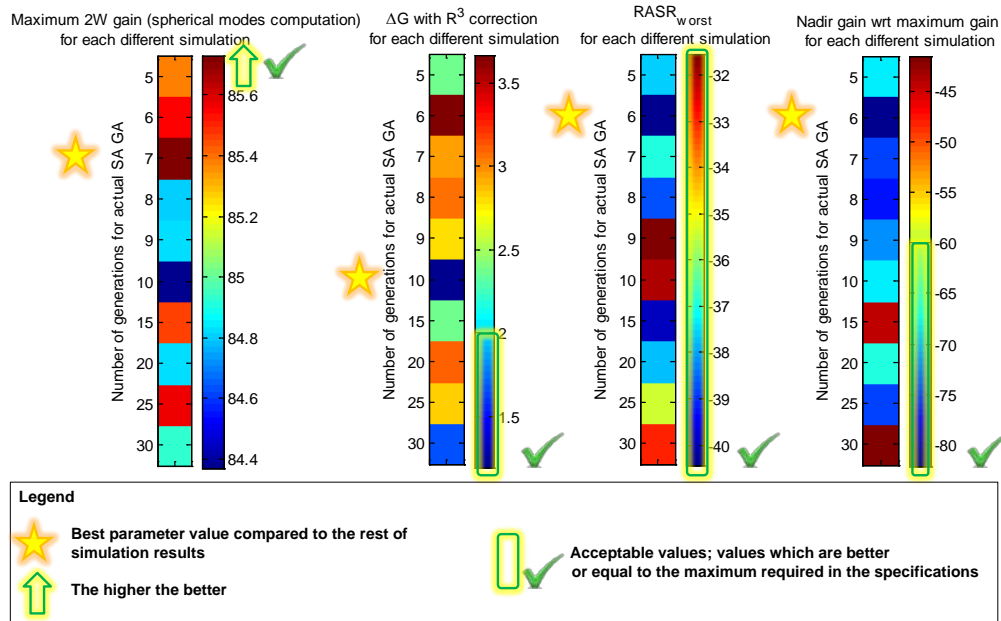


Figure 3.22: plots representing the magnitudes of the different evaluated parameters for the different simulations.

At the light of the results, it can be affirmed that increasing the number of generations in the GA using the actual SA has a good impact in the results obtained. The improvement of the results is slow but similarly to the ones obtained increasing the number of generations of the GA using ideal SA, reach a good trade-off between the different parameters.

Reaching similarly good results, it is preferable to increase the number of generations in the part of the optimization process using ideal SA, because it is less time-consuming.

3.3.1.4 GA number of individuals in the population variation

Ideally, the more individuals in the population, the quicker -in number of generation terms- the algorithm converges. The ideal number of individuals per generation is, as previously mentioned, between 1536 and 1920. In this section, the initial number of individuals, 80, is increased progressively up to 1600 in order to determine whether this parameter affects the improvement of the results obtained. The obtained results for the different simulations are gathered in Table 3.15.

Simulation number	Number of individuals per generation	Maximum 2W gain (computed using spherical modes) [dBi]	Gain variation in swath without R3 correction [dB]	Gain variation in swath with R3 correction [dB]	Worst RASR in swath [dB]	Nadir gain wrt max gain [dBi]
1	80	85.38	3.23	2.36	-37.54	-67.51
2	100	84.73	2.95	3.12	-34.64	-70.27
3	150	85.10	2.63	2.76	-35.31	-72.92
4	200	84.69	2.13	1.88	-38.94	-92.72
5	250	84.60	2.27	1.54	-33.15	-83.12
6	300	85.15	2.64	2.09	-38.38	-91.75
7	350	85.38	2.70	2.22	-36.10	-70.33
8	400	85.10	2.91	2.76	-40.72	-90.79
9	800	84.87	2.31	1.63	-32.08	-77.89
10	1600	83.89	1.55	0.81	-30.65	-86.68

Table 3.15: Main resultant parameters when varying the number of individuals in the population.

In this case, the last result is highly better in terms of ΔG than the ones obtained varying the number of generations. The maximum gain is not as good as desired, but it is the price to pay to obtain such a low gain variation in the swath value. In Figure 3.23 it can be easily appreciated that absolutely all the simulations fulfil the RASR and nadir null specifications. Then, concentrating on the other two parameters, it is observable that the maximum gain reduction is associated to the ΔG reduction. A good trade-off is reached in Simulation 9, where $\Delta G = 1.63$ dB and $G_{\max} = 84.87$ dBi.

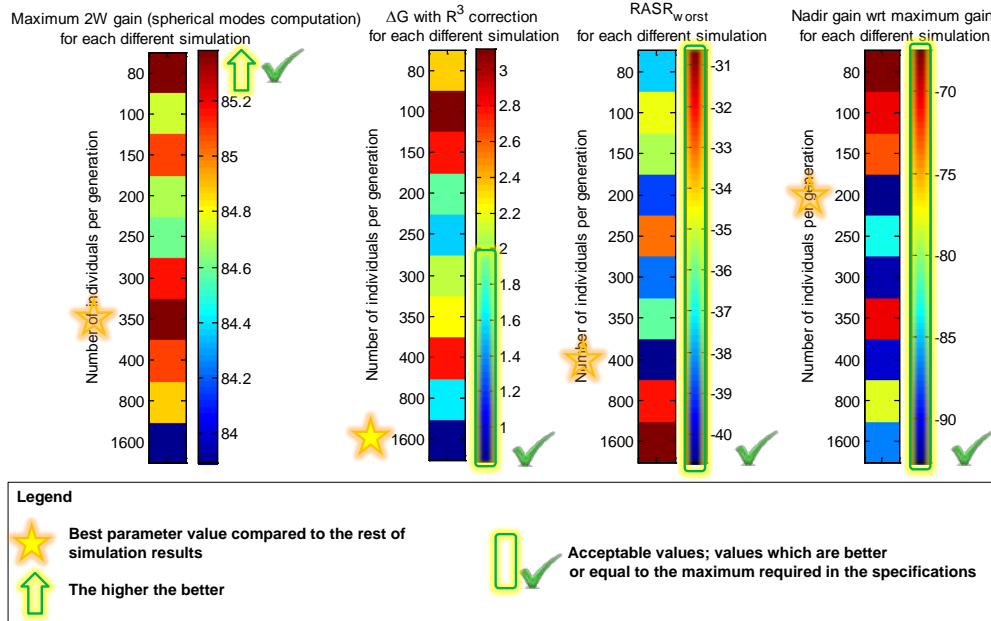


Figure 3.23: plots representing the magnitudes of the different evaluated parameters for the different simulations.

3.3.2 Optimiser Guidelines

At the light of the results obtained in the study undertaken in the last section, the guidelines to be followed when optimising a Stripmap beam are the following:

1. Set the number of individuals per generation at least to 400 or 800. Ideally the more the better, however 400 or 800 provide sufficiently evolved results in an acceptable period of time considering a trade-off between algorithm performance and time consumption.
2. Start optimizing using the default parameters (Table 3.7), except for the number of individuals per generation and the number of generations in the GA using the actual SA, where the recommendation is to set it at least to 10.
3. If the results are not satisfactory enough, reasonably vary the GA weights in order to find the adequate combination which provides the more adequate results.
4. If the results are still not satisfactory enough increase the number of generations for the GA using the ideal SA up to 300 (in order to save simulation time).

It is important to note that some specifications are impossible to fulfil when optimising determined beams. For instance, there is a limit in optimising the RASR parameter when the beams optimized are far range. To exemplify the situation, Figures 3.24 and 3.25 contain the RASR vs. incidence angle for the 26 different SM-S beams (Stripmap single polarization beams) for minimum and maximum orbit altitude, respectively. This parameter increases monotonously up to 0 dB at 60° of incidence angle (the SM-S₂₆ beam at an altitude of 536 Km). As the internal document on the instrument performance analysis (elaborated by the ECE team [3.5]) from where the figures have been extracted explains, the data has been simulated using SAR Tool (© EADS Astrium, UK) because this functionality has still not being completely implemented into the PAZ Antenna Model when the document was redacted.

In AMOR, the input swath file used in the Stripmap optimisation tool contains the geometric and signal parameters for an orbital height of 505 Km, and hence the reference figure to compare our results with is Figure 3.24. The basic element polarization used is H. As seen in the SM-S₂₆ case in Figure 3.24, the worst RASR in the swath can be worse than -2dB in H polarization for an altitude of 536 Km. For an altitude of 505 Km, this RASR for the Stripmap beam 26 is not as worse as -10 dB.

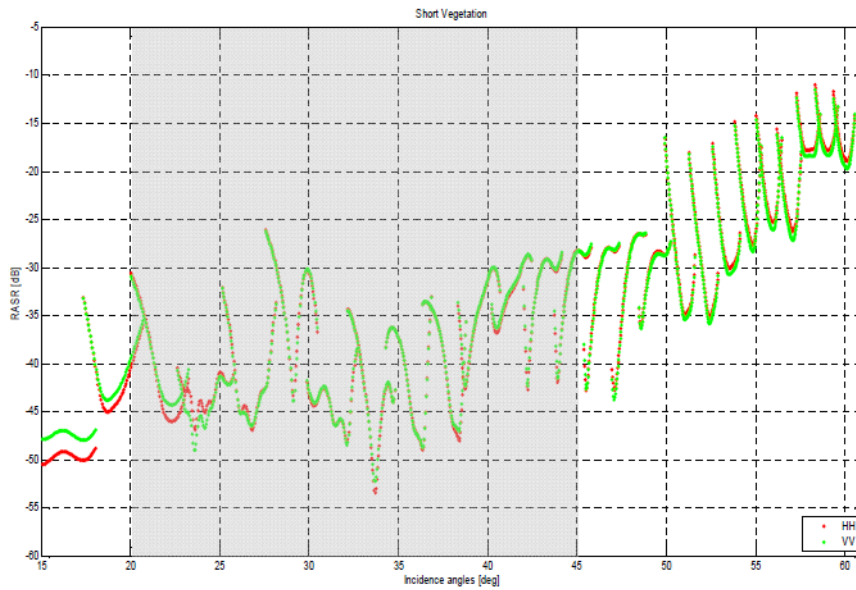


Figure 3.24: RASR vs. Incidence angle for an orbit height of approximately 505 Km. Figure extracted for an internal report written by the ECE team on the instrument performance analysis. This figure is valid only for the SM-S mode (Stripmap Single polarization mode) [3.5].

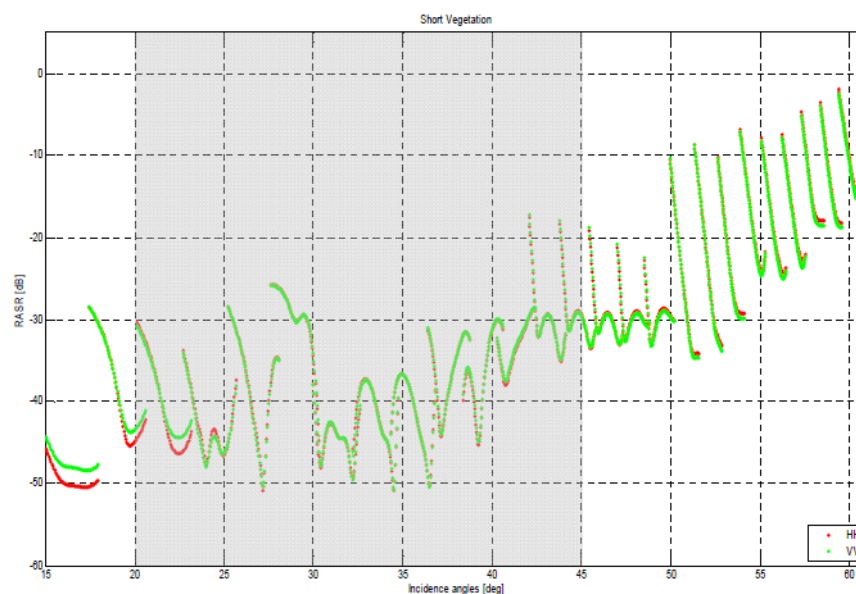


Figure 3.25: RASR vs. Incidence angle for an orbit height of approximately 536 Km. Figure extracted for an internal report written by the ECE team on the instrument performance analysis. This figure is valid only for the SM-S mode (Stripmap Single polarization mode) [3.5].

3.3.3 Guidelines Application

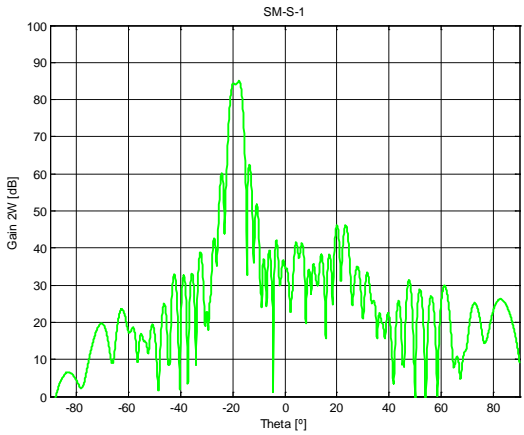
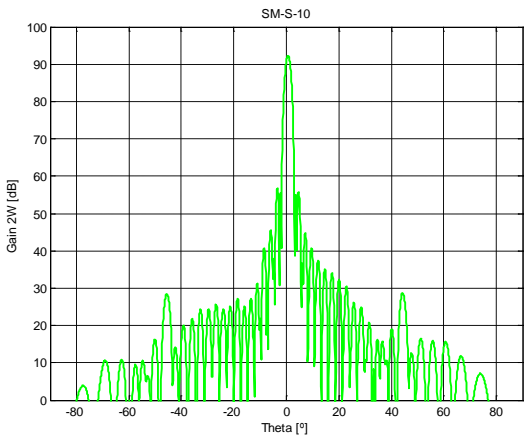
Finally, the guidelines and knowledge extracted in the former section are applied to three specific Stripmap beams. Since the first one has been deeply studied in the former section, its results are directly presented.

3.3.3.1 Test Cases Definition

The beams on which one will focus are three Stripmap (SM) beams (out of 26), namely: SM-S_1, SM-S_10 and SM-S_26. In this way, the study is done for a near-range swath (SM-S_1), a near-boresight swath (SM-S_10), and a far-range swath (SM-S_26). All the optimisations are applied to the 2W (two-way) EL (Elevation) antenna patterns of each SM mode. 2W because optimising TX and RX separately and independently does not always, not saying almost never, result in an optimal 2W pattern. EL plane because in the AZ (azimuth) plane the beams are very directive, because of the higher number of radiating elements in the AZ direction (which means very narrow beamwidths or good side lobe levels, for instance), and only beam steering is performed in this plane (in Spotlight mode).

In Table 3.16 the three test cases reference patterns provided by ECE are presented, along with the reference quality parameters they have to fulfil. The reference patterns are provided by ECE from an internal antenna simulator with reduced functions: it cannot consider deviations in the position of the TRMs; it only computes the patterns based on an ideal SA (not measured) and considering the SAs equal between them. In this way, this simulator can assume some simplifications in the computations that lead to a less time consuming optimisation, comparing with the optimiser developed in this Master Thesis.

Therefore, it is important to remark that the below presented reference patterns are generated from an ideal SA pattern. Hence, it is important to have in mind that the comparisons between the optimised patterns which are generated by the optimiser developed in this MT –UPC patterns hereinafter– and the ECE ones are not exactly under the same conditions.

	2W EL Reference Pattern	Quality Parameters
SM1		<ul style="list-style-type: none"> Gain of the main lobe > 83 dB <ul style="list-style-type: none"> Peak Gain achieved 85 dB Width of the main lobe in elevation > 3.145° Gain variation within swath (or peak-to-peak sensitivity) : <ul style="list-style-type: none"> Required < 2 dB Achieved = 0.70 dB Range Ambiguity <ul style="list-style-type: none"> Required < -20 dB Achieved = -49.4 dB Elevation and azimuth pointing direction: <ul style="list-style-type: none"> Beam Maximum: $(\theta_{EL}; \theta_{AZ}) = (-17.6; 0)^\circ$ Estimated Beam centre $(\theta_{EL}; \theta_{AZ}) = (-18.7; 0)^\circ$
SM10		<ul style="list-style-type: none"> Gain of the main lobe > 90 dB <ul style="list-style-type: none"> Peak Gain achieved 92.3 dB Width of the main lobe in elevation > 2.185° Gain variation within swath (or peak-to-peak sensitivity) : <ul style="list-style-type: none"> Required < 2 dB Achieved = 4.70 dB Range Ambiguity <ul style="list-style-type: none"> Required < -20 dB Achieved = -33.9 dB Elevation and azimuth pointing direction: <ul style="list-style-type: none"> Beam Maximum: $(\theta_{EL}; \theta_{AZ}) = (0.61; 0)^\circ$ Estimated Beam centre $(\theta_{EL}; \theta_{AZ}) = (0.49; 0)^\circ$

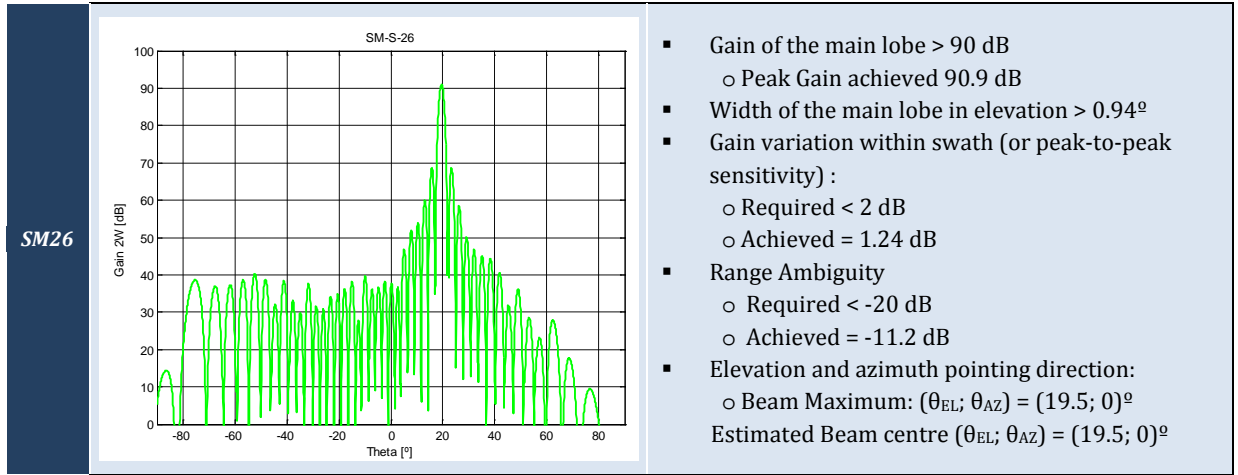


Table 3.16: Reference EL 2W patterns for the three cases of study, and quality parameters to fulfil. All the data in the table has been provided by ECE.

3.3.3.2 Simulation Results

The objective of the tool is to generate the excitations for the 26 Stripmap planned beams, according to the specified input parameters. The beams need to be optimum respect to the specified quality parameters.

In this section, the three cases formerly presented are optimised based on the guidelines established in 3.3.2. After the optimization process, the beams generated by the AMOR optimization tool are compared to the ones provided by ECE.

Even knowing that the comparison between ECE beams and AMOR ones is not totally fair, it can be useful to give a general idea on how right or wrong is each tool when optimizing a beam.

SM_S-1

Since the SM_S-1 beam has been sufficiently studied in Section 3.3.1, the results of the best simulation are directly presented.

With a number of individuals per generation equal to 800 and the rest of the default parameters, we obtain the 2-Way pattern in Figure 3.26 and the results in table 3.17 compared with the ones provided by ECE.

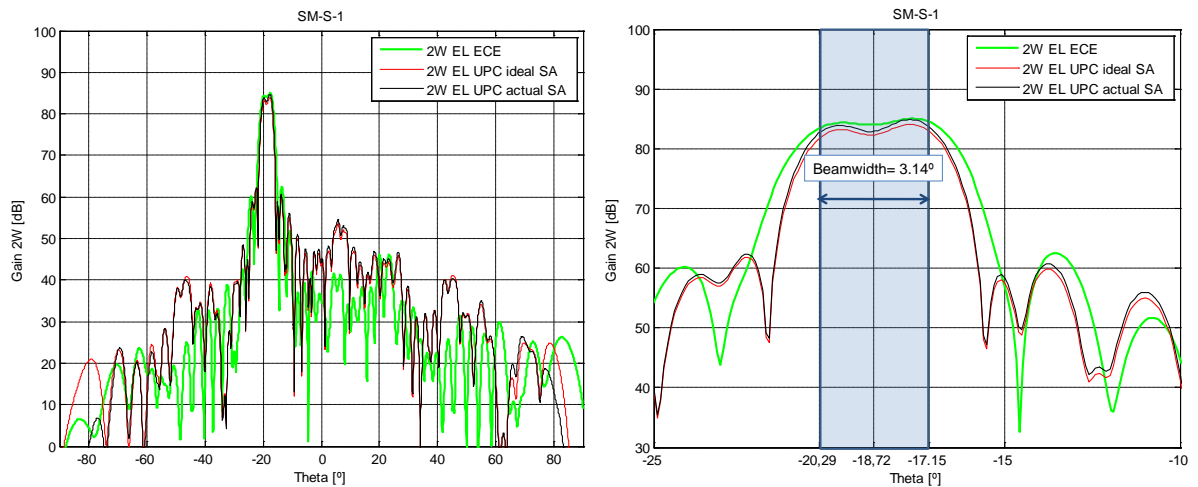


Figure 3.26: Comparison of the optimization results of the SM-S_1 beam: ECE vs. UPC beam. The green line corresponds to the ECE beam, the red line to the UPC resulting from the optimization using ideal SA patterns, and the black one resulting from the UPC's optimization with actual SA patterns.

Parameter	ECE	UPC
Maximum 2W gain (computed using spherical modes)	85	84.87
Gain variation in swath	0.70	1.63
Worst RASR in swath	-49.40	-32.08
Nadir gain with respect to maximum gain	-67.68	-77.89

Table 3.17: Comparison of the resulting parameters after optimizing the SM-S_1 beam: ECE results vs. UPC results.

In the SM-S_1 optimization process, remember that the critical parameter has been the gain variation within the swath. The AMOR beam fulfils all the specifications. The ECE one has approximately the same G_{\max} but with a lower ΔG . How can it be possible is explained by an inconsistency of the AZ and EL cuts found in the ECE SAR Tool³. If the ECE G_{\max} is not the one in the EL plane defined as it is defined in AMOR, and the gain level is also not computed in the same way and from ideal SAs instead of actual ones, the comparison is not fair at all and this kind of phenomena can occur. The logical thing would have been that a sharper AMOR beam would had a higher G_{\max} and worse ΔG . But another issue that has to be taken into account is that the considered beam is a 2-Way one, and hence the former reasoning can not be made as directly as if the beam was from a single antenna (1-Way).

The magnitudes and phases of the excitations to obtain the pattern optimized are plotted both for TX and RX (see Figure 3.27). In this case the magnitudes in RX follow a quasi-cosine like shape, and the phases slope is the same in TX and RX, which denotes the beam steering.

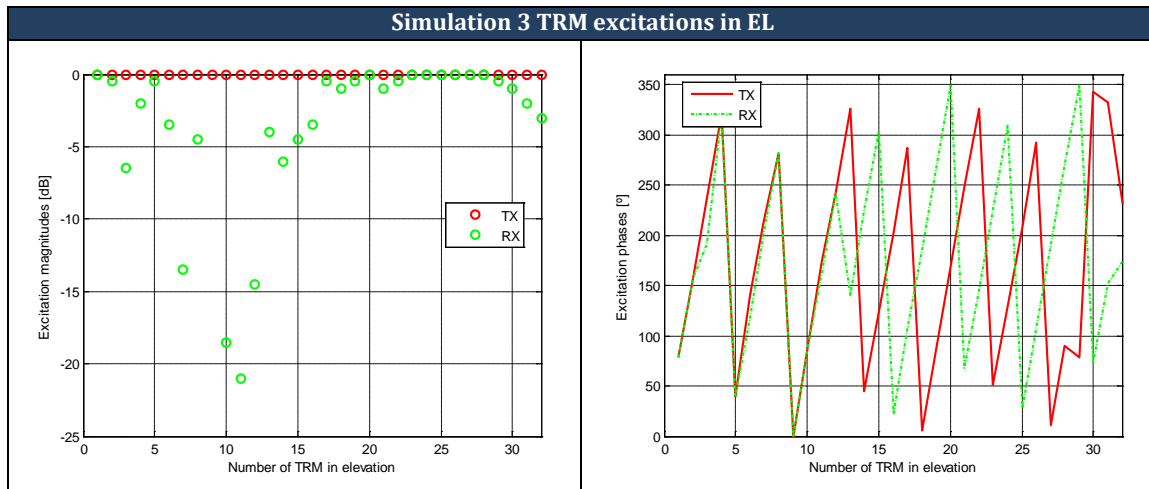


Figure 3.27: Comparison of the AMOR (in red) and ECE SAR Tool (in green) excitation RX magnitudes and TX and RX phases.

SM-S-10

In this case we need to start from the beginning: point 1 in the guidelines (although the number of individuals per generation is maintained equal to 80 in order to save time). The SM-S_10 optimization using the AMOR optimization tool fulfils all the specifications from the very beginning. However, since the ECE provided results have achieved a gain of 92.3dB, a couple of additional simulations are performed to enhance the gain in Simulation 1 of SM-S_10. In the case of ECE, however, the gain variation within the swath obtained for a gain of 92.3 dB has been more than 4dB which is, from the specifications point of view, unacceptable. Note that SM-S_10 mode is the more boresight-like mode, and hence its maximum achievable gain in swath is very close to the theoretical one (92.8 dB).

The effort in this beam is concentrated in reaching the higher maximum gain possible while having good ΔG and RASR values. The last simulation is performed assigning a 100% to w_1 , in order to evaluate which is the maximum possible gain for the SM10 and the correspondent ΔG value using the AMOR optimizer.

In the following table, the results obtained in the different simulations are gathered. Note that in the SM-S_10 case, to save time and since the initial result with default input parameters fulfils specifications, the only parameters that have been varied are the GA weights.

³ Explained in Appendix C.

UPC Simulation number	GA Weights w_1, w_2, w_3, w_4 [%]	G_{max} [dBi]	Gain variation in swath [dB]	RASR [dB]	Nadir gain wrt maximum gain [dBi]
1	20, 45, 25, 10	86.43	0.76	-23.28	-71.19
2	30, 35, 25, 20	85.97	0.64	-23.91	-78.52
3 ★	65, 20, 10, 5	86.76 ★	1.01	-22.02	-71.50
4	85, 5, 10, 0	89.70	4.47	-29.80	-59.35
5	100, 0, 0, 0	91.79	6.11	-19.20	-59.48
ECE simulation		92.3	4.70	-33.90	-82.75

Table 3.18: Comparison between the different optimization results between them and with the ECE reference ones for the SM-S₁₀ beam case.

Having into account that it is desired to obtain the maximum gain while fulfilling the $\Delta G < 2\text{dB}$ specification, the best result is the obtained in Simulation 3. The patterns obtained for Simulation 3 both in the GA using ideal SA and in the GA using actual SA (with directivity computed using the spherical modes expansion) are compared to the ECE provided one in Figure 3.28. Similar plots for the different simulations can be found in Appendix B, Figure B.1. As expected, less ΔG in the AMOR beam than in the ECE one implies higher secondary lobes and hence higher RASR levels, along with lower G_{max} value.

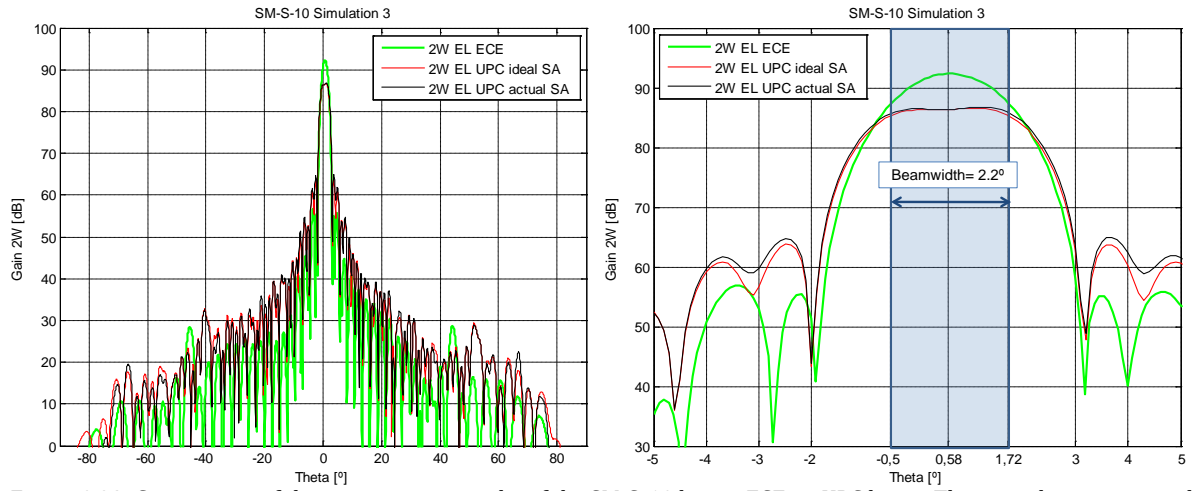


Figure 3.28: Comparison of the optimization results of the SM-S₁₀ beam: ECE vs. UPC beam. The green line corresponds to the ECE beam, the red line to the UPC resulting from the optimization using ideal SA patterns, and the black one resulting from the UPC's optimization with actual SA patterns.

The magnitudes and phases of the excitations to obtain the pattern optimized in Simulation 3 are plotted both for TX and RX (see Figure 3.29). In this case the magnitudes in RX follow a quasi-cosine like shape, like in SM-S₁, but the phases slope is very soft precisely because the beam is little steered. The phase in RX has an abrupt change in the last TRMs, superposed to the phase ramp which determines the beam steering.

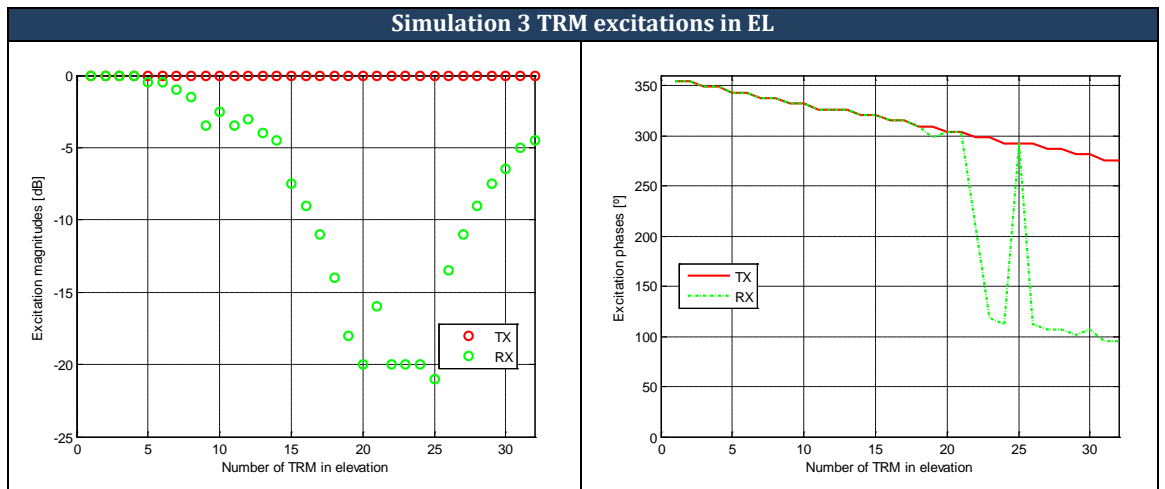


Figure 3.29: Magnitudes (left) and phases (right) for the excitation coefficients, both in TX and RX, obtained as a result in Simulation 3 of the SM-S₁₀ beam.

SM-S_26

The starting point is the default configuration of the input parameters (Table 3.7). From the very beginning it can be observed that the ΔG obtained is well below the upper limit established by the specifications (in part, due to the fact that the swaths are narrower for far range beams than for the near range ones) and the maximum gain is fairly high (again, caused by the narrower beamwidth of the main lobe, requiring a less flat-top beam to fulfil the required ΔG in the swath, and hence the gain can be higher) - approximately 86dB. However, the RASR is tremendously high, even being higher than 0dB.

From Figures 3.24 and 3.25 it is known that the RASR can not be as good as in nearer range beams, but in this case the optimization effort has to be centred in containing the RASR value while maintaining reasonable values of the gain variation in the swath and the maximum gain in the swath.

In this way, around 5 simulations are needed to complete the optimization process for the SM-S_26 Stripmap beam. Note that the optimization can be stopped after it reaches its end, in order not to spend too much time with the exact computation of the directivity when the main parameter values that are observed in the GA window are very distant from the desired ones from the very beginning.

Table 3.19 contains the main results of the different simulations carried out for the SM-S_26 beam, where the only parameters varied are the GA weights.

UPC Simulation number	GA Weights w_1, w_2, w_3, w_4 [%]	G_{max} [dBi]	Gain variation in swath [dB]	RASR [dB]	Nadir gain wrt maximum gain [dBi]
1	20, 45, 25, 10	85.63	0.06	0.84	-85.59
2	30, 10, 50, 10	88.97	0.48	-1.05	-77.85
3	20, 5, 70, 5	89.81	0.83	-2.01	-99.83
4	20, 0, 80, 0	90.28	1.04	-2.68	-60.08
5 ★	0, 0, 100, 0	85.62	1.49	-3.49 ★	-67.60
ECE simulation		90.90	1.24	-11.2	-73.86

Table 3.19: Comparison between the different optimization results between them and with the ECE reference ones for the SM-S_26 beam case.

In this case the critical parameter is the RASR, and the simulation which best suits the RASR specifications is number 5. The patterns obtained for Simulation 5 both in the GA using ideal SA and in the GA using actual SA (with directivity computed using the spherical modes expansion) are compared to the ECE provided one in Figure 3.30. Similar plots for the different simulations can be found in Appendix B, Figure B.2.

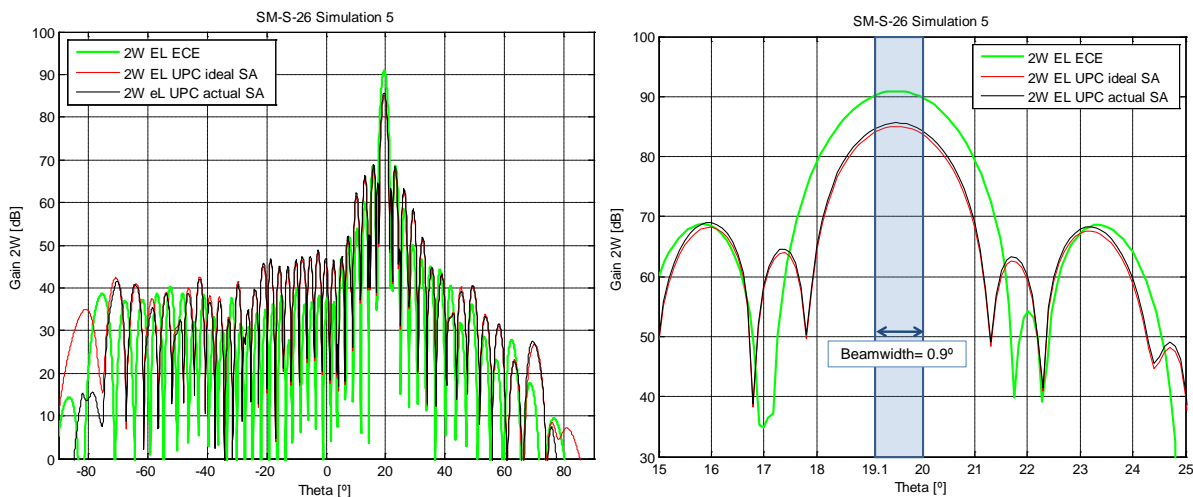


Figure 3.30: Comparison of the optimization results of the SM26 beam: ECE vs. UPC beam. The green line corresponds to the ECE beam, the red line to the UPC resulting from the optimization using ideal SA patterns, and the black one resulting from the UPC's optimization with actual SA patterns.

In this case, the RASR specification is not fulfilled. It may be improved increasing the number of individuals per generation, but it will never be as good as the -20dB specified in the general requirements. Like in SM-S_1, the

comparison is paradoxical: in AMOR beam the Gmax is lower than in ECE, however, the beam is not wider but even narrower, leading to a worse ΔG value in the AMOR beam. It can be due to the fact that the secondary lobes are higher. In this way, although the main beam is wider, the ECE pattern is more directive because its secondary lobes are lower.

The magnitudes and phases of the excitations to obtain the pattern optimized in Simulation 5 are plotted both for TX and RX (see Figure 3.31). In this case the magnitudes in RX do not follow any specific or identifiable shape. The phases slope is negative, oppositely to the ones of the SM-S_1 and SM-S_10 beams, because the beam steering is positive in the antenna angle domain.

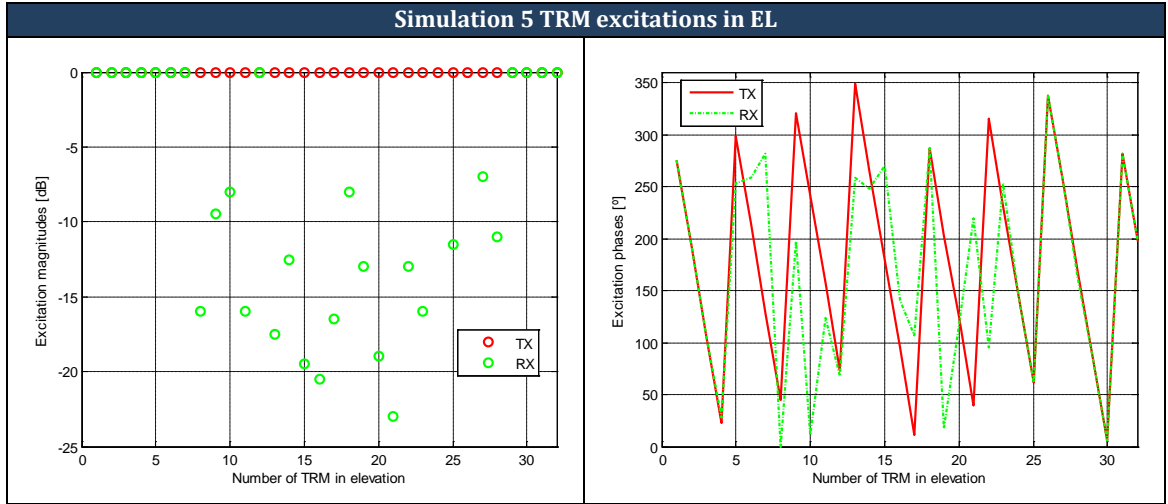













Figure 3.31: Magnitudes (left) and phases (right) for the excitation coefficients, both in TX and RX, obtained as a result in Simulation 5 of the SM-S_26 beam.

4 BUILDING BLOCKS OF AMOR

The antenna model structure is described in the present chapter. The directory tree of the Antenna Model software package is explained, and the modeller main subroutines are introduced in order to better understand the way the software tool is implemented.

4.1 Directory Tree

The Antenna Modeller code uses the following tree of directories under the AMOR main folder:

 Array_Descriptions	Contains <i>.mat</i> files (Matlab® compressed file format) where several array descriptions are stored.	
 Basic_Elements	Folder where all the measured subarrays (basic array elements) are stored in an individual <i>.mat</i> file. This <i>.mat</i> file is generated by combining into single file individual embedded SA measurements stored in the same subfolder. Raw subarray measurements are preprocessed (using the Preprocessing window) to increase the sampling, as required for further accurate computations of array directivity.	
 Controls	Library of functions required to build the GUI of AMOR.	
 Docs	This folder contains documents such as <i>AMOR_Versions.doc</i> (summary of differences between the several versions of AMOR) and the AMOR user manual.	
 Errors	It stores the different input files for the mechanical and thermoelastic error computations. Error files are grouped into specific folders. Only a folder called <i>Mechanical_Panel</i> is found till now. Inside, different text files having different mechanical panel error configurations can be found. In the present version of AMOR (v4.0) a folder called <i>Actual_Working_TRMs</i> stores the matrices used to indicate which TRM are failing or working properly.	
 Excitations	Inside the Excitation directories there are six folders containing text files describing the excitation coefficients for the several beams allowed by the different operating modes of the instrument. Namely: <i>Boresight</i> , <i>Stripmap</i> , <i>Spotlight</i> and <i>ScanSAR</i> . Also there is a folder containing the excitation coefficients for squinting the Spotlight beams, <i>Squints4Spot</i> . An additional folder named <i>User_Defined</i> allows having sets of excitation coefficients defined by the user for testing purposes.	
 Menu	Contains scripts required to design the Graphical User Interface and build the windows used by the modeller tools, that is, the <i>Array Description</i> window, the <i>Error</i> window, the <i>Analysis</i> window, the <i>Synthesis</i> window, the <i>Help</i> window, and the <i>About</i> window.	
 Results	It contains 6 folders:	
	 Pattern_Cuts	In this folder the text files having azimuth and elevation pattern cuts according to the definition given in Section 3.2.3, together with a text file summarizing the TX, RX and 2W antenna performance are stored.
	 AZ_Pattern_Cuts	It contains the text files for an azimuth pattern cut (that is, the pattern cut for a plane with constant ϕ).
	 Directivity_Files	It stores, in <i>.mat</i> file the antenna directivity using the pattern integration method.












	 3D_Patterns	It contains 3D antenna patterns stored in compressed MatLab files (.mat).
	 Stripmap_Optimisation	Containing different folders where the TRMs excitation coefficients resulting from different optimisations of the Stripmap mode are stored.
	 Temp	Intermediate results that involve spherical modes are stored in this folder.
 Routines	It contains 4 folders:	
	 Run	It contains scripts detailing the algorithmic of the several functionalities of AMOR.
	 Main	In this folder, there are the main procedures on each of the algorithms under the <i>Run</i> folder.
	 Subroutines	Here one can find scripts or subroutines that perform tasks required in several algorithms. These tasks are packed as functions and could be sorted adequately to build new functionalities not yet implemented.
	 Tools	It contains routines with specific analysis utility that are not directly used in AMOR but could be used in the future.

Table 4.2: AMOR directory tree.

The specific format of the aforementioned input and output files is described in the modeller User Manual.

4.2 Main Subroutines

The tasks developed by the main subroutines included in folder *Subroutines* are summarized in the following paragraphs. These subroutines are the modeller engines and can be called independently to carry out specialized and repetitive functions which can be combined in a script to generate and analyze sequentially large number of beams.

 Sub_PAZ_PatternCuts_pSF	Computes the far fields (copolar and crosspolar, or theta and phi components) radiated by a given antenna configuration at given spatial directions. The antenna configuration is defined by the chosen basic element matrix, operating frequency, separation between subarrays, positioning errors, excitation coefficients (including failing TRMs) and pattern to be computed (TX, RX or 2W). The spatial directions where the fields are computed are specified by a pair of vectors having the spatial θ and ϕ directions. To compute the patterns this subroutine uses the previously preprocessed fields radiated by each subarray element. The subroutine output provides the electric field intensities radiated by the whole array.
 Sub_PAZ_PatternCorrections_pSF	Computes the corrections to be added to the patterns obtained by the subroutine <i>Sub_PAZ_PatternCuts_pSF</i> to get directivity patterns (from the radiation intensities previously obtained). To compute the corrections the inputs to the subroutine are the basic elements matrix and the excitation coefficients feeding the basic elements. Also the malfunctioning TRMs are accounted for through a matrix that provides information about the ones. The corrections provide directivities based on the formulation of Section 3.2.2.2.
 Sub_PAZ_PatternCorrections_SphericalModes_pSF	Its function is the same as the abovementioned subroutine, except for the method used to compute the directivity. It uses the formulation presented in Section 3.2.2.4. It calculates directivity corrections in a more accurate way than the former routine, but taking more time to perform the computations. It is used by default in all the operations performed in the analysis window.

 Sub_PAZ_ReadingMeasurementsGUV	It reads on-ground measured radiation patterns of embedded subarrays stored in a GUV text file and allocates these data in a copolar and crosspolar matrix. GUV files contain copolar/crosspolar far field samples in the uv -domain whereas the data used by AMOR require sampling in a spherical domain ($\theta\phi$).
 Sub_PAZ_uvplanes	Used to compute the spatial directions corresponding to the azimuth and elevation pattern cuts in addition with the angles required for plotting the resulting patterns.
 Sub_PAZ_PatternCharacterization	It computes several pattern characteristics for a given pattern cut, such as maximum pattern level for the cut (directivity or fields, depending on the input vector), the beam pointing direction, the -3dB beamwidth and the side lobe level. Beam pointing direction is considered to be the beam maximum direction or the beam centre direction. By default, beam pointing direction is considered to be the beam centre as defined in Figure 3.9 in Section 3.2.3.
 Sub_PAZ_Find_BeamCenter	Used to compute the spatial directions of the beam centre and beam maximum of a copolar pattern for a given antenna configuration (basic elements/s, separation between elements, and pattern -TX, RX, or 2W). These directions are determined following an iterative procedure briefly described (for a two way pattern) in the algorithm of Figure 3.12 (right), in Section 3.2.3.
 Sub_PAZ_DiscretizePhases	It provides the discretized phases of the TRMs excitation coefficients to the given number of bits.
 Sub_PAZ_SavePatternResults	Subroutine that stores a pattern cut (EL or AZ) in a text file. The pattern has been previously computed using <i>Sub_PAZ_PatternCuts_pSF</i> .
 Sub_PAZ_SaveTRMCoeffs	This subroutine is used to store the excitation coefficients to be applied to the array in transmitting and receiving modes.
 Sub_PAZ_SN2FFT_ModesComputation	Used to compute the spherical mode expansion (Q_{1nm} and Q_{2nm}) of a given field distribution, according to formulation in Equation 3.11 in Section 3.2.2.4.
 Sub_PAZ_CodifyingExcitations	Codifies a given set of excitation coefficients according to the number of bits of phase shifters and amplifiers.
 Sub_PAZ_cpxp2thph	It converts from copolar/crosspolar to theta/phi components (or the other way round) following the Ludwig 3 definition.
 Sub_PAZ_GA_FitnessFunction	It computes the partial fitness of a given pattern array configuration and set of excitation coefficients. It also computes the partial fitness attending to a set of some radar parameter goals previously defined by the user.
 Sub_PAZ_ComputingAllAmbiguities	Returns the location of all the ambiguous zones required for further RASR computation given a normal satellite configuration and swath definition.
 Sub_PAZ_RASR_Computation	Using the geometrical parameters provided by the function <i>Sub_PAZ_ComputeAllAmbiguities.m</i> it computes the RASR levels at a given number of samples in the swath.

Table 4.3: AMOR main subroutines.

5 CONCLUSIONS AND FUTURE WORK

AMOR is in a constant evolution, and, though at the time this Master Thesis document is redacted there is still some work to do regarding the antenna model, one can clearly distinguish between present achievements and next-future work.

At the present, a complete antenna model capable of analysing and synthesizing many different antenna beams has been developed. AMOR allows loading any antenna configuration and analysing or synthesizing it. The basic elements of the phased array antenna can be any (all equal or all different between them, isotropic, formula-based or measured), they can be placed at any location in the antenna (equally spaced –as ideally, or non-equally spaced accounting for positioning errors), and the antenna element number can be any (the only restriction is that the antenna must be planar –including the linear antenna case). All of this taking into account many possible errors: TRM failures and/or deviations, thermo-elastic errors, etc; and performing accurate directivity computations.

The optimizing tool is capable of optimizing any Stripmap beam reaching an optimal trade-off solution between the different specified requirements. Therefore the major difficulty of the problem has been successfully overcome: adequately defining the fitness function to represent mathematically through a single value (the total fitness value) the quality of a solution from a multiple-objective optimisation problem. However, some points have to be improved:

- The RASR levels are higher in the AMOR optimised beams when compared to the ECE SAR Tool ones. In addition, obtaining a comparable gain, the AMOR beams are narrower and sharper than the ECE SAR Tool ones. Although knowing that the comparison is not made in totally fair conditions, these discrepancies which make the SAR Tool results better (always speaking in the short term, with a time limitation in the optimization) are probably due to the difference in the initial population generation.

Both tools apply techniques to widen the swath in RX. In AMOR initial population the swath is made wider by magnitude tapering of the RX pattern. However, while in the ECE case the TX pattern admits a phase tapering to widen the swath in TX and make it flatter, the AMOR initial population provides TX patterns with a phase tapering only to obtain the desired beam steering.

In this sense a phase-spoiling technique is strongly recommended to improve AMOR initial population, helping by this to a quicker convergence of the algorithm to an optimal solution with wider and flatter swaths and lower RASR levels. At the time of writing this document, the mentioned technique is just been applied.

- It has been detected that the tool would present a main difficulty to a potential user: adequately tuning the weights of the fitness function used by the GA to converge to the optimal solution, depending on the beam under test. These weights are very sensitive to changes, and an adjustment of the limiting function (which is used to have a limited dynamic range for each partial fitness function) is suggested as a future task in order to improve the algorithm functioning and to facilitate its tuning.

Apart from the abovementioned improvements, there is still some verification to do regarding the optimizer behaviour:

- To check the optimizer when using measured data. This is also being done at the time this document is written.
- To make the optimizer capable of re-optimize a beam when, during in-flight measurements, any failure is detected.

The work developed in this thesis benefits from a constant revision, multiple assessments and expertise derived from the people at ECE SEOSAR/PAZ mission. The final validation of the work done here will be through its application to a real-case scenario.

Appendix A_{STATE OF THE ART}

During the last decade, many SAR missions have been planned, designed and carried out by different countries. Their main objective is the Earth Observation (EO), for different purposes. Some recent SAR missions, sorted by order of satellite launch date are:

- *ENVISAT (Environmental Satellite)*
- *ALOS (Advanced Land Observing Satellite)*
- *TerraSAR-X*
- *RADARSAT-2 (RADAR Satellite)*
- *COSMO-SkyMed (Constellation of Small Satellites for Mediterranean Basin Observation)*

And, of course, the one to which the present work is applied:

- *SEOSAR/PAZ (Spanish Earth Observation Synthetic Aperture Radar)*

In the following sections, each one of the mentioned missions is briefly revised in order to have in mind both their main objective and the performance of their antenna model compared with the SEOSAR/PAZ one.

A.1 Missions Overview

All the reviewed SAR missions are intended for Earth Observation (EO). They are global; hence they observe ground, atmosphere, oceans and icecaps. The overall functionalities are to support science research, and also to facilitate the development of operational and commercial applications. In addition, they can offer products to support both civil and military applications. Specific tasks they develop are the monitoring of water, land cover, carbon and global climate. Some of the missions combine the SAR instruments, which provide all-weather and day-night observations, with optical sensors.

These kinds of missions have made possible:

- Cloud penetration, which allows the access to subtropical and tropical regions
- Detection of man-made structures such as buildings and metal surfaces like bridges, roofs, power lines, fences, or wind energy parks, in order to exert control and territory survey
- Generation of geographical maps at high resolution levels for commercial and military applications, wetlands mapping, geological mapping, and topographic mapping
- Support to agricultural mapping and agricultural crop monitoring
- Maritime surveillance: ship detection and tracking, oil spill and pollution detection, sea ice mapping, ship routing, iceberg detection
- Region observations for environmental monitoring: flood extension mapping, burned extension mapping, land subsidence monitoring, assess coastal erosion and sea/river pollution
- Information distribution for disaster mitigation: estimation of the spatial and qualitative extent of damage caused by hazardous events to help with logistics planning, long term prediction and trend analysis of events, development of early warning systems to track the real time evolution of events to avoid or reduce damage
- Monitoring of surface deformation caused by earthquake-driven phenomena and volcanic activities
- Research in the polar regions for ice sheet flow rate estimations
- Terrestrial defence surveillance and target identification for national security applications

In the case of the Spanish mission, it is expected that PAZ will provide information in order to fight the piracy in Somalia waters, where in summer 2010 a Spanish fishing boat was kidnapped, as an example [A.1].

Not all the above mentioned applications have the same time requirements regarding data servicing. The most critical of them need short System Response Time (time between user's demand and the information release). Some systems have the capability of being configured in different modes to satisfy the user's needs. For instance, in the COSMO-SkyMed mission the system can operate in three different modes [A.2]:

- Routine mode: the images to be acquired are requested to the constellation once a day. The system can satisfy the user request in 72 hours.
- Crisis mode: the requests are sent twice a day and the user's request is satisfied in 36 hours.
- Very urgent mode: it is asynchronous and hence allows the servicing of an image acquisition request with the minimum possible latency. The requests can be satisfied in 18 hours.

Different missions work at different frequency bands; for instance L band used in ALOS mission is better in terms of atmosphere penetration than working at higher frequencies.

The considered SAR missions description is briefed in Table A.1, while the main characteristics of their available operational modes are gathered in Table A.2. In Table A.3 some images of the different missions are shown.

Mission Overview	
ENVISAT	ENVISAT is an European advanced polar-orbiting EO satellite working at C-band built by the European Space Agency (ESA), launched as follow-on of the satellites ERS-1 and ERS-2. While its predecessors acquired images being steered at a fixed angle of 23 degrees, ENVISAT is equipped with an instrument capable of being electronically oriented - ASAR (Advanced Synthetic Aperture Radar).
ALOS	ALOS is an L-band Japanese SAR mission. It became operational since its launch. It was developed as a demonstration satellite with improved performance in comparison to JAXA (Japan Aerospace Exploration Agency) previous Earth observation satellites (the Japan Earth Observing Satellite, JERS-1, or the Observing Satellites, ADEOS and ADEOS-II, for instance) and designed to fill the gap created by the termination of JERS-1 on October 12, 1998. ALOS development and operation project was realized as a joint project of METI (Japanese Ministry of Economy, Trade and Industry) and JAXA.
TerraSAR-X	The German satellite TerraSAR-X is built in a Public Private Partnership (PPP). Its objective is to allow EO with additional capabilities with respect to previous missions, providing value-added SAR data in the X-band for research and development purposes and for scientific and commercial applications. This is accomplished thanks to the number of operation modes available, different polarisations and resolutions. The mission is carried out both by a public entity – the German Federal Ministry of Education and Research (Bundesministerium für Bildung und Forschung, BMBF) and the German Aerospace Centre (Deutsches Zentrum für Luft- und Raumfahrt; DLR), and a private entity which is Astrium GmbH.
RADARSAT-2	The Canadian next-generation satellite RADARSAT-2 is the follow-on to RADARSAT-1. Working at C-band , it has been designed with significant technical advancements: 3m high-resolution imaging, flexibility in selection of polarisation, left and right-looking imaging options, superior data storage, more precise measurements of spacecraft position and attitude , additional beam modes, more frequent revisits, and increased downlink margin enabling reception of data from lower-cost receiving antenna systems. The RADARSAT-2 is a commercial Canadian SAR satellite fruit of collaboration between government – the Canadian Space Agency (CSA), and industry - MacDonald, Dettwiler and Associates Ltd. (MDA).

COSMO-SkyMed	<p>The COSMO-SkyMed system is an Italian EO mission which consists of a constellation of four LEO mid-sized satellites, each equipped with a multi-mode high-resolution SAR that can operate under any weather conditions, visibility and with very short revisiting time. In 2007 and 2008 ASI (<i>Agenzia Spaziale Italiana</i>; the Italian Space Agency) launched three out of four X-band SAR satellites involved in the program. The fourth satellite to complete the constellation will be launched in 2010 (planned to be launched on October 30th, 2010 [A.3]). The mission is intended for both civil and military use.</p> <p>The Italian Earth Observation program COSMO-SkyMed, one of the most innovative Earth Observation programmes, is financed by the Italian Ministry of Education, some Universities and Scientific Research and by the Italian Space Agency (ASI) and the Ministry of Defence (MoD). ASI in cooperation with MoD manages the contract assigned to an Italian industrial team, where Thales Alenia Space Italia (TAS-I), in charge to develop the project, is the Prime Contractor.</p>
SEOSAR / PAZ	<p>The PAZ Spanish satellite is equipped with an X-band SAR instrument, mounted in a hexagonal platform made of carbon fibre (inherited from TerraSAR-X) supplied by Astrium GmbH. The instrument radiating part (the antenna array) incorporates the printed radiator technology developed by Astrium in its centre in Madrid-Barajas, used with success in other programs like Envisat, Spainsat, Inmarsat or Galileo.</p> <p>The PAZ satellite will be the first of two satellites (the second is named Imagenio) to capture images which will compose the Spanish Earth Observation (SEOSAR) program (<i>Programa Nacional de Observación de la Tierra</i>, PNOT). It has very diversified functionalities, since it is addressed to multiple defence and security applications as well as to civil applications. The second satellite, Ingenio, will incorporate an optical technology to basically cover civil necessities. This will lead Spain to be the first European country having a dual observation system with a double use (civil and military).</p> <p>EADS Casa España (Astrium España) is the main contractor, responsible for the development and satellite construction, with functions like being responsible of the system engineering, the integration, the satellite test and its validation and in-orbit delivery completely operative. INTA is responsible for the ground segment which includes two control ground stations (in Torrejón and Maspalomas). Hisdesat is the operator and the commercial exploitatory of the satellite, acting as its owner and with the Spanish Defence Ministry (Ministerio de Defensa) as its principal client.</p>

Table A.1: Overview of the most recent SAR missions

	ENVISAT	ALOS	TerraSAR-X	RADARSAT-2	COSMO-SkyMed				PAZ
Launch Date	March 1, 2002	January 24, 2006	June 15, 2007	December 14, 2007	COSMO-SkyMed-1 June 7, 2007	COSMO-SkyMed-2 December 2007	COSMO-SkyMed-3 October 25, 2008	COSMO-SkyMed-4 October 30th, 2010 [A.3]	Planned for 2012
Launch vehicle	Ariane 5	H-IIA	Dnepr 1	Soyouz	Delta II				-
Launch Site	Korou Space Centre, French Guyana	Tanegashima Space Centre, Japan	Baikonur, Kazakhstan	Baikonur, Kazakhstan	Vanderberg Air Force Base (VAFB), California(US)				-
Launch Configuration Dimensions	10.5 m (envelope Ø 4.57m)	-	4.88m (envelope Ø 2.4m)	-	-				-
In-orbit Configuration	26 x 10 x 5 m	27.8 x 9 x 6.7 m	-	-	-				-
Satellite Mass	8211 kg	4000 kg	1230 kg	-	1700 kg				1200 kg
Payload Mass	2050 kg	-	~ 400 kg	-					
Expected Lifetime	5 years	≥ 3 year	≥ 5 year	≥ 7 year	5 year				
Orbit Altitude	780 km	691.5 km	514.8 km	797.7 km	619.6 km				510km
Orbit Inclination	98°	98.16°	97.44 °	98.55°	97.86°				98.44°
Recurrent Cycle or Period	35 days	46 days	11 days	24 days	16 days				
Frequency Band	C (5.331GHz)	L (1.27GHz)	X (9.65GHz)	C (5.405GHz)	X				X (9.65GHz)
SAR Antenna Dimensions	-	8.9m (azimuth) x 2.9 m (range)	0.7m (width) x 4.8 m (length)	15m x 1.47 m	5.7 m (long) / 1.4 m (high)				0.7 m (width) x 4.794 m (length)

Table A.2: All the missions have a Sun-synchronous orbit configuration (polar, near-polar or circular), and their channel polarization is HH, HV, VH or VV ([A.4],[A.5], [A.6], [A.7], [A.8], [A.9], [A.10], [A.11], [A.1], [A.12]).

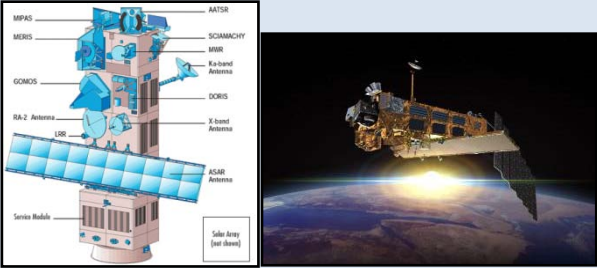



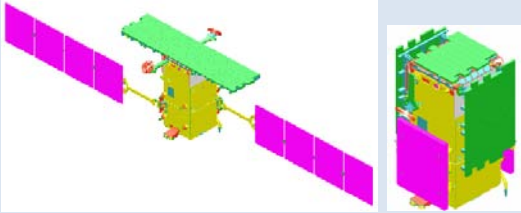
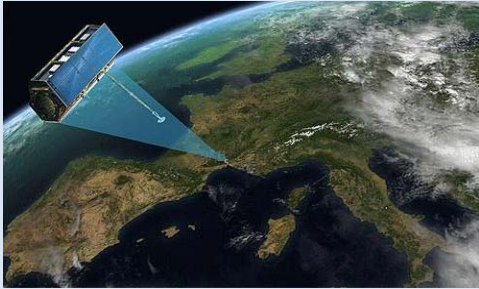
ENVISAT (Environmental Satellite)	ALOS (Advanced Land Observing Satellite)	TerraSAR-X
 <p>Figure A.1: ENVISAT instruments sketch [A.13] (upper) and simulated image of the satellite in space (lower) [A.14].</p>	 <p>Figure A.2: Advanced Land Observing Satellite [A.6A.6] (left), and artist's concept of ALOS (right) [A.15].</p>	 <p>Figure A.3: TerraSAR-X satellite artist view [A.16].</p> <p>The solar panel is mounted on top of the satellite bus. The SAR antenna is visible on the bottom side. The X-band downlink antenna is mounted on a small boom in order to avoid interference with the SAR-antenna.</p>
RADARSAT-2 (RADAR Satellite)	COSMO-SkyMed (Constellation of Small Satellites for Mediterranean basin Observation)	SEOSAR / PAZ (Spanish Earth Observation Synthetic Aperture Radar)
 <p>Figure A.4: RADARSAT-2 satellite artist concept view [A.10].</p>	 <p>Figure A.5: COSMO-SkyMed satellite Pictorial representation: deployed (left) and stowed (right) configurations. The green structure corresponds to the antenna while the pink one to the solar panels [A.11].</p>	 <p>Figure A.6: Artist concept view of PAZ [A.17]</p>

Table A.3: Some images of the considered SAR missions.

A.2 Antenna Description

In this section, the antennas used in the considered missions are described (Table A.4), and the operational modes which provide are listed together with their main characteristics (Table A.5).

Antenna Description	
ENVISAT	<p>ASAR, the broadest instrument onboard Envisat satellite, is an active phased array antenna formed by 320 TRMs, organized in 32 rows of ten modules to allow electronic beam steering in elevation. The 320 TRMs are grouped in 20 tiles. Each tile is a self-contained fully operating sub-system which includes four Power Supply Units, a Tile Control Interface Unit, two microstrip RF distribution corporate feeds and 16 subarrays. Each subarray is connected to a TRM with independent connection for the two polarizations.</p> <p><i>Figure A.7: ASAR mounted on ENVISAT in the anechoic chamber (left) and ASAR instrument isolated (right) [A.13].</i></p>
ALOS	<p>The PALSAR instrument is composed of four sub paddles, each of which is 2.9 m in range \times 2.2 m in azimuth. Each sub paddle has 20 TRMs (1 TRM row in azimuth \times 20 columns in range). Thus, it carries 80 TRMs, which allow incidence angle quick change and other functions like polarimetry and scanning SAR – ScanSAR) generating 2 kW of transmission power (each TRM has 25W transmission power).</p> <p><i>Figure A.8: PALSAR sensor [A.18]</i></p>
TerraSAR-X	<p><i>Figure A.9: TerraSAR-X S/C with SAR antenna [A.19].</i></p> <p>The antenna is 4.8 m long and 0.7 m wide and consists of 384 subarrays composed by pairs of 40 cm long slotted waveguides (see Figure A.10), one for each polarisation (horizontal and vertical).</p> <p>The subarrays are arranged in 12 panels in azimuth direction (columns) each composed of 32 subarrays (rows). The nominal antenna pointing in elevation is 33.8° from nadir. Right and left looking acquisition is realised by satellite roll manoeuvres. Each individual subarray is driven by a TRM adjustable in amplitude and phase by applying complex excitation coefficients. This enables beam steering and adaptive beam forming both in azimuth and elevation direction. More than 12000 different beams can be commanded for the multitude of standard acquisition modes possible on TerraSAR-X.</p> <p><i>Figure A.10: Dual polarised subarray with TRM [A.19].</i></p>

RADARSAT-2

The RADARSAT-2 antenna is a 15 m by 1.47 m divided in two wings, each having two SAR panel assemblies (nominally 0.15 m thick). It is hence formed by 512 subarrays with 20 element (patch) linear array with dual linear polarization capability. The subarrays are distributed in 32 rows in the elevation (range) direction and 16 columns (4 columns per panel, with 4 panels in total) in the azimuth direction. There are 512 TRM elements, as mentioned before, each one dedicated to excite one single subarray. Each TRM can switch between transmit and receive mode. Each subarray includes the 1:20 power dividing network to feed the 20 elements present in each subarray. The described antenna structure is depicted in Figure A.11.

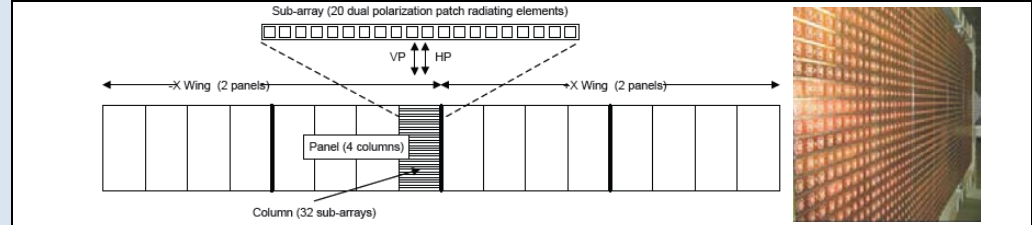


Figure A.11: SAR payload diagram of the RADARSAT-2 satellite (left) and the fabricated antenna structure [A.20].

COSMO-SkyMed

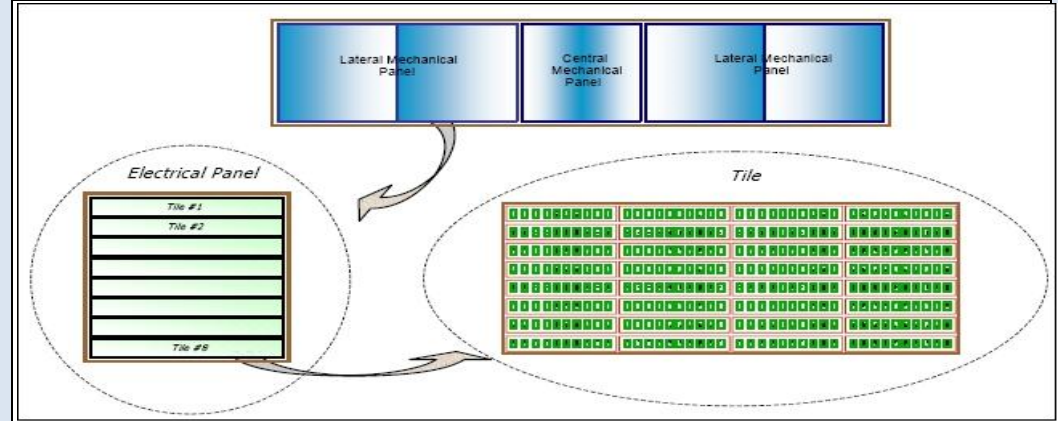


Figure A.12: Image showing the SAR antenna structure. In blue, the 5 panels containing 8 tiles each. In each tile there are 32 subarrays consisting on a linear array formed by 10 patch antennas [A.21].

The antenna used is formed by 40 tiles each including 32 transmit/receive modules (TRMs) each one feeding a patch linear array (H and V polarisation). Figure A.13 helps to understand its structure, from the panels to the subarray formed by patches arranged forming tiles.

PAZ

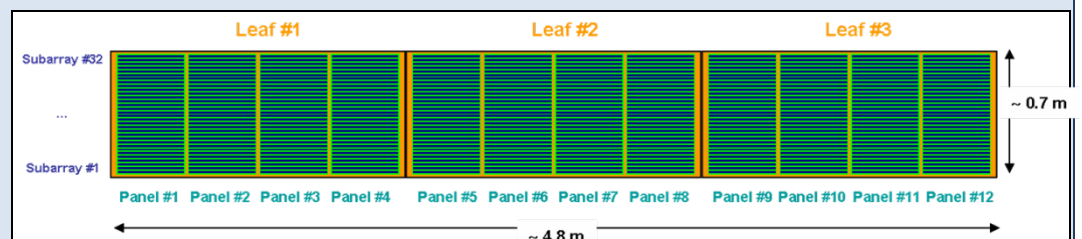


Figure A.13: Antenna array for PAZ sketch. Subarray referencing at panel and leaf level [A.22].

The PAZ array is 4.8 m long (along satellite flight direction) and 0.7 m wide. It consists of 384 subarrays of 16 annular slots excited by two orthogonal striplines providing H and V polarization. The subarrays constitute a planar array with 12 panels in the azimuth direction (columns), each with 32 SAs (rows). Four panels form a leaf. In Figure A.16 the SA referencing is shown. The individual subarrays are driven by (TRMs) that allow an adjustment in amplitude and phase of the beam excitation coefficients by applying complex excitation coefficients.

Table A.4: Antenna description of the six issued SAR missions.

Antenna Models for SAR Applications

			Polarisation	Spatial Resolution	Swath Width	Incidence angle	Swaths	
ENVISAT: ASAR	ScanSAR	Wide Swath (WS)	VV or HH	150 x 150 m (nominal product)	400 km		5	
		Global Monitoring Mode (GMM)	VV or HH	1 km	400 km		5	
	Stripmap or Image Mode (IM)		VV or HH	30 m (for precision product)	56 km (sw 7) – 100 km (sw 1)		7	
	Wave Mode (WM)		VV or HH	Vignettes of 10 km x 10 km spaced 100 km	5 km		-	
	Alternating Polarisation (AP) (same imaging geometry than IM)		2 simultaneous images from the same area in HH and VV, HH and HV, or VV and VH	30 m (for precision product)	-		7	
ALOS: PALSAR	High resolution		HH or VV	7–44 m	40–70 km	8°-60°		
			HH+HV or VV+VH	14-88 m	40–70 km	8°-60°		
	ScanSAR		HH or VV	100 m (multilook)	250–350 km	18°-43°		
	Polarimetry		HH+HV+VH+VV	24–89 m	20–65 km	18°-43°		
TerraSAR-X	High Resolution SpotLight (HS)			Azimuth	Range			
	SpotLight (SL)			1 m	1.5–3.5 m	10 km	20°-55°	
	Stripmap (SM)			2 m	1.5–3.5 m	10 km	20°-55°	
	ScanSAR (SC)			3 m	1.7–3.5 m	30 km	20°-45°	
				16 m	1.7 –3.5 m	100 km	20°-45°	
RADARSAT-2	Ultra-Fine		Single Polarisation	Range x Azimuth				
	Multi-Look Fine			3 x 3 m	20 km	30°- 49°		
	Fine			8 x 8 m	50 km	30°- 50°		
	Standard		Single or Dual Polarisation	8 x 8 m	50 km	30°- 50°		
	Wide			25 x 26 m	100 km	20°- 49°		
	ScanSAR Narrow			30 x26 m	150 km	20°- 45°		
	ScanSAR Wide			50 x 50 m	300 km	20°- 46°		
	Extended High		100 x 100 m	500 km	20°- 49°			
	Fine Quad-Pol		Single Polarisation	18 x 26 m	75 km	49°- 60°		
	Standard Quad-Pol		Quad Polarisation	12 x 8 m	25 km	20°- 41°		
				25 x 8 m	25 km	20°- 41°		
COSMO-SkyMed	Hugeregion (ScanSAR)			Muti-look	Single-look			
	Wideregion (ScanSAR)		Single HH/HV/VH/VV	100 x 100 m	30 x 30 m	200 x 200 km	20° -59.5°	
	Himage (Stripmap)		Single, HH/HV/VH/VV	30 x 30 m	16 x 16 m	100 x 100 km	20° -59.5°	
	Pingpong (Stripmap)		Single, HH/HV/VH/VV	5 x 5 m	3 x 3 m	40 x 40 km	20° -59.5°	
	Mode-2 (Spotlight)		Alternating, 2 pol. Selectable among HH, VV, VH and HV	20 x 20 m	15 x 15 m	30 x 30 km	20° -59.5°	
PAZ			Single, HH or VV	-	1 x 1 m	10 x 10 km	20° -59.5°	
	SM-S		HH, VV	Azimuth	Range			
	SM-D		HH-VV, HH-HV, VV-VH	2.5m	2.5m	10 km	20° - 45.365°	32
	WSM-S		HH,VV	5m	5m	5 km – 5.5 km	20° - 45.365°	34
	WSM-D		HH-HV, HH-VV, VV-VH	2.5m	2.5m	25 km (except 1 swath of 23.8 km)	20° - 45.969°	13
	SC, 1 azimuth look		HH, VV	5m	5m	9.9 km	20° - 45.195°	32
	SC, 2 azimuth looks		HH, VV	14.3m (1 azimuth look)	15m (4 range looks, 3.75m single look resolution)	75 km (each swath formed by 3 subswaths of 26.3 km each, 2km overlap)	20° - 45.598°	4
	SL-S		HH, VV	15m (2 azimuth looks)	15m (2 range looks, 7.5m single look resolution)	75 km (each swath formed by 3 subswaths of 26.3 km each, 2km overlap)	20° - 45.598°	4
	SL-D		HH-HV, HH-VV, VV-VH	1m (single look)	1m (@<29°) – 1.48m (@20°)	10 km	20° - 55.025°	24
	HR-S		HH,VV	2m	2m	10 km	20° - 55.025°	19
HR-D		HH-HV, HH-VV, VV-VH	1m	0.67m (@ 55°) -1.6m (@ 20°)	10 km	20° - 55.025°	12	
			1.3m	1.34m (@ 55°) – 3.21m (@ 20°)	10 km	20° - 55.025°	13	

Table A.5: Main characteristics of the operational modes of each SAR mission ([A.23], [A.24], [A.7], [A.24], [A.9], [A.25], [A.26], [A.10], [A.2], [A.27], [A.28],[A.29],[A.12]).

The PAZ satellite is designed to proportionate six different nominal operating modes namely: Stripmap single polarization (SM-S), Stripmap dual polarisation (SM-D), Stripmap single polarization wide swath (WSM-S), Stripmap dual polarization wide swath (WSM-D), ScanSAR (SC), Spotlight single polarisation (SL-S), Spotlight dual polarisation (SL-D), High Resolution Spotlight single polarisation (HR-S) and High Resolution Spotlight dual polarisation (HR-D).

The requirements described in Table A.5 come from a deep preliminary instrument performance study and will be confirmed by ECE as the different analysis tests will be done.

A.3 Antenna Model

Regarding the antenna model, in the case of Envisat/ASAR instrument the SAR system uses in-orbit antenna pattern measurements for correction in calibration process. This is possible because ASAR acquires SAR images with only eight different antenna beams (a low number of beams). Albeit at ASAR an antenna model was implemented, the more accurate antenna patterns were obtained from in-orbit measurements. There is some information on the Envisat antenna modeller in [A.30] and [A.32]; however it has been inaccessible to the author of this thesis. Although this inconvenience, it can be certainly affirmed that the method used to optimise has been the Genetic Algorithm approach. Further the approach in which is based the Envisat antenna model was applied to TerraSAR-X.

In the ALOS/PALSAR case, the number of beams is 23, still being a low number of beams. There is no public information found on the antenna modeller used. There is some information on a developed antenna model in the RADARSAT-2 and COSMO-SkyMed missions. These antenna models are also based in Genetic Algorithm in order to perform the antenna pattern optimisation.

The antenna model is of vital importance in modern SAR satellites, where novel calibration techniques have been developed to accomplish the objectives that imply the mission constraints. The novel SAR systems, which allow many different acquisition modes and hence a multitude of different antenna beams are needed for consistent calibration of the modes, have very tight accuracy requirements and the calibration process duration is limited to a short period of time.

A.3.1 TerraSAR-X

Some information on the TerraSAR-X antenna model can be found in [A.33]. The TerraSAR-X antenna model was used to derive the high number of different antenna beams (approximately 12000) generated by active antenna steering, necessary to perform accurate pattern correction during SAR processing. This makes possible to calibrate a high number of the used antenna beams with high accuracy and in a very time/cost effective way. The real measurement of all antenna beams in all operation modes, as performed for the ASAR instrument of ENVISAT across the rainforest, is too time-consuming.

The Antenna Model mathematically calculates radiation patterns having into account diverse inputs. One important input is the on-ground measurement of patterns from the embedded subarray patterns. Then, the beam excitation coefficients (amplitude and phase) of each individual TRM are applied to these measured subarray patterns. It is also necessary to determine the exact geometrical array antenna dimensions of (including the actual distances between subarrays) and the actual SAR instrument state like drifting and/or failed individual TRMs.

The antenna model has to generate antenna settings for optimal instrument performance, apart from the validation on-ground adjusting some of the simulated patterns to the actual measured ones. It is important, for instance, to achieve high sensitivity over a large angular range as well as good suppression of ambiguities. The optimization is performed varying the antenna TRMs excitation coefficients, which are optimized comparing the actual pattern with a given template (defined from some given quality parameters) and the best pattern obtained up to that time. The obtained antenna pattern must not violate the template. This optimization is based on the algorithms already developed for the ASAR instrument of ENVISAT. The antenna model optimiser generates a set of excitation coefficients prior to the mission that can be adapted during the mission time by means of a re-optimisation in case of drifts or failures in the TRMs.

After the Antenna Model validation and verification by an in-flight measurement of a limited number of beams, the thousands of reference patterns can be accurately derived. The complex excitation coefficients are stored in tables, one table for each possible beam, in form of amplitude and phase values row and column-wise. Another tables used are the ones describing drifting or failed antenna elements. These matrices are used to optimise the excitation coefficients in order to obtain an optimal antenna performance even having some TRMs failures. Both the excitation laws and the error matrix are different for transmit and receive. In case of the excitation coefficients, the differentiation between transmit and receive matrices allows greater flexibility for beam steering. The tables are

available on-board the satellite and can be updated if required (TRM failures, changes in the acquisition requirements, incorporation of new beams during normal operation, etc.).

A.3.2 RADARSAT-2

The APSW (antenna pattern synthesis workstation) is the antenna model designed for RADARSAT-2, and, like any other SAR antenna model should do, performs two main tasks: antenna pattern modelling and antenna pattern synthesis.

From the conclusions extracted for the ASAR instrument [A.32A.32] on the convenience of using the Genetic Algorithm to perform antenna synthesis in detriment of algorithms such as the Woodward Synthesis or Fourier Method, Touzi et al. chose the Genetic Algorithm to be implemented in the APSW. Its main objective is to determine the excitation law to be applied to the TRMs in order to obtain a predefined antenna pattern, by fulfilling a set of requirements specified by the manufacturer. APSW outputs the optimum TRM excitation amplitude and phases, the optimised antenna pattern parameters, and fitness curves.

A.3.3 COSMO-SkyMed

COSMO-SkyMed antenna model simulator is called Pharsim (PHased ARray SIMulator), and is based on array factor computation by mean of Fast Fourier Transform applied on the excitation matrix. The simulator developer is Thales Alenia Space Italia in the frame of SAR calibration activities.

Regarding the synthesis, the patterns are synthesised using Genetic Algorithms; maximising the 2-way directivity in the pointing direction and keeping sidelobes below an input mask. 1-way patterns are synthesised using template masks, while the 2-way ones using optimisation of radar parameters. The synthesis allows retrieving the excitation for nominal beams after estimating the effects of eventual mechanical deformations from the measured patterns ([A.33], [A.34]). In Figure A.14, one of the outputs generated by the program is reproduced:

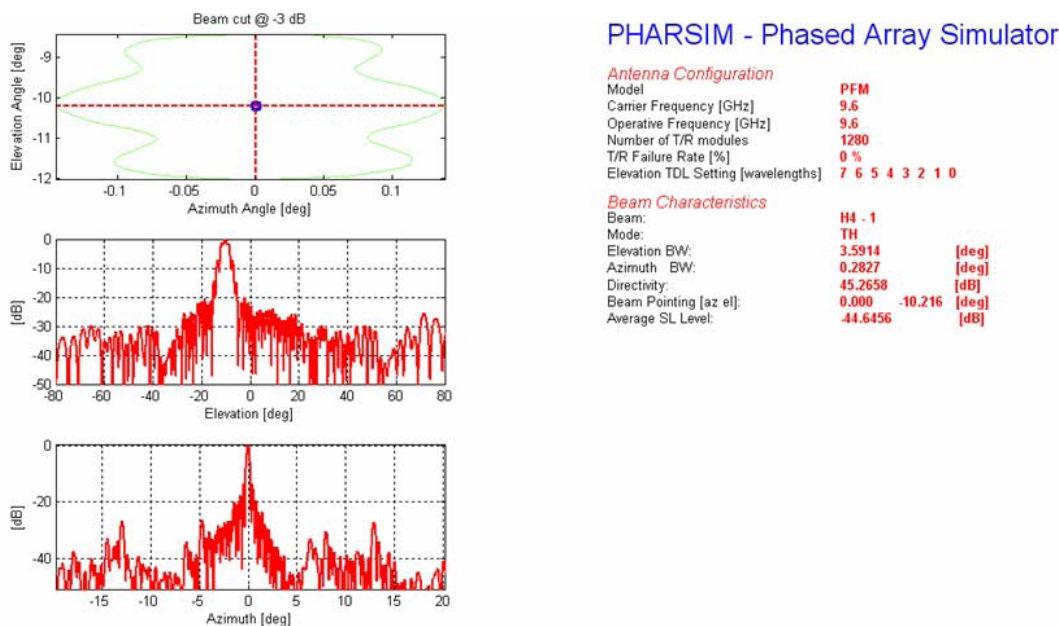


Fig. A.14: Example of an output of the COSMO-SkyMed beam optimiser [A.34].

In [A.34] it is explained that Pharsim has been validated versus an electromagnetic model where measured data is loaded and numerous non-ideal effects are taken into account: mutual coupling, mismatching and non-linear effects. They concluded that there is a high correlation between the two models. In addition, what Pharsim does to reduce computation load is to perform a Fast Fourier Transform of the amplitude-phase excitation matrix to obtain the array factor. This is possible for an equi-spaced regular grid, which means that the SAs are equi-spaced and fixed. Hence, from all this information it is deduced that Pharsim does not optimises the beams taking into account measured but ideal SA antenna patterns. And not only during the optimisation; Pharsim does not use actual SAs pattern to analyse antenna beams. What it actually does is, after the optimisation or the pattern generation from ideal SAs patterns, it

performs a correction of the excitations by importing data coming from near-field pre-flight measures and in-flight calibration data. In this way, the predicted beam is achieved by matching information on antenna configuration, near field measures and in-flight calibration data.

A.3.4 SEOSAR/PAZ

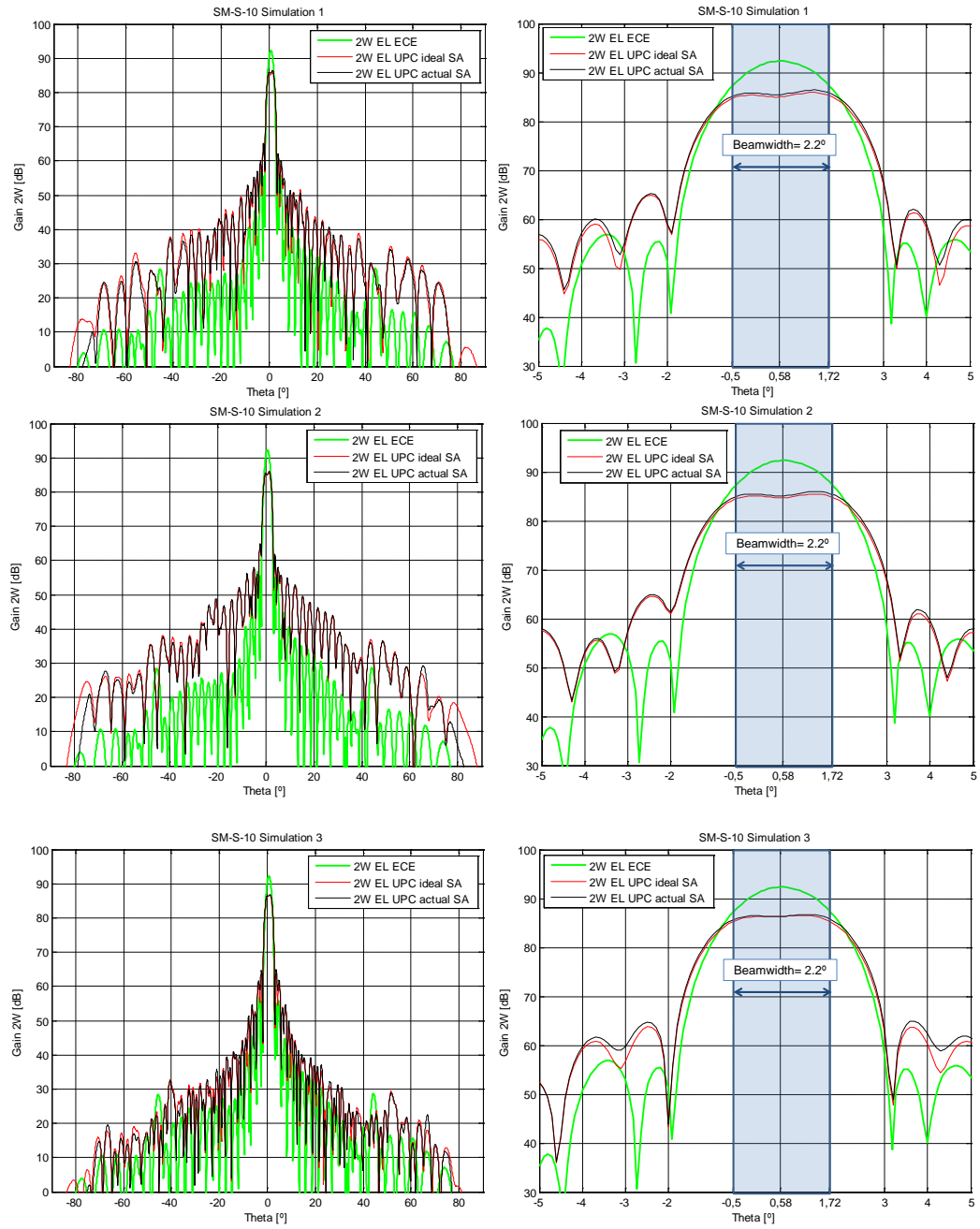
Since the next two chapters are entirely devoted to explain the antenna model architecture the optimiser developed for that software tool, the only comment to make in this section is that the chosen algorithm optimisation tool for that model is, one more time, the Genetic Algorithm approach.

The reader is hence encouraged to learn more about the PAZ antenna model, namely AMOR (Antenna MOdelleR), and especially about the method used to optimise the antenna beams in chapters 2 and 3. The former information is difficult to find in literature. As antenna model developers, our aim is to throw some light in aspects that every antenna model for SAR applications developer has to face in the design and development phase of its task. In this way we hope to help the reader to avoid losing time in aspects that probably another designer has faced before.

Appendix B SIMULATION RESULTS

In this Appendix the extra results from the simulations performed in Section 3.3.3.2 are presented:

- In Figure B.1 the results corresponding to the 5 simulations performed to tune the weights for the SM-S_10 beam,
- In Figure B.2 the results for the 5 simulations performed to tune the weights for the SM-S_26 beam.



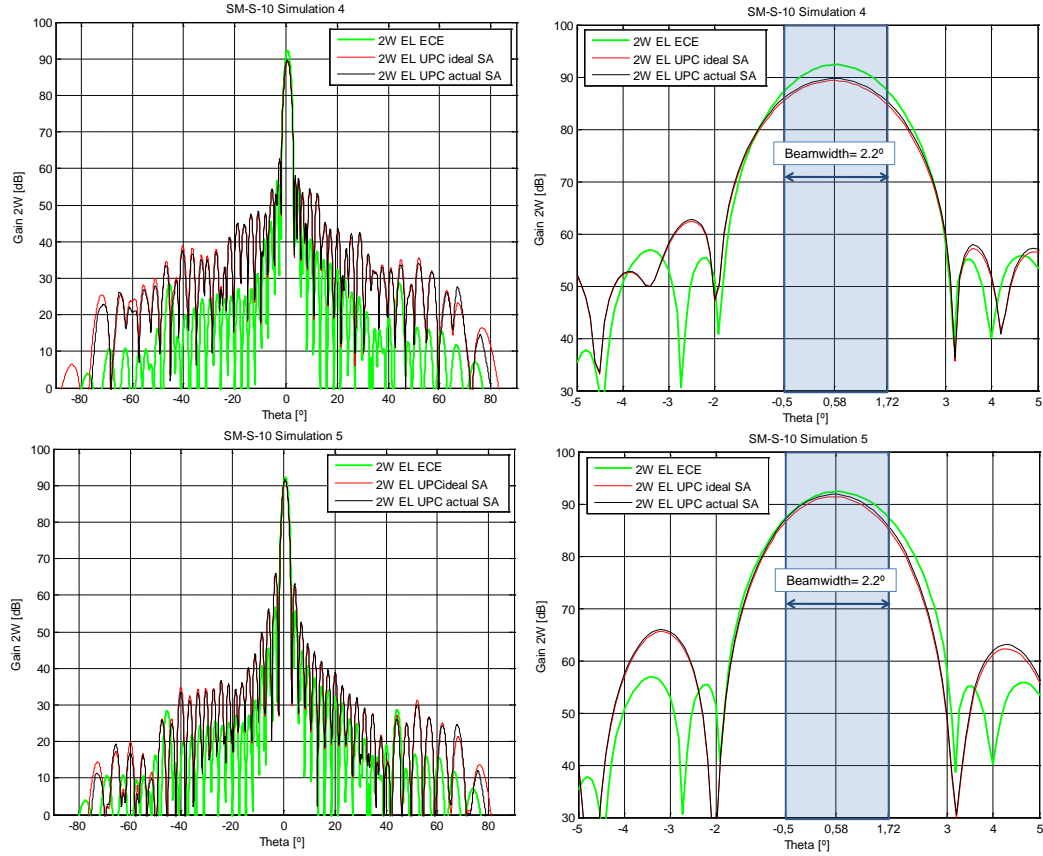
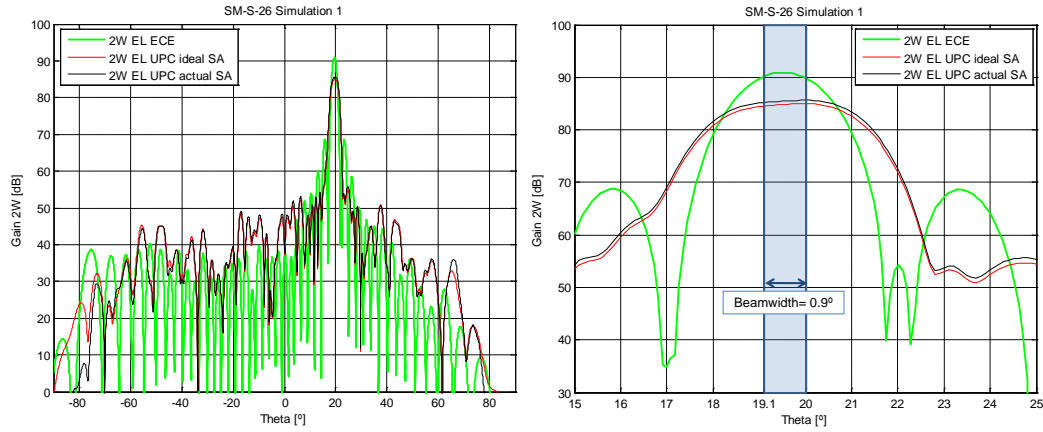


Figure B.1: Comparison of the optimization results of the SM10 beam: ECE vs. UPC beam for the 5 simulations performed. The green line corresponds to the ECE beam, the red line to the UPC resulting from the optimization using ideal SA patterns, and the black one resulting from the UPC's optimization with actual SA patterns.



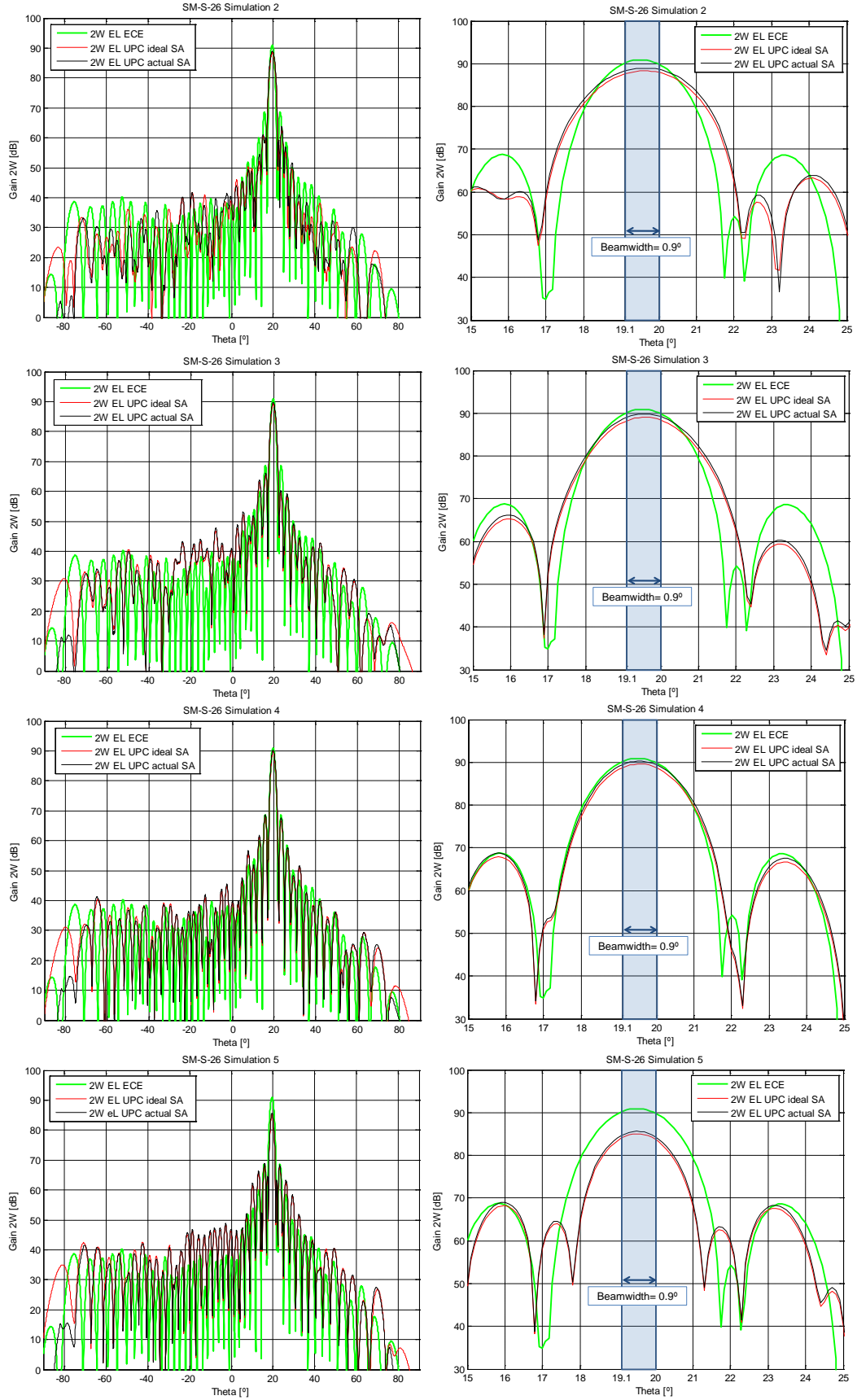


Figure B.2: Comparison of the optimization results of the SM26 beam: ECE vs. UPC beam for the 5 simulations performed. The green line corresponds to the ECE beam, the red line to the UPC resulting from the optimization using ideal SA patterns, and the black one resulting from the UPC's optimization with actual SA patterns.

Appendix C

AZIMUTH AND ELEVATION PLANES INCONSISTENCE

An inconsistency in the results provided by the ECE SAR Tool has been detected while comparing exactly the same pattern generated from coefficients provided by ECE when plotted using ECE tool and AMOR. It was found that starting from the same coefficients both patterns are different in gain level (more than 1dB). The shape is practically the same, but with an offset that makes the UPC generated beam more than 1dB less directive. After many comparisons and deliberations, it was found that the EL and AZ pattern cuts provided by the ECE tool are not consistent, since they must have the same maximum gain in the point where the cuts intersect, and this does not happens (Figure 4.13 and 4.14). This means that the cuts are not done passing exactly over the same point in the main lobe. The AMOR tool performs correctly those cuts. However, this means that the comparisons presented in Chapter 3 are not totally fair for two reasons:

1. The ECE tool always uses ideal pattern SAs, while the UPC tool also uses actual SA patterns. This way, AMOR is able of accounting for differences in the SA patterns, errors on the SAs positioning in the manufacturing process, and even for errors in TRMs.
2. It seems that there is a disagreement between ECE Tool and AMOR in the definition of the AZ and EL planes. In addition, it seems to be an inconsistent result between the levels of the AZ and EL planes provided by the ECE Tool. Hence, the EL cuts which are compared between tools are not performed in the same plane and this makes difficult to compare in fair conditions both results.

In Figure C.1 it can be observed how using the same set of coefficients for both tools, specifically the ones used to generated the SM-S_1 beam, the ECE cuts are inconsistent, at least according to our definition. Concretely, the AZ cut is done at $\varphi=0^\circ$, and the EL one at $\varphi=90^\circ$, in AMOR case, and the power value in the nominal centre of the swath ($\theta=0^\circ$ in the AZ plane, and $\theta=-18.72^\circ$ in the EL plane) is exactly the same. On the contrary, in the ECE generated beam, with the formerly mentioned EL and AZ cuts definition, the power in the centre of the swath for AZ and EL planes does not coincide.

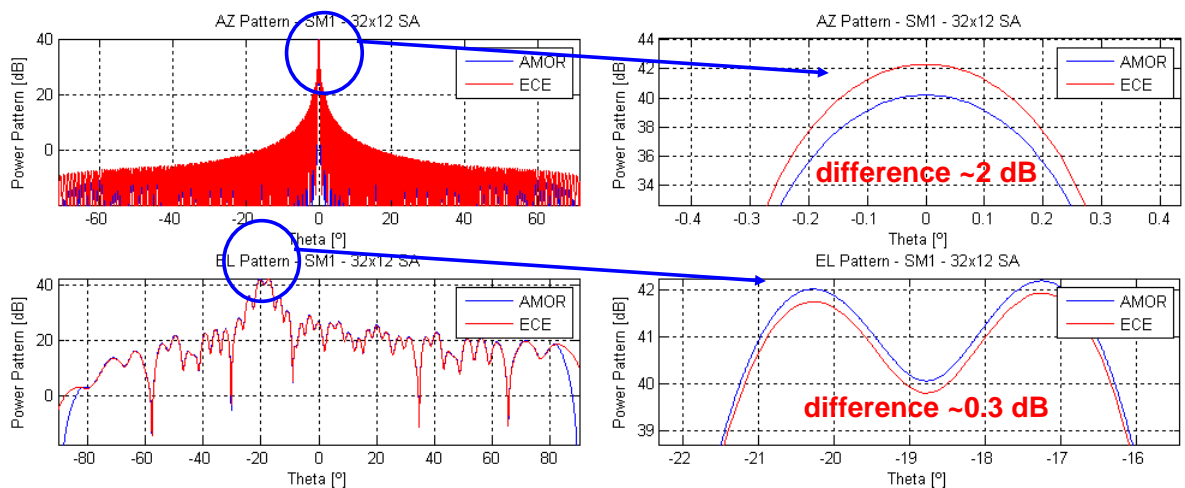


Figure C.1: Comparison of the power patterns for the TX SM-S_1 beam: ECE vs. AMOR beam. Zoom in the swath. The AMOR power values in the centre of the swath coincide, while in the ECE case this they differ in 2.3 dB.

If the patterns are normalized in order to check if at least their shape is the same, it is observed that the AZ pattern is quite different between both tools while the EL pattern is the same for both. It is very probable that the cuts are defined in different planes (Figure C.2).

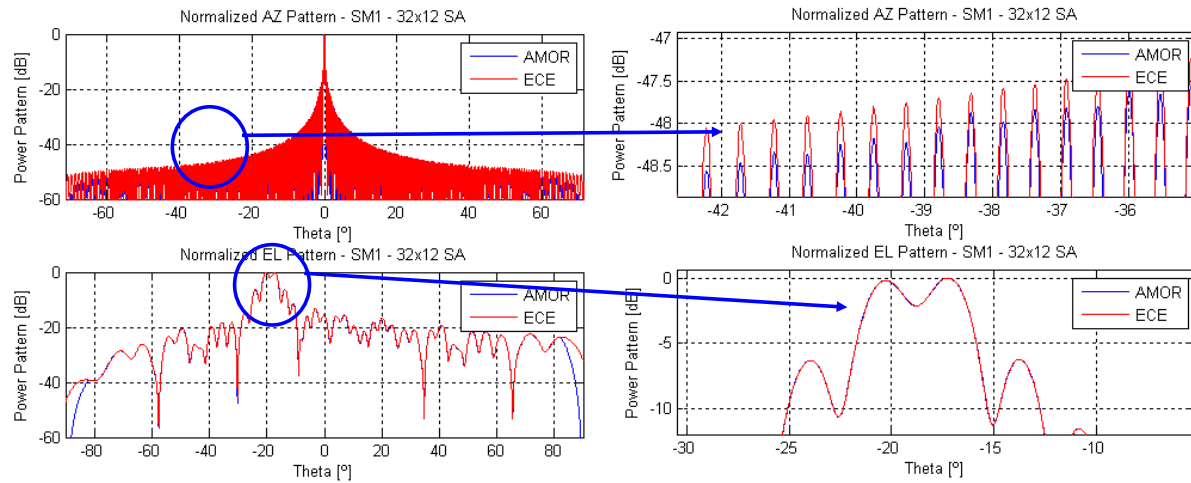


Figure C.: Comparison of the power patterns for the TX SM-S₁ beam: ECE vs. AMOR beam. Zoom in the swath. The AMOR power values in the centre of the swath coincide, while in the ECE case this they differ in 2.3 dB.

Appendix D

PUBLICATIONS

In the present annex the publication associated to the work developed in this Master Thesis is attached:

- M. Labriola, J.M. González-Arbesú, J. Romeu Robert, I. Calafell Rueda, J. Sánchez Palma, P. Saameño Pérez, J. Closa Soteras, A. Solana González, “AMOR: an Antenna MOdeleR for the Spanish SAR Satellite (PAZ)”, Proceeding of Advanced RF Sensing Instruments (ARSI), ESA-ESTEC, Noordwijk, 16-18 November 2009 (Full conference paper publ. in proceedings book).

AMOR: an Antenna MOdeleR for the Spanish SAR Satellite (PAZ)

M. Labriola⁽¹⁾, J.M. González Arbesú⁽²⁾, J. Romeu Robert⁽²⁾, I. Calafell Rueda⁽²⁾, J. Sánchez Palma⁽¹⁾, P. Saameño Pérez⁽¹⁾, J. Closa Soteras⁽¹⁾, A. Solana González⁽¹⁾

⁽¹⁾EADS CASA Espacio
Av. Aragón, 404, 28022 Madrid (Spain)
E-mail: zx_massimo.labriola@casa-espacio.es

⁽²⁾ Universitat Politècnica de Catalunya
Campus Nord. C/Jordi Girona, 1-3, 08034, Barcelona (Spain)
E-mail: jmgonzalez@tsc.upc.edu

ABSTRACT

PAZ is a highly flexible X-band SAR Satellite which primary objective is global Earth Observation to serve the strategic needs of the Spanish Government within the National Earth Observation Programme.

The SAR Satellite will be capable to provide high quality SAR images with a variety of sizes and resolution ranging from medium over wide regions up to very high resolution (e.g. meter and sub-meter). Operational flexibility with multi-mode, multi-polarization and left and right looking attitude is one of the major PAZ system requirements leading to a quite large number of different instrument configurations and antenna beams. The main function of the antenna model is to derive the two dimensional antenna patterns for all the modes, swaths, polarizations and transmit/receive combinations needed for image acquisition and processing.

The methodology of the antenna model design, the validation/verification methods as well as first results obtained with AMOR are presented in detail in this paper.

INTRODUCTION

SEOSAR/PAZ is the first Spanish Satellite based on the use of a high resolution X-band Synthetic Aperture Radar (SAR). The entire System is being developed under control and supervision of Hisdesat, who is also responsible of the satellite operation and data exploitation services. EADS CASA Espacio is the Satellite prime contractor company leading a wide industrial consortium, while INTA (Instituto Nacional de Técnica Aeroespacial) is responsible of developing the Ground Segment [1].

The SAR instrument comprises an X band active phased array antenna with an operation instantaneous bandwidth up to 300 MHz. The antenna which size is 4.8 m length and 0.7 m width consists of 12 panels in azimuth direction— assembled in three mechanical leaves – each with 32 dual-polarized subarrays [2]. Each individual subarray is driven by a transmit-receive module (TRM) adjustable in amplitude and phase by applying complex excitation coefficients. This enables beam steering and adaptive beam forming in both azimuth and elevation directions. For the variety of standard acquisition modes possible, such as Stripmap, ScanSAR or Spotlight, and the several experimental modes more than ten thousand beams can be programmed and commanded. This multitude of beams is one highlight but also a great challenge for the whole mission and it represents the main driver for the need of an accurate antenna model. In fact, the traditional (ASAR) approach based on the calibration of individual beams and in-orbit measurement of single antenna pattern is not feasible because it requires an unacceptable effort and cost, taking into account the short Commissioning Phase (CP). Owing to this high degree of flexibility of the instrument and tight radiometric performance requirements, a different approach is needed to reach an efficient end-to-end system calibration.

ANTENNA MODEL

Concept

PAZ operation and calibration approach is built around an Antenna Model. This tool is used to accurately determine the antenna beam patterns combining mathematical models with highly precise on-ground characterization data, post-launch external verification measurements and periodic in-flight TR modules calibration.

This article summarizes the different functionalities provided by Antenna MOdeleR (AMOR) in order to fulfil the best performance of the radar instrument and to correct the SAR images radiometry. AMOR is developed by the Universitat Politècnica de Catalunya (UPC) under EADS Casa Espacio contract. As aforementioned, it will allow the reconstruction of the antenna radiation patterns by superposition of measured embedded subarray patterns weighted by beam excitation coefficients, considering the antenna geometry and elements referencing. Another important function to be included in AMOR is the beam excitation coefficients optimization, in order to optimize the performance in terms of Noise Equivalent Sigma Zero (NESZ) and ambiguity ratios; an eventually re-computation may be in response to TRMs failure or degradation. Furthermore the tool includes the analysis of the effects due to eventual antenna subarray misalignment and planarity errors, favouring a better fit to the desired patterns. Frequency dependence as well as thermo-elastic deformations are assessed. AMOR validation/verification strategy is also presented, describing the steps necessary to achieve the needed AMOR accuracy in order to comply with the specified products quality.

AMOR Functionalities & Future Developments

The antenna modeller AMOR is being implemented using Matlab® and it runs in personal computers and even in notebooks. Its primary goal is the design, analysis and synthesis of the PAZ front-end antenna patterns in to order to achieve maximum-performance sensing data in a much more operational basis. For that reason the AMOR GUI (Graphical User

Interface) makes a distinction between the Analysis and Synthesis procedures in addition to its Array Description procedure. The influence of errors in the antenna performance is also accounted for and an Error Analysis tool is included in the code. In Fig. 1 a screenshot of the Array Description tool is shown.

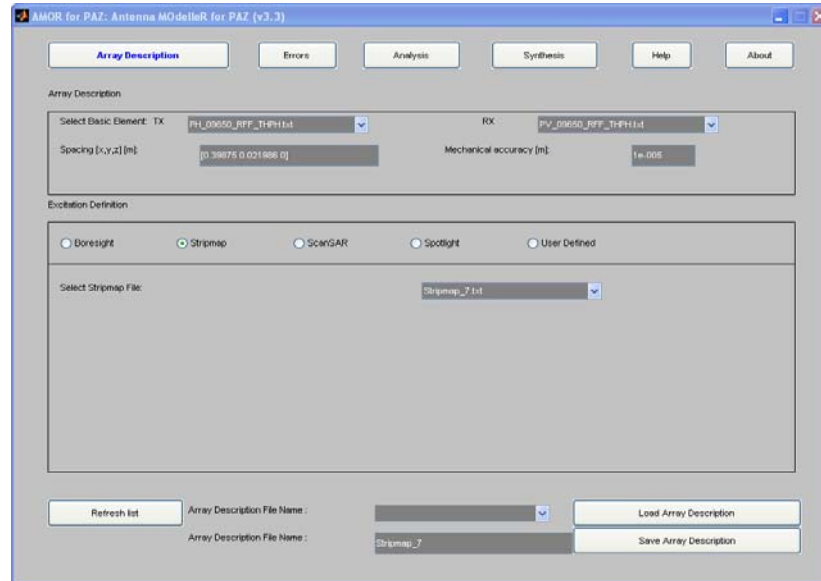


Fig. 1: Array Description window of AMOR. Buttons in the upper side of the window are calls to the tools available in the code. Some of them are the Error analysis tool, the array Analysis tool, and the Synthesis of excitation coefficients tool.

AMOR allows the computation of the copolar and crosspolar transmitting (Tx) and receiving (Rx) antenna patterns of the SAR instrument together with the copolar and crosspolar two-way (2W) antenna patterns. Theta and phi components of the Tx, Rx and 2W radiation patterns are also computed. The patterns of the subarrays can be different in transmitting or receiving modes due to the chosen polarization, being either vertical or horizontal depending on the operating mode of the instrument. The resulting patterns can be visualized in a standard Cartesian presentation for the elevation and azimuth planes and the main parameters of the pattern automatically determined for a quick analysis of the results. Also three dimensional power patterns plots can be generated to assess the absence of notorious secondary lobes. The accurate computation of the antenna directivity for the Tx and Rx pattern is an additional functionality included in AMOR.

Until the moment, to compute these patterns the measurements of an isolated subarray or an ideal subarray with the required polarization can be chosen as an input. In the future the measured patterns of embedded subarrays will be used as baseline. However, and although not implemented yet in the present interface, the software is ready for using several measured (or simulated) subarray patterns simultaneously, in order to account for the slight differences in the radiation patterns of the subarrays when embedded in different positions in the whole array. The data concerning the patterns of the subarrays can be stored as far field samples, or even as spherical modal coefficients of the subarray for a more complete and accurate computation of the far.

As previously mentioned the software is able to analyze the different operational modes of the instrument (Stripmap, ScanSAR, Spotlight), and also a User Defined set of coefficients for designing and/or testing purposes. The coefficients that command a given antenna configuration are the combination of TRM Tx/Rx phase and Rx gain values stored in look up tables like in the satellite. In Fig. 2 a snapshot of the Analysis tool and some of its results are shown when characterizing a Stripmap beam, while Fig. 3 highlights the resulting 3D pattern.

The use of symmetries in the subarray is also a feature in AMOR, allowing the evaluation of a better configuration of the array structure for reducing the crosspolar levels. Although this feature is not going to be used in the future it has revealed as very useful in the design phase of the array configuration.

Mechanical errors due to imperfections in the antenna manufacturing and its deformation in-flight due to the variation of thermal conditions at panel and antenna level (modelled as shifts along x, y, and/or z-axis with respect to their nominal positions and a rotation along each of their axis –yaw, roll, pitch), together with errors due to TRM failures or deviations from their nominal values are also being implemented in AMOR.

An important objective of the code is the capability of synthesizing the excitation coefficients to be applied to the TRMs through its Synthesis tool. This synthesis procedure has to derive an optimized 2W antenna pattern matching a given template. The template is related with several instrument performances such as: gain and beamwidth of the main lobe, side lobe levels, elevation and azimuth beam pointing directions, gain variations within the swath, ambiguity levels, null positions in certain directions and higher gain towards higher elevation angles within the main lobe. The possibility to include deviations in the TRM settings (determined by PN-gating technique) or failing modules either in Tx and Rx or both shall be considered when computing the coefficients.

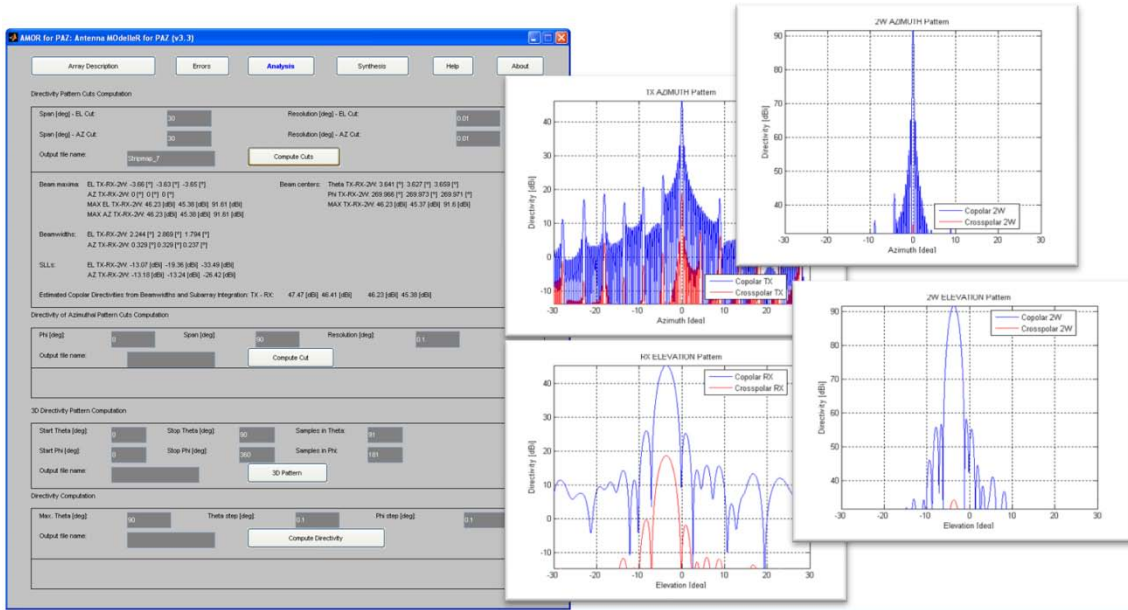


Fig. 2: Analysis window of AMOR. Some of the resulting pattern cuts (for the Tc, Rx, and 2W azimuth plane) are shown on the right. The main parameters of interest for the resulting patterns are shown in the Analysis window.

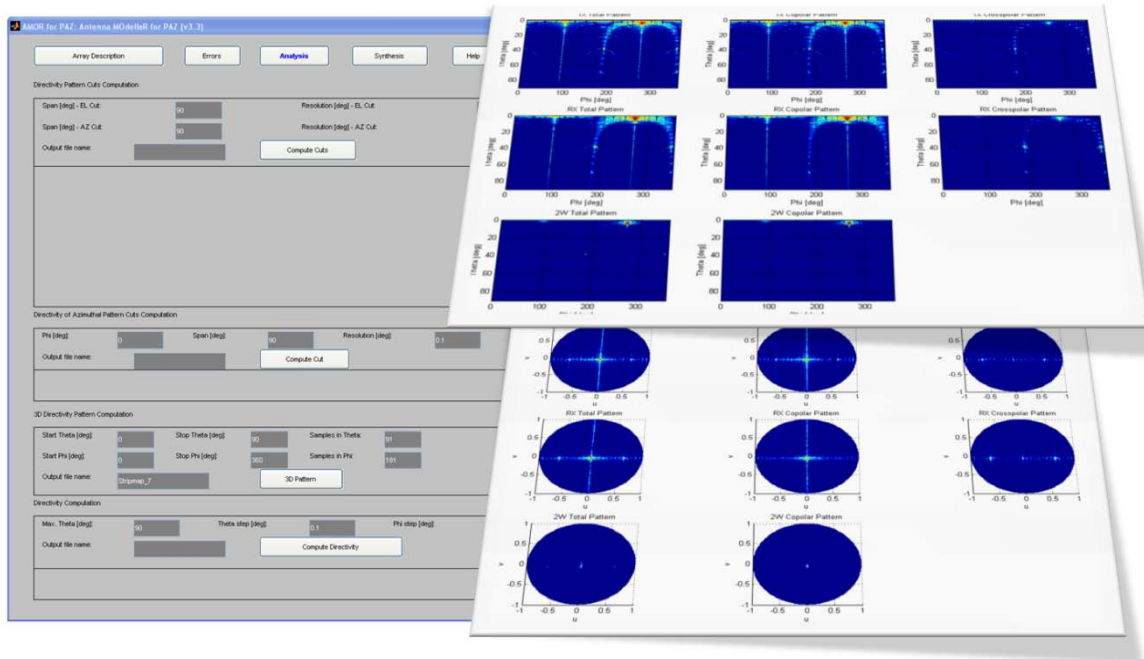


Fig. 3: Analysis window of AMOR. Two ways of showing the three dimensional Tx, Rx, and 2W copolar and crosspolar power patterns.

AMOR VALIDATION & VERIFICATION METHODS

The life cycle of the Antenna Model is briefly summarized in Fig. 4. The scheme here proposed forms part of the more general System engineering and calibration section included into Ground Segment architecture [3]. AMOR V&V chart is dictated by the peculiar PAZ System calibration philosophy [4], basically driven by: (i) the huge number of beams to be commanded and calibrated, (ii) the high-performance radiometric requirements and (iii) the short CP.

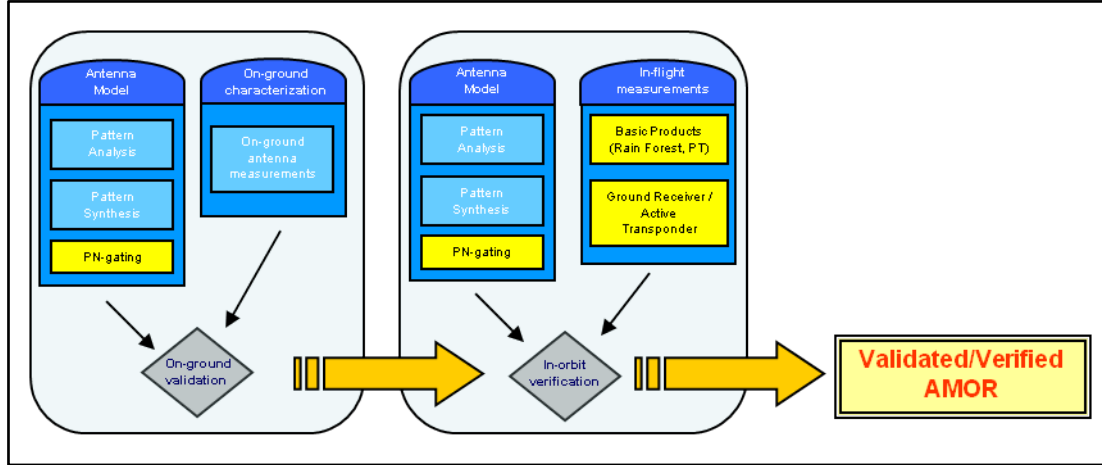


Fig. 4: AMOR validation/verification flow chart

Starting from the design guidelines described in the previous sections, AMOR will be firstly validated on-ground before launch and therefore an in-orbit verification process will be performed during the first months of the CP [5]. To do this, an extensive on-ground characterization of the instrument behaviour, antenna radiation, mechanical and electrical seems to be necessary to achieve well-calibrated SAR products during the whole mission lifetime. The pre-flight tests provide reference to the acquired data in-orbit (e.g. antenna patterns, instruments drifts, etc.) and they will directly feed into the antenna model. This activity may involve different steps of iteration once the validation has commenced.

Pre-launch Validation

Embedded subarray patterns (considering mutual coupling between radiating subarrays, VSWR and insertion loss) and the nominal gain and phase excitations applied to each subarray are required as a direct inputs for antenna model. The antenna model will be tuned in the sense that the predicted antenna patterns fit well (i.e. achieve the specified accuracy) to the measured ones and it will be validated by comparison of modelled with measured patterns. The validation approach makes use of a reduced set of beams measured in Tx and Rx modes, for both polarization (vertical and horizontal) and at different frequencies: a good selection of them could be based on the pointing and the beamwidth criteria. It's worth noting that AMOR built process will be tracked and checked at different levels:

- I. individual subarray
- II. single panel (embedded subarrays)
- III. one leaf (one third of the antenna)

in order to validate the model for the complete antenna.

In-orbit Verification

The second next step foresees an in-orbit verification process to prove the performance for the whole antenna in space; this important task will be executed during the first weeks after launch. The verification will be performed with really measured beams and can be divided into three main tasks:

- Elevation pattern shape
- Peak-to-peak gain variation
- Azimuth pattern shape

The Amazon rainforest will be the primary area for measurements of elevation beam patterns because of the stability and homogeneity of the radar back-scattering over extended areas. The pattern shape is clearly visible in the SAR raw data and it will be corrected with the modelled reference patterns. AMOR will be also capable to predict peak-to-peak gain, thus gain offset between different beams, by an opportune processing of ScanSAR data. The verification of the antenna pattern in the azimuth direction will be performed by using measurements acquired over strong point scatterers (2-way azimuth pattern estimation) or by analyzing SAR specific acquisition over a deployed network of ground receivers/active transponders.

After its completely in-flight verification, the properly working antenna model will also help for the determination of the absolute calibration factor, thus the equivalent radar cross section of targets, contributing to save valuable time during the commissioning and the operation phase.

CONCLUSIONS

E2E System calibration shall take minimum operation time and cope with System degradation neither with impact on performance nor the need for long re-calibration periods. After the lessons learnt during the TerraSAR-X commissioning, an effective calibration philosophy emerges which basically shifts the calibration effort from space to ground in order to assure a commissioning phase of less than six months.

The key element of this new concept is a mathematical antenna model based upon accurate on-ground measurements of the instrument, a set of post-launch external measurements to be performed during the initial commissioning period, periodic in-flight internal characterisation, and the internal calibration data to be performed during and together with the sensing data. AMOR plays an important role in the performance prediction of the entire instrument and allows for dynamic re-calibration during operational lifetime, so its required accuracy has to be carefully managed and verified.

REFERENCES

- [1] F. Cerezo, M. Fernández , A. Borges, J. Sánchez Palma, J. Lomba, R. Trigo, J. Ureña, E. Vez, M. López, “The Spanish Earth Observation Programme”, Advanced RF Sensors and Remote Sensing Instruments 2009
- [2] F. Monjas Sanz, M. I. Martín Hervás, “Dual polarized subarray for Spaceborne SAR at X-band”, EUCAP 2009
- [3] PAZ ECE Team, “Satellite to Ground Segment Interface Description”, Internal Technical Note (PAZ-ECE-SSC-TNO-0053), 2009
- [4] P. Saameño Pérez, J. Closa Soteras, M. Labriola, J. Sánchez Palma, A. Solana González, F. López Dekker, A. García Mondejar, A. Broquetas Ibars , “Radiometric Budget Characterization of X-Band SAR Instrument On-Board PAZ”, Advanced RF Sensors and Remote Sensing Instruments 2009
- [5] M. Bachmann, M. Schwerdt and B. Bräutigam, “Accurate Antenna Pattern Modelling for Phased Array Antennas in SAR Applications – Demonstration on TerraSAR-X”, International Journal of Antennas and Propagation 2009

REFERENCES AND BIBLIOGRAPHY

In the following sections the cited references through the Master Thesis document are listed. References refer to books, papers, articles, conference proceedings and even web pages from which some information has been consulted in order to explain a concept, or some image has been taken.

In addition, a bibliography is also included. Bibliography refers to books, papers, articles, conference proceedings or web pages that have been consulted during the Master Thesis document elaboration and in the previous stage but are not explicitly cited during the text. They are not cited because the information found on them is not directly used in the document. However, this bibliography may help the reader, like has helped the author, to understand more deeply some concepts discussed in the document. For this reason including it is considered important.

R.1 Chapter 2

R.1.1 References

- [2.1] M.R. Spiegel, *Schaum's Mathematical Handbook of Formulas and Tables*, McGraw-Hill, 1968
- [2.2] C.A. Balanis, *Antenna Theory: Analysis and Design*, John Wiley & Sons Inc., 2nd edition, 1997
- [2.3] J.M. González-Arbesú, I. Calafell Rueda, J. Romeu Robert, Internal Technical Note (PAZ-UPC-SSY-RPT-0004), July 2009
- [2.4] J.E. Hansen, *Spherical Near-Field Antenna Measurements*, Peter Peregrinus Ltd., IEEE Electromagnetic Waves Series 26, 1988
- [2.5] PAZ ECE Team, *Antenna Model Development and Validation Plan*, Internal Technical Note (PAZ-ECE_IIE-PLN-0040), October 2008

R.2 Chapter 3

R.2.1 References

- [3.1] Michael Johnson, Yahya Rahmat-Samii, *Genetic Algorithms in Engineering Electromagnetics*, IEEE Antennas and Propagation Magazine, Vol. 39, No. 4, August 1997
- [3.2] Antenna Pattern Synthesis_150410-2
- [3.3] ECE Team, *Antenna Pattern Synthesis for Paz*, 2010
- [3.4] Yahya Rahmat-Samii and Eric Michielssen, *Electromagnetic Optimization by Genetic Algorithms*, John Wiley & Sons, 1999
- [3.5] PAZ ECE Team, *Instrument Performance Analysis*, Internal Technical Note (PAZ-ECE-SSY-ANA-0039), October 2010

R.2.2 Bibliography

- *Genetic Algorithm and Direct Search Toolbox™ 2. User's Guide*, The MathWorks, Inc., 2009

R.3 ANNEX A

R.3.1 References

- [A.1] <http://www.astrium.eads.net/es/news/satellite-paz-una-solucion-de-seguridad-y-defensa-de-astrium-en-espana.html> [Accessed July 2010]
- [A.2] F. Covello, F. Battazza, A. Coletta, G. Manoni, G. Valentini, "COSMO-SkyMed Mission Status: Three out of Four Satellites in Orbit", IGARSS 2009
- [A.3] <http://spaceflightnow.com/tracking/index.html> [Accessed July 2010]
- [A.4] Jacques Louet, Stefano Bruzzi, "ENVISAT Mission & System", IEEE, 1999
- [A.5] <http://www.lsespace.com/missions/envisat.php> [Accessed March 2010]
- [A.6] Ake Rosenqvist, Masanobu Shimada, "ALOS PALSAR: A Pathfinder Mission for Global-Scale Monitoring of the Environment", IEEE Transactions on Geoscience and Remote Sensing, Vol. 45, No. 11, November 2007
- [A.7] PALSAR Reference guide, ERSDAC (Earth Remote Sensing Data Analysis Center), 3rd ed., March 2006
- [A.8] J. Herrman, A. González Bottero, "TerraSAR-X Mission: The New Generation in High Resolution Satellites", Anais XIII Simpósio Brasileiro de Sensoramento Remoto, Florianópolis, Brasil, 21-26 abril 2007, INPE, p.7063-7070
- [A.9] A. Roth, M. Eineder, B. Schättler, "TerraSAR-X: A New Perspective for Applications Requiring High Resolution Spaceborne SAR Data"
- [A.10] <http://www.radarsat2.info/> [Accessed March 2010]
- [A.11] "COSMO-SkyMed Mission, COSMO-SkyMed System Description & User Guide", Italian Space Agency
- [A.12] PAZ ECE Team, "Instrument performance analysis", Internal Technical Note (PAZ-ECE-SSY-ANA-0039), October 2008
- [A.13] <http://envisat.esa.int> [Accessed March 2010]
- [A.14] <http://www.knmi.nl/~eskes/projects/asset.html> [Accessed July 2010]
- [A.15] Masanobu Shimada, Takeo Tadono, Ake Rosenqvist, "Advanced Land Observing Satellite (ALOS) and Monitoring Global Environmental Change", Proceedings of the IEEE, Vol. 98, No. 5, May 2010
- [A.16] Stephan Buckreuss, Achim Roth, "The TerraSAR-X Mission", 2nd STG/IPY SAR Coordination meeting, Oberpfaffenhofen, Sept 30, 2008
- [A.17] M. Labriola, J. Sánchez Palma, P. Saameño Pérez, J. Closa Soteras, A. Solana González, J.M. González Arbesú, J. Romeu Robert, I. Calafell Rueda, "AMOR: an Antenna MOdeller for the Spanish SAR Satellite (PAZ)", Presented in Advanced RF Sensing Instruments (ARSI), ESA-ESTEC, Noordwijk, November 18th, 2009
- [A.18] <http://www.eorc.jaxa.jp/ALOS/en/about/palsar.htm> [Accessed May 2010]
- [A.19] B. Grafmüller, A. Herschlein, C. Fischer, "The TerraSAR-X Antenna System", IEEE 2005
- [A.20] S. Riendeau, C. Grenier, "RADARSAT-2 Antenna", 2007 IEEE
- [A.21] http://www.eoportal.org/directory/pres_COSMOSkyMedConstellationof4SARSatellites.html [Accessed May 2010]
- [A.22] PAZ ECE Team, "Satellite technical description", Internal Technical Note (PAZ-ECE-SSY-TNO-0042), October 2008

- [A.23] Betlem Rosich, Manfred Zink, Ramón Torres, Josep Closa, Christopher Buck, "ASAR Instrument Performance and Product Quality Status", IEEE
- [A.24] Masanobu Shimada, Osamu Isoguchi, Takeo Tadono and Kazuo Isono, "PALSAR Radiometric and Geometric Calibration", IEEE TRANSACTIONS ON GEOSCIENCE AND REMOTE SENSING, VOL. 47, NO. 12, DECEMBER 2009
- [A.25] Wolfgang Keydel & Alberto Moreira, "TerraSAR-X and TanDEM-X. Two Innovative Remote Sensing Stars for Space-borne Earth Observation", DLR
- [A.26] Bernhard Buckl, "DLR Agency Report", WGISS-21 Budapest, May 12th, 2006
- [A.27] "ASI-COSMO-SkyMed Brouchure", e-geos, an ANSI/Telespazio company
- [A.28] L. Candela, F. Caltagirone, "COSMO-SkyMed. Mission Definition. Main Application and Products", POLinSAR, January 2003
- [A.29] PAZ ECE Team, "Satellite system specification", Internal Technical Note (PAZ-ECE-SSC-TNO-0012), October 2008
- [A.30] L. Alvarez-Pérez, M. Schwerdt, D. Hounam, R. Torres, C. Buck, and M. Zink, "Antenna Pattern Optimization for the ENVISAT ASAR Antenna with Failed Elements," in 25th ESA Antenna Workshop on Satellite Antenna Technology, Noordwijk, Netherlands, 2002
- [A.31] J. Mittermayer, A. Moreira, "Antenna Pattern Synthesis Optimization for the Elevation Pattern of the ASAR Instrument", CEOS Workshop, Toulouse/France, 22-29 October 1999
- [A.32] Markus Bachmann, Marco Schwerdt, and Benjamin Bräutigam, "Accurate Antenna Pattern Modelling for Phased Array Antennas in SAR Applications – Demonstration on TerraSAR-X", Application Article, Hindawi Publishing Corporation, International Journal of Antennas and Propagation, Vol. 2009, Article ID 492505
- [A.33] A. Torre, L. Cereoli, "Cosmo-SkyMed: First Results of SAR In-Flight Calibration", 2008 IEEE]
- [A.34] L. Cereoli, A. Torre, "The Role of Performance Modelling in Active Phased Array SAR", IEEE 2007

R.3.2 Bibliography

- http://www.naturalsciences.be/institute/structure/geology/gsb_website/research/satellite/satellite [Accessed July 2010]
- <http://www.spotimage.com/web/es/276-envisat-y-ers.php> [Accessed February 2010]
- Takanori Iwata, "Advanced Land Observation Satellite (ALOS): On-Orbit Status and Platform Calibration",
- <http://www.eorc.jaxa.jp/ALOS/en/index.htm> [Accessed July 2010]
- Irena Hajnsek & TSX TEAM, "TerraSar-X Mission: Application and Data Access. 2 years in Orbit (since June 2007)", 29 June 2009
- B. Bräutigam, M. Schwerdt, M. Bachmann, B. Döring, "Results form TerraSAR-X Geometric and Radiometric Calibration"
- M. Schwerdt, D. Hounam, J. L. Alvarez-Pérez, and T. Molkenhthin, "The calibration concept of TerraSAR-X, a multiple mode high resolution SAR," Can. J. Remote Sens., vol. 31, no. 1, pp. 30–36, Feb. 2005
- M. Schwerdt, D. Hounam, B. Bräutigam, and J. L. Alvarez-Pérez, "TerraSAR-X: Calibration concept of a multiple mode high resolution SAR," in Proc. 25th Int. Geosci. Remote Sens. Symp., Seoul, Korea, 2005, pp. 4874–4877
- Markus Bachmann, Marco Schwerdt, Benjamin Bräutigam, "TerraSAR-X In-Orbit Antenna Model Verification Results", Proceedings of the 4th European Radar Conference, Munich, Germany, October 2007
- Markus Bachmann, Marco Schwerdt, and Benjamin Bräutigam, "Accurate Antenna Pattern Modelling for Phased Array Antennas in SAR Applications – Demonstration on TerraSAR-X", Application Article, Hindawi Publishing Corporation, International Journal of Antennas and Propagation, Vol. 2009, Article ID 492505
- COSMO3_Mbook, "COSMO-SkyMed COSMO-3. Delta Launch Vehicle Programs", Boeing, ASI, Thales Alenia Space, United Launch Alliance
- <http://www.ottawacitizen.com/Technology/Coastline+surveillance+boost/1758661/story.html> [Accessed March 2010]
- R. Touzi, C.E. Livingstone and R. Filfil, "RADARSAT 2 Antenna Modelling and Synthesis Using the Genetic

Algorithms", Geoscience and Remote Sensing Symposium, 2005. IGARSS '05. Proceedings. 2005 IEEE International , vol.4, no., pp. 2262- 2265, 25-29 July 2005

- G. Valentini, F. Battazza, A. Coletta, F. Covello, G. Manoni, "Achievements and Perspectives of the COSMO-SkyMed Mission", Progress In Electromagnetics Research Symposium Proceedings, Moscow, Russia, August 18-21, 2009
- <http://www.e-geos.it/cosmoMission.htm> [Accessed July 2010]

ACRONYMS

A list of the acronyms used in the chapters of the present Master Thesis is presented below. The acronyms used in Appendix A different from the ones in the chapters are not included for the sake of brevity.

AMOR	Antenna MOdelleR
AZ	Azimuth
EL	Elevation
LSB	Least Significant Bit
MSB	Most Significant Bit
NESZ	Noise Equivalent Sigma Zero
GA	Genetic Algorithm
GUI	Graphical User Interface
RX	Reception
SA	Sub Array
SAR	Synthetic Aperture Radar
SEOSAR	Spanish Earth Observation SAR
TRM	Transmit-Receive Module
TX	Transmission
2W	Two-Way
3D	Three Dimensions